

Characterisation of the Metabolic
Phenotype of the Fmo5 Knockout
Mouse

Flora Helen Scott

UCL

Biochemistry

I, Flora Helen Scott confirm that the work presented in this thesis is my own. Where information has been derived from other sources, I confirm that this has been indicated in the thesis.

Abstract

Through the use of a knockout mouse line, we have identified flavin-containing monooxygenase 5 (FMO5) as a regulator of energy homeostasis. The characterisation of the FMO5 knockout (FMO5 KO) phenotype reveals the mutant animals are resistant to age-related and diet-induced weight gain when compared to age-matched wild-type (WT) controls. The FMO5 KO mice exhibit higher insulin sensitivity and need lower circulating insulin to maintain normal glycaemia. The knockout mice are also more responsive to an exogenous dose of insulin and they do not gain weight when fed a high fat diet.

FMO5 is expressed in the murine digestive tract of WT animals and is further induced in high-fat feeding. Investigations into the intestine of the knockout animal reveal differences in the intestinal microbiota and a different processing of a colonic hormone, RELM β . This hormone is involved in intestinal inflammation and less was detected in circulation of the knockout mouse. Furthermore, lower levels of circulating cytokine TNF α was detected and inflammation of adipose tissue, peripheral to the intestine, was found to be lower in the knockout mice.

The findings implicate FMO5 to be a modulator of the intestinal environment and an mediator of inflammation. By influencing the processing of RELM β , the protein contributes to the systemic inflammatory profile of the animal. Reduced inflammation of sites such as adipose tissue in the absence of the protein correlates with higher insulin sensitivity and a leaner animal.

Acknowledgements

First and foremost I would like to thank Professor Elizabeth Shephard. Your guidance and encouragement has enabled me to succeed as a scientist and also as an individual. You have taught me so many lessons and your mentorship has led me in an exciting path of research and an even more insightful time of personal development. I will forever be grateful for the wisdom and attributes you have instilled in me and never forget my time working with you. It has been a real pleasure, thank you.

I am also indebted to my mum and dad. Your love and support has given me the strength to embark on everything I have done. You have paved the way for all of my achievements with your unshakable support, your confidence in me and our extraordinary friendship. I also thank my brothers and sisters, Tom, Holly, Matty and Clare. Having you all by my side has been wonderful in times of celebration and even more so in times of desperation. And to Keval; the honorary Scott, I owe my sanity. Your unfathomable support has kept me upright over the last four years and your friendship has kept me smiling throughout. Thank you all, I couldn't have got to here without you.

I also thank my secondary supervisors; Professor Ivan Gout and Dr Joanne Santini, and Professor Ian Phillips for their guidance in the project. I am additionally grateful for the founts of knowledge named Dr Sunil Veeravalli, Dr Yugo Tsuchiya and Dr Anoop Kumar. Your support and extensive discussions through troublesome experiments have stifled tears and got me to the results, thank you. I also thank Dr Max Yun and Phillip Gates for their experimental expertise and aid in investigations.

I must also credit the brilliant students who have participated in the research presented in this thesis; Simina Istrate, George Featherstone, Jim Leng, Tim Hwong Kung, Diede Fennema and in particular Brett O'Brien and Clarissa Coveney. In given the task of teaching you, I have learnt a great deal from each one of you, thank you. I have also been very lucky to share the last four years with some incredible friends, in particular I would like to mention (the now Dr) Liz Rodriguez. Your hand in diffusing scientific and personal meltdowns has been fundamental in keeping me together, thank you. Lastly, thank you Michael, Ian and Rob for never failing to brighten my day!

Table of Contents

Chapter 1: Introduction	12
1.1 FLAVIN CONTAINING MONOOXYGENASES.....	13
1.1.1 Catalysis	14
1.1.2 FMO1	17
1.1.3 FMO2	17
1.1.4 FMO3	18
1.1.5 FMO4	19
1.1.6 FMO5	19
1.1.7 An Endogenous Role of the FMOs	20
1.1.8 FMO5 as an Atypical FMO.....	22
1.2 INTESTINAL BACTERIA	24
1.2.1 Development and Ageing.....	25
1.2.2 Energy Homeostasis.....	26
1.2.3 Dysbioses in Disorders.....	27
1.2.4 Host Genetics	28
1.3 GENERAL AIMS OF THE PROJECT	30
Chapter 2: Materials and Methods	31
2.1 ANIMAL HUSBANDRY	32
2.1.1 Mice.....	32
2.1.2 Blood Collection	32
2.1.3 High-Fat Feeding.....	32
2.1.4 Antibiotic Treatment	33
2.1.5 Faecal Sample Collection.....	33
2.1.6 Glucose Tolerance Test.....	34
2.1.7 Insulin Sensitivity Test.....	35
2.1.8 Tissue Insulin Sensitivity Test	36
2.1.9 Animal Dissection and Tissue Collection	36
2.2 PLASMA MEASUREMENTS AND BIOCHEMICAL ANALYSES	38
2.2.1 Glucose.....	38
2.2.2 Insulin.....	38
2.2.3 Lipopolysaccharide (LPS).....	38
2.2.4 Resistin Like Molecule β (RELM β).....	39

2.2.5	Tumour Necrosis Factor α (TNF α)	39
2.2.6	Lipid Profiling	39
2.3	INTESTINAL MICROBIOTA ANALYSIS	40
2.3.1	Isolation of Faecal DNA.....	40
2.3.2	Selection of Primers	40
2.3.3	Polymerase Chain Reaction (PCR) Amplification of 16S rRNA Gene Sequences	41
2.3.4	Ligation of 16S rRNA Gene Sequences.....	41
2.3.5	Preparation of Chemically Competent Cells	41
2.3.6	Transformation of Chemically Competent Cells.....	42
2.3.7	Preparation of Electrocompetent Cells.....	42
2.3.8	Transformation of Electrocompetent Cells	43
2.3.9	Selection of Successful Transformants	43
2.3.10	Phylogeny Classification.....	45
2.4	WESTERN BLOT ANALYSIS.....	46
2.4.1	Sample Collection Protein Isolation.....	46
2.4.2	Protein Precipitation.....	48
2.4.3	Protein Determination by BCA assay	48
2.4.4	Protein Determination by Coomassie Protein Assay	49
2.4.5	Sample Preparation for Electrophoresis	49
2.4.6	Electrophoresis	50
2.4.7	Protein Transfer.....	50
2.4.8	Blocking of the Membrane.....	51
2.4.9	Incubation with Primary Antibody.....	52
2.4.10	Incubations with Secondary Antibody	53
2.4.11	Detection Methods	54
2.5	HISTOLOGY AND IMMUNOHISTOCHEMISTRY	55
2.5.1	Embedding and Cutting.....	55
2.5.2	Hematoxylin and Eosin Staining.....	55
2.5.3	Alcian Blue Staining	55
2.5.4	Immunohistochemistry.....	55
2.5.5	Slide Scanning.....	56
2.5.6	Goblet Cell Quantification	56
2.6	STATISICAL ANALYSIS.....	57

Chapter 3: The FMO5 KO Mouse	58
3.1 INTRODUCTION.....	59
3.1.1 Mouse Knockout Models	59
3.1.2 The FMO5 Knockout Mouse	60
3.2 EXPERIMENTAL QUESTIONS AND AIMS.....	66
3.3 RESULTS.....	67
3.3.1 The Glucose Phenotype of the FMO5 KO mice in Ageing	67
3.3.2 The FMO5 KO Animal is Resistant to High-fat Diet Induced Weight Gain	74
3.3.3 The Effect of an Antibiotic Treatment in the WT and FMO5 KO Animal	82
3.4 CONCLUSIONS.....	86
 Chapter 4 – The Intestine and the Commensal Microbiota.....	 87
4.1 INTRODUCTION.....	88
4.1.1 Intestinal Epithelial Cells	88
4.1.2 The Intestinal Microbiota	89
4.1.3 Goblet Cells.....	91
4.1.4 Resistin Like Molecule β	93
4.2 EXPERIMENTAL QUESTIONS AND AIMS.....	102
4.3 RESULTS.....	103
4.3.1 A Perturbed Intestinal Microbiota in the FMO5 KO Animal	103
4.3.2 The Response of the Intestinal Microbiota To High-Fat Feeding.....	107
4.3.3 FMO5 is Expressed in the Murine Digestive Tract.....	112
4.3.4 No Gross Morphological Differences in the WT and FMO5 KO Digestive Tract.....	117
4.3.5 FMO5 Expression is Induced in Response to the High-Fat Diet	120
4.3.6 A Disparity in RELM β Expression in the WT and FMO5 KO Animal	121
4.3.7 RELM β Expression is Induced in Response to the High-Fat Diet.....	125
4.3.8 A difference in Colonic Goblet Cells in the FMO5 KO Animal.....	127
4.3.9 RELM β and FMO5 Expression Following Antibiotic Treatment	132
4.4 CONCLUSIONS.....	134

Chapter 5 - Low-grade Inflammation in Metabolic Disorders.....	135
5.1 INTRODUCTION.....	136
5.1.1 Inflammation and Metabolism	136
5.1.2 Adipose Tissue	137
5.1.3 Inflammation and Insulin Signaling.....	139
5.1.4 The Intestine and Metabolic Endotoxaemia.....	143
5.1.5 Complement Component 3.....	146
5.2 EXPERIMENTAL QUESTIONS AND AIMS.....	148
5.3 RESULTS.....	149
5.3.1 Adipose tissue C3 expression is reduced in the FMO5 KO Mouse	149
5.3.2 FMO5 KO Adipose Tissue is more Insulin Sensitive	150
5.3.3 Plasma Endotoxin Measurement.....	152
5.3.4 Difference in Plasma RELM β in the WT and FMO5 KO Animal.....	153
5.3.5 Changes in Circulating TNF α in the WT and FMO5 KO Animal.....	155
5.4 CONCLUSIONS.....	157
Chapter 6 - Discussion.....	159
6.1 Summary	160
6.2 Mechanism	163
6.3 The FMO5 KO Mouse	164
6.4 Conclusions and Future Work	166
7. Appendix	167
9. List of Abbreviations.....	169
8. References	172

List of Figures

Chapter 1 – Introduction

- Figure 1.1- The catalytic cycle of an FMO 15
- Figure 1.2 - Proposed short-circuiting of the FMO catalytic cycle 21

Chapter 2 – Materials and Methods

- Figure 2.1 – pGEMT vector 44

Chapter 3 – The FMO5 KO Mouse

- Figure 3.1 – Generation of the FMO5 KO mouse 61
- Figure 3.2 – Difference in age-related weight gain 62
- Figure 3.3 – Differences in plasma glucose at 15 and 30 weeks 63
- Figure 3.4 – Plasma cholesterol measurements of 15-week old mice 64
- Figure 3.5 – Glucose tolerance of 15- and 30- week old animals 68
- Figure 3.6 – Plasma insulin of 15- and 30-week old animals 69
- Figure 3.7 – Insulin sensitivity of 10-week old animals 70
- Figure 3.8 – Plasma measurements of 10-week old mice 71
- Figure 3.9 – Body weight measurements of mice fed standard chow or a high-fat diet 74
- Figure 3.10 – Plasma glucose of mice fed a standard chow or high-fat diet 75
- Figure 3.11 – Glucose tolerance of animals fed a standard chow or high-fat diet 77
- Figure 3.12 – Plasma insulin of animals fed standard chow or a high-fat diet 78
- Figure 3.13 – Plasma cholesterol measurements of animals fed a standard chow or high-fat diet 80
- Figure 3.14 – Plasma glucose of control and antibiotic treated animals 83
- Figure 3.15 – Glucose tolerance of control and antibiotic treated animals 84
- Figure 3.16 – Plasma insulin of control and antibiotic treated (AB) animals 85

Chapter 4 – The Intestine and the Commensal Microbiota

Figure 4.1 – Phyla level analysis of the intestinal microbiota of 7-week, 10-week and 30-week old WT and FMO5 KO mice	104
Figure 4.2 – Phyla level analysis of the intestinal microbiota of 30-week WT and FMO5 KO mice fed a standard chow or a high fat diet	108
Figure 4.3 – FMO5 expression in the murine digestive tract	112
Figure 4.4 – Immunohistochemical detection of FMO5 in stomach mucosa	113
Figure 4.5 – Immunohistochemical detection of FMO5 in small intestine mucosa	114
Figure 4.6 – Immunohistochemical detection of FMO5 in mucosal crypts of the colon	116
Figure 4.7 – Gross morphology of WT and FMO5 KO stomach	117
Figure 4.8 – Gross morphology of WT and FMO5 KO small intestine	118
Figure 4.9 – Gross morphology of WT and FMO5 KO colon	119
Figure 4.10 – Faecal FMO5 expression following high fat feeding	120
Figure 4.11 – Expression of RELM β in colon contents of WT and FMO5 KO animals	121
Figure 4.12 – Goblet cell expression of RELM β in WT and FMO5 KO colon	123
Figure 4.13 – Faecal expression of RELM β in the WT and FMO5 KO mouse	124
Figure 4.14 – Faecal RELM β expression following high fat feeding	125
Figure 4.15 – Goblet cell staining of WT and FMO5 KO colonic mucosa	128
Figure 4.16 – Measurement of colon crypt length in WT and FMO5 KO mice	129
Figure 4.17 – Goblet cell quantification in WT and FMO5 KO colonic crypts	129
Figure 4.18 – Goblet cell number normalised to colon crypt length in WT and FMO5 KO mice	130
Figure 4.19 – Faecal RELM β expression following antibiotic treatment	132
Figure 4.20 – Faecal FMO5 expression following antibiotic treatment	133

Chapter 5 – Low-grade Inflammation in Metabolic Disorders

Figure 5.1 – Adipose tissue levels of complement component 3 in the WT and FMO5 KO animal	149
Figure 5.2 – Adipose tissue insulin sensitivity measurement in WT and FMO5 KO animals	150
Figure 5.3 – Plasma endotoxin levels in the WT and FMO5 KO animal	152
Figure 5.4 – Plasma levels of RELM β in the WT and FMO5 KO animal	153
Figure 5.5 – Plasma levels of RELM β in WT and FMO5 KO mice fed a high fat diet	154
Figure 5.6 – Plasma levels of TNF α in control and antibiotic treated WT and FMO5 KO mice	155

List of Tables

Table 4.1 – Phyla level analysis of the intestinal microbiota of 7-week, 10-week and 30-week old WT and FMO5 KO mice	104
Table 4.2 – Family level analysis of the intestinal bacteria of 7-week, 10-week and 30-week old WT and FMO5 KO mice	106
Table 4.3 – Phyla level analysis of the intestinal microbiota of 30-week old WT and FMO5 KO mice fed standard chow or a high fat	108
Table 4.4 – Family level analysis of the intestinal bacteria of 30-week old WT and FMO5 KO mice fed standard chow or a high fat diet	109
Table 5.1 – Plasma levels of RELM β in WT and FMO5 KO mice fed standard chow or a high fat diet	155

Chapter 1: Introduction

The investigations presented in this thesis are regarding flavin-containing monooxygenase 5. This chapter will briefly introduce the members of the flavin-containing monooxygenase gene family and discuss their role in endogenous, as well as xenobiotic metabolism. Experiments described in following chapters were conducted to characterise the phenotype of the flavin-containing monooxygenase 5 knockout mouse (FMO5 KO) in comparison to the wild-type (WT). One of the most striking phenotypes of the FMO5 KO is an attenuation in age-related weight gain. The recent proposal of the intestinal microbiota as an integral entity of the host, capable of modulating energy storage, led us to consider this population in the WT and FMO5 KO. The commensal bacteria of the intestine and its involvement in the host phenotype will therefore also be discussed in this chapter.

1.1 FLAVIN CONTAINING MONOOXYGENASES

Xenobiotic metabolism is a critical function of any living organism. Metabolism of foreign compounds, such as therapeutic drugs, pesticides and dietary constituents, ensures the elimination of non-nutritional or potentially toxic agents. Second to cytochrome P450s (CYPs), the flavin-containing monooxygenases (FMOs) play a fundamental role in the Phase I processing of such foreign chemicals. The FMOs are present in the endoplasmic reticulum (ER) membrane of several different tissues and catalyse the oxidation of nucleophilic nitrogen-, sulfur-, selenium- and phosphorous-containing compounds. Generally, the oxygenated product is less toxic or pharmacologically active and the modification facilitates further processing (Phase II) or elimination of the parent compound. In 1971 Zeigler purified the first FMO from porcine liver microsomes (Ziegler and Mitchell, 1972). Shortly after, two groups independently isolated an FMO from rabbit lung microsomes that was distinct to the hepatic form in activity and physical stability (Williams et al., 1984; Tynes et al., 1985). This was evidence for the existence of multiple forms of FMOs and since, a further three additional isoforms have been identified. The proteins were named, in order of their identification, FMO1-5 (Lawton and Philpot, 1993).

In humans there are 11 *FMO* genes, five of which encode the functional proteins FMO1-5. Human FMOs 1-5 share 51-57% sequence identity and FMOs isolated

from other mammals have >80% sequence identity to their human orthologues (Phillips et al., 1995). All five genes are located on chromosome 1. *FMOs 1-4* are contained within a cluster in the region q24.3, also containing a pseudogene (*FMO6p*). *FMO5* however, is not part of this cluster, and lies closer to the centromere in region 1q21.1. Another cluster consisting of five additional pseudogenes (*FMO7p to 11p*) has also been identified on chromosome 1. The gene family is thought to be a result of several gene duplications estimated to have occurred over 200 million years ago, long before the divergence of mammals from their common ancestor 85 million years ago. We can therefore predict the five functional *FMO* genes *FMO1-5* are common among all mammals (Hernandez et al., 2004; Phillips et al., 2007). Like humans, out of the nine members of the *Fmo* gene family in mice, only *Fmo1* through 5 produce functional protein products. Similarly, *Fmo1*, 2, 3, and 4 are clustered together on chromosome 1 whereas *Fmo5* is located separately on chromosome 3 (Hernandez et al., 2004).

1.1.1 Catalysis

No crystal structure has been obtained for mammalian FMOs, however information can be inferred from the crystal structure of the yeast FMO (Eswaramoorthy et al., 2006). The *Schizosaccharomyces pombe* wild-type FMO has been crystallised, along with the protein-cofactor and protein-substrate complexes. Structures however reveal the cytosolic yeast protein has a mechanism distinct to that of the mammalian FMOs. From kinetic evidence, the mechanism of action of mammalian and bacterial FMOs instead seems very similar (Ziegler, 2002). Using NADPH and FAD, FMOs oxygenate a soft nucleophile (Figure 1.1).

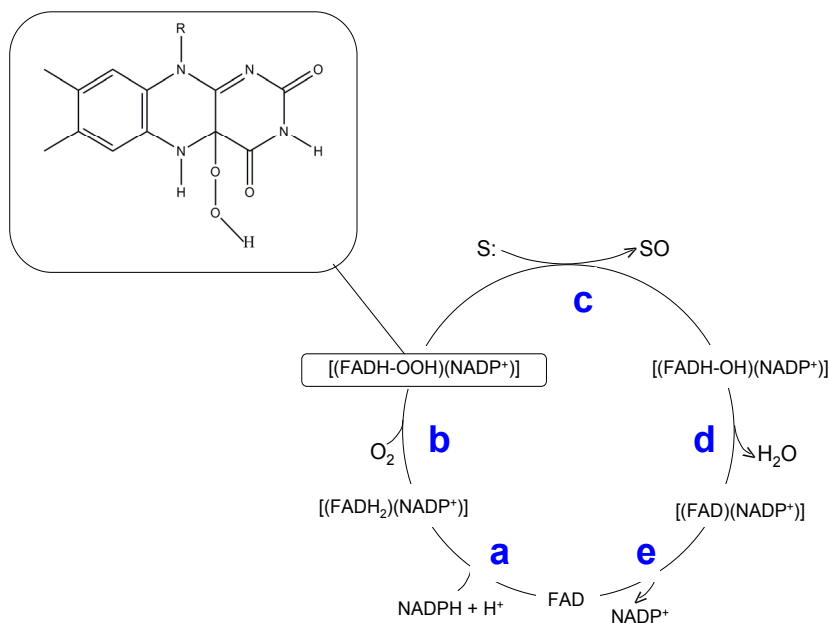


Figure 1.1- The catalytic cycle of an FMO. FAD is reduced after the association of NADPH (a). Upon the addition of molecular oxygen, a hydroperoxyflavin (FADH-OOH) is formed (b). Nucleophilic attack from the distal O atom of the hydroperoxyflavin (shown inset) results in the oxygenation of the parent compound S (c). Water is then released from the hydroxyflavin (d) reforming FAD and, finally NADP⁺ is released (e). Figure adapted with permission from Phillips, I. R., & Shephard, E. A. (2008). Flavin-containing monooxygenases: mutations, disease and drug response. *Trends in Pharmacological Sciences*, 29(6), 294–301.

The catalytic cycle begins with the association of NADPH and the reduction of FAD to FADH₂ (Figure 1.1-a). Upon the addition of molecular oxygen (Figure 1.1-b), a hydroperoxyflavin is formed (shown inset). Even in the absence of substrate, this complex is stable and is believed to be the most predominant form of the enzyme in the cell. Contact with a substrate (S) containing a soft nucleophile results in nucleophilic attack of the distal oxygen atom of the hydroperoxyflavin and oxygenation of the parent compound (Figure 1.1-c). Water is then released from the hydroxyflavin, regenerating FAD (Figure 1.1-d) and finally NADP⁺ is released (figure 1-e) (Krueger and Williams, 2005; Phillips et al., 2007; Testa and Krämer, 2007).

The unique property of this catalysis, with respect to most other enzymes that use oxygen, is the ability of FMOs to activate molecular oxygen in the absence of substrate. The 'loaded gun' nature of the FMOs is thought to explain the broad substrate range of the family; the determining factor for substrate specificity therefore being the substrate's ability to access the active site (Ziegler, 2002; Zhang et al., 2007). Using tertiary amine substrates, with carbon chains of varying length, Zhang et al. showed catalysis of FMO1 was independent of chain length, suggesting the hydroperoxyflavin of this isoform is easily accessed by the substrate. Catalysis by FMO3, and more so FMO5, was however dependent on the aliphatic chain length. FMO5 was proposed to have a much deeper active site, requiring a chain of at least 5 carbon atoms to deliver the soft nucleophile for catalysis (Zhang et al., 2007).

More recently investigations have also proposed certain mammalian FMOs can mediate catalysis in a mechanism distinct to the other family members. Baeyer-Villiger monooxygenases, another group of flavin-containing enzymes, convert a ketone group to its corresponding ester using dioxygen and NAD(P)H. Similar to the catalysis described above, an intermediate hydroperoxyflavin is formed, which mediates substrate oxygenation (Fraaije et al., 2002). FMO1 was initially found to catalyse the Baeyer-Villiger oxidation of salicylaldehyde to pycrocatechol (Chen et al., 1995) and more recently Lai et al. have shown specifically FMO5 is able to perform Baeyer-Villiger catalysis of a potential anti-cancer therapeutic (Lai et al., 2011). Taken together with several other factors discussed below, we suggest FMO1 and, in particular, FMO5 may behave as atypical FMOs.

Although the substrate specificities of the isoforms overlap (Krueger and Williams, 2005), the FMOs exhibit distinct developmental and tissue-specific patterns of expression. Each isoform will be briefly introduced.

1.1.2 *FMO1*

FMO1 has the widest range of substrates of the FMO family. Although expressed in several organs, its main site of expression in humans is the kidney (Krueger and Williams, 2005; Zhang and Cashman, 2005). In most other mammals studied, FMO1 is one of the most prominent enzymes of the liver, however the *FMO1* gene is silenced shortly after birth in humans (Dolphin et al., 1991; Koukouritaki et al., 2002). This is in contrast to the kidney, where gene expression increases after birth (Phillips et al., 1995; Krause et al., 2003) and the amount of FMO1 protein exceeds the total concentration of renal CYPs (Shephard and Phillips, 2010). This indicates the prominent role for FMO1 in human renal metabolism of drugs.

Five nonsynonymous single nucleotide polymorphisms of *FMO1* have been identified, however these mutations happen at a very low frequency in a discrete number of populations (Phillips et al., 2007). FMO1 mRNA has however been shown to be dysregulated in certain pathologies. *FMO1* expression is up regulated in tissue samples from patients suffering with atrial fibrillation, an arrhythmia thought to be caused by oxidative stress (Kim et al., 2003). FMO1 mRNA was also originally reported to be downregulated in the spinal cord in amyotrophic lateral sclerosis (ALS); a neuro-muscular disorder caused by the continuous loss of spinal cord, brain stem and motor cortex neurons (Malaspina et al., 2001). However, using a mouse model for ALS, Gagliardi et al. went on to report FMO1 mRNA was contrastingly up regulated in diseased spinal cord (Gagliardi et al., 2010). The ALS mediated increase in FMO1 mRNA was however gender dependent, occurring specifically in males, which may explain the disagreement with Malaspina et al. The role of FMO1 in the development of atrial fibrillation and ALS remains unclear, however Gagliardi et al. propose the induction of *Fmo1* expression may be in response to the increase in oxidative stress, which is characteristic of both pathologies.

1.1.3 *FMO2*

In humans and most mammals the main site of FMO2 expression is the lung, where it is the most prominent enzyme of this tissue. In humans, the protein is however mostly non-functional due to a nonsense mutation contained within an allele (*FMO2**2). Most humans are homozygous for *FMO2**2, however the ancestral allele

(*FMO2*1*), which produces the full-length functional protein, has been identified in African American individuals (Dolphin et al., 1998). In fact, it is estimated that around 220 million individuals in Africa express functional FMO2 (Veeramah et al., 2008). This has implications when considering the bioactivation functionality of the enzyme. For example, thiourea and its derivatives undergo S-oxygenation catalysed by FMO2, resulting in exposure of the individual to more toxic metabolites. Recent investigations have identified that FMO2 indeed oxygenates two anti-tubercular drugs, thiacetazone and ethionamide, producing harmful metabolites and reducing the amount of the available prodrug (Francois et al., 2009). Therefore, great consideration should be taken in the prescription and distribution of therapeutics in Africa, which are a substrate for FMO2 mediated metabolism (Phillips et al., 2007; Veeramah et al., 2008).

1.1.4 FMO3

Alongside FMO1, FMO3 is one of the most important FMOs in human xenobiotic metabolism. Gene expression is switched on after birth in the liver, where FMO3 reaches concentrations close to that of the most prominent hepatic CYPs (Koukouritaki et al., 2002; Phillips et al., 2007). Whereas birth appears necessary to induce the repression of *FMO1* in the liver (described above) induction of *FMO3* is not as tightly linked to birth; the age at which expression is switched on varies from birth to two years of age. The resultant possible absence of a hepatic FMO in the first years of life diminishes the ability of the organism to metabolise therapeutic drugs. Hence, further examination of this temporal switch is required to understand the toxicology and efficacy of certain paediatric therapies. Post puberty, FMO3 is not expressed in specifically the male mouse liver (Cherrington et al., 1998), hence the adult male mouse is a natural hepatic FMO3 knockout model.

The *FMO3* gene has gained interest in light of the disease trimethylaminuria (TMAU) being attributed to polymorphisms of *FMO3* (Dolphin et al., 1997). Distinct to the other family members, *FMO3* is highly polymorphic. Loss of function mutations within the gene abolishes the ability of an individual to *N*-oxygenate the odorous dietary-derived trimethylamine (TMA) to its non-odorous *N*-oxide. TMA is instead secreted in the breath, sweat and urine of the affected individual and the disease

manifests as an unpleasant smell, similar to that of rotting fish (Mitchell and Smith, 2001). Little can be done to treat sufferers, however microbial intervention targeting intestinal flora that produces TMA has been recommended. In addition, a diet restricted in TMA precursors, i.e. choline and lecithin, has been shown to help (Phillips et al., 2007).

It is also expected that patients diagnosed with TMAU will have an altered response to therapeutics that are substrates of FMO3. This is indeed the case in treatment of familial adenomatous polyposis with the pro-drug sulindac. Inactivation of sulindac is, in part, catalysed by FMO3, and individuals possessing loss of function variants of *FMO3* had a better response to sulindac treatment (Hisamuddin et al., 2005).

1.1.5 *FMO4*

FMO4 mRNA is found in the liver and kidney amongst many other human tissues, however protein expression levels are comparatively low. Little is known about the enzymes substrate specificity, due to the instability of the protein preventing functional studies (Hernandez et al., 2004; Zhang and Cashman, 2005).

1.1.6 *FMO5*

Like FMO4, little is known about the substrate specificity of FMO5. However, unlike FMO4, FMO5 is highly expressed in certain tissues making it a more intriguing isoform. *FMO5* expression has been reported in both mouse and human liver. It was found to be the most predominant isoform in mouse liver and expression in humans nearly equaled that of *FMO3*, which was previously thought to be the most important hepatic FMO (Janmohamed et al., 2004; Zhang and Cashman, 2005). FMO5 mRNA is also the most prevalent of the *FMO* genes in the small intestine and is expressed in other human tissues including brain and skin, albeit at much lower levels than the liver (Janmohamed et al., 2001; Zhang and Cashman, 2005). The consideration of FMO5 as an unusual FMO will be discussed further.

1.1.7 An Endogenous Role of the FMOs

As well as a role in the metabolism of xenobiotics, it is possible the enzyme family also serves a physiological role. The FMOs are not normally induced by environmental factors and genetic factors are thought to be responsible for the inter-individual variations reported. Genetic variations are however very rare, often isolated to a single population and at a very low frequency. The very few nonsynonymous mutations found, in particular of *FMO1* and *FMO5*, suggests a potential endogenous role of these FMOs (Furnes et al., 2003; Sevasti B Koukouritaki, 2005; Motika et al., 2007).

In addition to the few diseases described above, an association with the FMOs and diabetes has also been recorded. Studies show streptozocin-mediated insulin deficient and, to a lesser extent, congenitally insulin resistant animals have higher hepatic FMO activity (Rouer et al., 1988; Borbás et al., 2006). Conversely, *FMO5* expression was found to be downregulated in livers of type 2 diabetic patients (Takamura et al., 2004). Functional information is however sparse and although insightful, the changes identified in the disease states do not clarify whether FMO modification is a cause or consequence of disease pathogenesis. Regardless, it is evidence for changes in FMO expression and activity in disturbances of endogenous metabolism.

Furthermore, although rare, some endogenous compounds have been identified as FMO substrates. As described previously, specifically FMO3 metabolises dietary-derived trimethylamine. Methionine (Duescher et al., 1994), cysteine-s-conjugates (Sausen and Elfarra, 1990) and lipoic acid (Krueger and Williams, 2005) have also been recognised as targets of FMO mediated oxidation, however the physiological relevance of these catalyses remains unknown. More interestingly, hepatic microsomes have shown FMOs to be capable of oxidizing cysteamine to cystamine. Cystamine is a powerful thiol oxidant, critical for the formation of disulphide bonds and correct protein assembly. Along with its known location on the ER membrane, Poulsen et al. therefore proposed the FMOs to be implicated in the folding of nascent proteins by influencing the local oxidising environment (Poulsen and Ziegler, 1977). Indeed in the case of yeast, where there is only one FMO, an FMO knockout strain was defective in the active expression of specifically ER proteins containing disulphide bonds. It is clear the lone cytosolic FMO in yeast is a fundamental part of

the redox machinery, as the knockout was also unable to grow in the presence of reducing agents (Suh et al., 1999). Therefore, it is possible FMOs may function in a general endogenous capacity by regulating the thiol:disulphide ratio.

Most recently, a potential ‘short-circuiting’ of the catalytic cycle has been reported of the FMOs. Normally, a soft nucleophile that can gain access will react with the hydroperoxyflavin. However, another uncoupled function of the enzyme exists. Instead of oxygenating a substrate, an FMO can also oxidise NADPH, generating a superoxide anion or H_2O_2 (figure 1.2-x). This has been shown for FMO1, 2 and 4 and is surprisingly accelerated in the presence of a substrate (Siddens et al., 2014). Considering the ‘loaded gun’ nature of an FMO, i.e. the predominant form of the enzyme is the C4a hydroperoxyflavin; this continual cycling and generation of reactive oxygen species (ROS) may be physiologically relevant. Therefore, in addition to potentially influencing the oxidising environment of a cell, FMOs may also contribute to the production of ROS, which are now regarded as functional signaling molecules themselves (Neish, 2009).

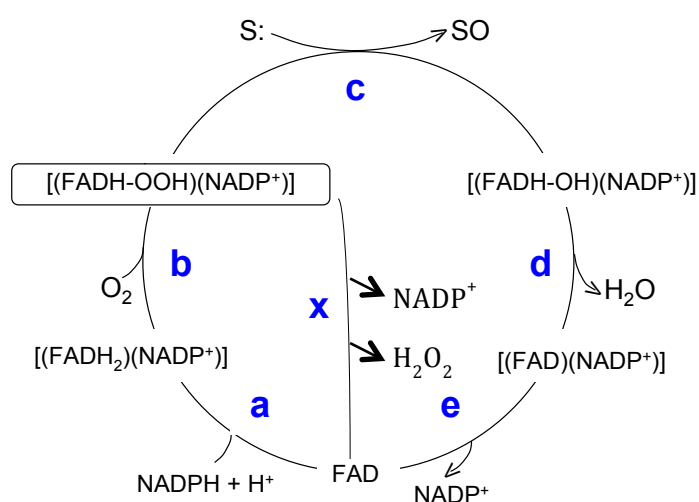


Figure 1.2 - Proposed short-circuiting of the FMO catalytic cycle. Association of NADPH and the reduction of FAD (a) followed by the addition of molecular oxygen results in the formation of the hydroperoxyflavin (b). Instead of the oxygenation of a substrate (c) and release of H_2O (d) oxidised NADPH (NADP^+) and a H_2O_2 molecule is released (x).

1.1.8 FMO5 as an Atypical FMO

FMO5 is an isoform that has gained a particular amount of attention as an atypical FMO. As described previously, regardless of its pervasive expression, very little is known about the isoform's function and substrate specificity and a role is yet to be defined for the enzyme in xenobiotic metabolism (Phillips et al., 2007). FMO5 shows no catalytic activity towards known FMO substrates trimethylamine (Lang et al., 1998), methimazole (Overby et al., 1995) and benzydamine (Lang and Rettie, 2000). Tertiary amine containing 5-DPT and 8-DPT are substrates for FMO5, although catalytic activity was much higher in the other isoforms FMO1 and 3 (Zhang et al., 2007). S-methyl-esonarimod is also an FMO5 substrate in both humans and mice (Ohmi et al., 2003; Zhang et al., 2007).

Along with its substrate profile, FMO5 also differs from the other FMOs in physical properties such as thermal and pH stability (Krueger and Williams, 2005; Zhang et al., 2007) and protein expression further separates the isoform from its family members. It is inducible; in cellular assays, FMO5 was induced following treatment with hyperforin (Krusekopf and Roots, 2005), a progesterone analogue (Miller et al., 1997) and rifampin (Rae et al., 2001), and large interindividual differences are reported (Overby et al., 1997). Additionally, in contrast to other isoforms, hepatic FMO5 is not influenced by gender. Cherrington et al. reported higher FMO1 activity in females and FMO3 is exclusively expressed in the female mouse, whereas FMO5 expression is gender independent.

Most intriguingly, FMO5 is also found to behave distinctly to the other isoforms in particular models of intestinal inflammation. During murine infection with *Citrobacter rodentium*; a model of human enteropathogenic *Escherichia coli* infection that results in intestinal inflammation, unlike the reduced expression of the other *Fmos*, the level of hepatic *Fmo5* mRNA was unchanged. Characterisation of hepatic *Fmo* expression was further investigated in a mouse line lacking toll like receptor 4 (HeJ). Dextran sodium sulphate treatment (a chemical model of colonic inflammation) in HeJ mice specifically induces *Fmo5* expression. Induction of *Fmo5* suggests a specific role of the isoform in the stress response to this extreme model of intestinal injury. LPS treatment resulted in downregulation of *Fmos 1, 3* and *5*, however, unlike the other orally delivered agents, LPS was injected intraperitoneally

(Zhang et al., 2009). This is evidence for the FMO5 isoform being differentially regulated by inflammatory mediators of the intestine and, in corroboration with all other observed characteristics, warrants further investigation of this atypical FMO.

Due to the lack of specific inhibitors, and the inefficiency of antibody-mediated catalytic inhibition, the further characterisation of FMOs requires the utilization of mouse knockout models (Shephard and Phillips, 2010). Specific FMO mouse knockout models have been used to clarify the participation of particular isoforms in xenobiotic metabolism (Hernandez et al., 2009) and, in further investigations, have also highlighted a potential endogenous role of isoforms FMO1 and 5 (Veeravalli et al., 2014; Gonzalez Malagon et al., unpublished). This will be further discussed in chapter 3.

1.2 INTESTINAL BACTERIA

A vast array of bacteria colonises the human gastrointestinal tract. With over a 100 trillion microorganisms present, it is one of the most extensively populated microbial communities on earth (Ley et al., 2006a). It is estimated the collection of microbes is comprised of more than 400 bacterial species, the number of microbial cells exceeding that of total human cells in the body (Palmer et al., 2007). Within this community, only 8 of the known 55 bacterial divisions are represented and the composition is strongly dominated by two phyla; Bacteroidetes and Firmicutes (Bäckhed et al., 2005; Ley et al., 2006a; Krajmalnik-Brown et al., 2012). The collective genomes of the bacteria residing in the gut, the microbiome, contain more genes than that of the host and therefore can be considered as an integral entity of the human body; a supplement which is now known to be essential for human health. The collection of microorganisms has coevolved with the host, resulting in the specialisation of energy harvest from the available sources (the host diet) alongside the adaptation of the host to utilise such products (Neish, 2009; Burcelin et al., 2011). Amongst many proposed roles, the microbiome functions to complement the host genome in protection against pathogens, the production of vitamins and co-factors and the catabolism of dietary components which are resistant to host-mediated digestion (Palmer et al., 2007; Zoetendal et al., 2008; Neish, 2009; Thomas et al., 2011).

Even though there are extensive inter-individual differences in the microbial populations of the gut, it has been speculated that there is an essential core at the functional (i.e. gene) level. Despite the dynamic property of the community, with external factors such as diet having a dramatic effect on composition, the microbial population is thought to be relatively stable at the phyla level in healthy individuals (Palmer et al., 2007; Thomas et al., 2011; Walker et al., 2011). Although variation at the species level has been observed, a cross continent study of individuals from four countries only identified three enterotypes. These three classifications of the microbiota, which differ in routes of energy harvest related to the available substrates in the colon, do not appear to be nation or continent specific (Arumugam et al., 2011). This further demonstrates the presence of a 'functional core' of the microbiota, with a distinct number of stable host-microbial symbiotic states.

1.2.1 Development and Ageing

At birth, the gastrointestinal (GI) tract is free from bacteria, however after delivery colonisation begins and progresses dependent on functional requirement. It is thought that the infant gut microbiota is a very simple community, predominately composed of *Lactobacillus* and *Bifidobacteria* species. This is thought to be due, but not restricted, to the ability of these genera to digest human milk (Koropatkin et al., 2012). Given a more sophisticated requirement of the microbiota by the host, and hence competition therein, a more diverse population develops. Within the first two years of life a more complex ‘adult-like’ environment is established (Palmer et al., 2007; Angelakis et al., 2012). For instance, with the introduction of more complex components of the diet (cereals, fruits, vegetables etc.) organisms which metabolise the resultant glycans will prevail, namely the Bacteroidetes, Firmicutes and Actinobacteria phyla (Koropatkin et al., 2012).

Although the establishment of the microbiota has received a lot of attention, little is known about the changes in the population with the progression of age in later life. It is now well understood that the microbiota has a substantial role in the health of the host, providing nutrients and protection from pathogens (Neish, 2009). A hypothesis that has recently therefore emerged, is that an age-related change in composition of the gut microbiota may be responsible for a decline in the well-being of an individual and perhaps progression of disease (Biagi et al., 2010). Limited investigations into this question have, however produced conflicting results with respect to the ratio of the two most dominant phyla in the gut, Firmicutes to Bacteroidetes (F:B). F:B has been reported to increase (Mariat et al., 2009), decrease (Marathe et al., 2012) or remain stable with age (Biagi et al., 2010). This phenomenon may be due to the varying origins of the individuals sampled or, in fact be dependent on the method of analysis used. In a more detailed analysis of lower taxonomy levels however, significant differences were found in samples of the most aged individuals. This group had a lower abundance of *Bifidobacteria* species and members of the clostridia class, both groups are thought to be beneficial in the health status of an individual. These changes correlated with a more inflamed status of the individual (Biagi et al., 2010) and several other studies are in agreement with this trend, perhaps highlighting a new aspect of the gut microbiota (Hopkins et al., 2001; Mariat et al., 2009). Many elderly people are receiving antibiotic treatment that, with an already perturbed gut

microbiota, may have deleterious effects. This therefore presents a definitive time in which pre and probiotics should be considered to promote beneficial bacteria residing in the gut, with the aim of conferring advantageous health consequences.

1.2.2 Energy Homeostasis

The significance of the microbiota in host energy homeostasis is simplistically illustrated in the comparison of animals raised in the absence of any microorganisms (germ-free) and those with a microbiota developed from birth (conventionally raised). When compared to their age and genotype matched germ-free counterpart, conventionally raised animals have more body fat even though they consume less chow. Introduction of the intestinal microbiota into germ-free animals (conventionalisation) results in an increase in body fat, and specifically epididymal fat pad weight, with values now equaling that of the conventionally raised animal. Conventionalisation of the germ-free animal was also associated with elevated plasma insulin and glucose and impaired insulin sensitivity and glucose tolerance (Bäckhed et al., 2004). Bäckhed et al. went on to show the germ-free mouse was also protected from diet-induced obesity and explained the difference to be a result of gut microbiota mediated induction of lipoprotein lipase and suppression of fatty acid oxidation in the conventional animal (Bäckhed et al., 2007). Since however, the germ-free mediated protection from diet-induced obesity has been shown to be diet composition-dependent and the molecular mechanisms proposed by Bäckhed et al. have been disputed (Fleissner et al., 2010).

Regardless, from these early experiments, we know the presence of the microbiota can influence the intestinal absorption of dietary energy and the host genes involved in energy expenditure and storage. Akin to this, an explosion of studies using antibiotics to reduce the microbial load of the intestine have shown an improved glucose tolerance in standard chow conditions (Vijay-Kumar et al., 2010; Bech-Nielsen et al., 2012) and ameliorated metabolic consequences (i.e. weight gain, hyperglycaemia and impaired insulin signaling) of high-fat feeding (Membrez et al., 2008; Cani et al., 2008a; Carvalho et al., 2012; Murphy et al., 2013). Of note, consequences of these sub-therapeutic, or 'low-dose', defined treatment regimes are

converse to the growth promoting, and obesity associated outcomes associated with sustained antibiotic use (Ternak, 2005; Swann et al., 2011).

1.2.3 Dysbioses in Disorders

A multitude of studies have linked several disease states to a deviation from a functional core of the microbiota and, as a consequence, the number of functions now attributed to this population of organisms in host homeostasis is ever increasing. Disorders from Crohn's disease (Dicksved et al., 2008) to autism (Song et al., 2004) have been associated with a disturbed intestinal microbiota. The former perhaps unsurprisingly as Crohn's disease is an inflammatory disorder of the gut, however, although cause or consequence is not clarified, the latter provides evidence for consideration of this population in pathologies not just concerning the digestive tract.

A potential role of the gut microbiota in specifically the development of metabolic disorders has received a lot of interest. Recently obesity has become a prevalent problem in both developing and industrialised countries, the most recent data indicating a staggering 68% of the population of the United States, over 20 years old, are obese. It is a serious perturbed health state of an individual, often accompanied by the incidence of several other metabolic disorders such as type 2 diabetes, cardiovascular disease, inflammation and hypertension (Kallus and Brandt, 2012). A simple idea is that obesity is a state resultant of energy intake far exceeding that of energy expenditure. However, a consensus is emerging that some individuals seem more susceptible to this state than others (Krajmalnik-Brown et al., 2012; Angelakis et al., 2012; Kallus and Brandt, 2012). With the intestinal bacteria identified as a contributor to host digestion and energy storage (Bäckhed et al., 2004; 2007), this population has subsequently been the focus of the search for non-canonical methods to alleviate the prevalence of obesity. Indeed, changes in the microbiota (Ley et al., 2005; Turnbaugh et al., 2009a) and its corresponding microbiome (Turnbaugh et al., 2006) are reported in the obese state, which are thought to increase the ability of the host to harvest energy from the diet (Ley, 2010). Hence, microbiota modulation was proposed to be a potential therapeutic intervention in obesity. This hypothesis will be explored further in chapter 4.

Diabetes is another metabolic disorder that has been extensively linked with a dysbiosis of the gastrointestinal tract. Type 1 diabetes is an autoimmune disease, in which activated immune cells destroy insulin-producing pancreatic beta cells, and an importance of the gut microbiota in disease occurrence has been implied. The ‘Hygiene Hypothesis’ proposes that inadequate exposure to microbial antigens, and resultant dysregulation of immune effector cells, is detrimental. As a result, the rise in autoimmune and inflammatory disorders has been attributed to the advent of antibacterial products producing a dysbiosis of their own (Neish, 2009; Russell et al., 2012). It has been shown that exposure to antigens early in life did reduce the risk of developing type 1 diabetes in diabetes prone rats. Furthermore, a causative role of the gut microbiota in disease development was indicated when faecal flora differences predated the onset of diabetes in the animals (Brugman et al., 2004; 2006). An additional more established link has developed between the gut microbiota and type 2 diabetes. Type 2 diabetes is an acquired disorder, governed by certain genetic factors and lifestyle, in which tissues become insulin resistant. Insulin signaling and function is under the inhibitory control of inflammation. In its expanse and proximity to the host intestinal cells, the intestinal microbiota has been postulated as a factor which would increase the inflammatory tone of an individual, thereby capable of influencing insulin signaling (Boroni Moreira and de Cássia Gonçalves Alfenas, 2012). This is exemplified in investigations of germ-free and antibiotic treated animals (described above); absence and reduction of the intestinal microbiota improved parameters of insulin sensitivity and glucose tolerance. The role of the microbiota in insulin signaling will be further explored in chapters 3 and 5.

1.2.4 Host Genetics

Although the importance of the host genome in shaping the gut microbiota has been presented (Zoetendal et al., 2001; Benson et al., 2010), very little information exists on how specific genetic variation may influence the population of bacteria in the gut. Mouse lines lacking either toll-like receptor 5 or resistin-like molecule β are found to have a different microbiota compared to their wild-type counterparts (Hildebrandt et al., 2009; Vijay-Kumar et al., 2010). These findings are perhaps to be anticipated as these proteins are involved in intestinal homeostasis; an immune receptor of the of intestinal epithelial cells and a goblet cell-secreted hormone of the intestinal lumen

respectively. Furthermore, mice with mutations in the leptin gene (*ob/ob*) (Ley et al., 2005), leptin receptor (*db/db*) (Geurts et al., 2011) and PPAR γ (Zuo et al., 2011) also present with an altered intestinal microbiota. However, as these genetic disturbances are associated with the development and severity of the obese state, it remains unclear whether the dysbiosis is a direct consequence of genetics, or secondary to the perturbed energy state of an individual. To briefly consider the reverse relationship, the microbiota is in fact found to be capable of modulating expression of host genes of predominantly, but not limited to, intestinal function (Pai and Kang, 2008; Claus et al., 2011; Sahasakul et al., 2012). What has emerged as a much more dominating influence of bacterial composition in the human and murine gut is diet (Moreno-Indias et al., 2014) and the influence of diet and genetics will be further described in chapter 4.

In summary, the resident microbes of the intestinal tract clearly have a strong influence on host physiology; their presence alters energy absorption from the diet, metabolism of such energy and the maintenance of good health in an individual. After development, the microbiota is relatively stable and is influenced by genetics and even more so diet. Although there is now a wealth of information regarding dysbioses occurring in disorders and unfavourable metabolic outcomes, currently information does not distinguish between a cause or consequence of this association. More recently gut transplants employed in pathologies such as Crohn's disease illustrate the complexity of the paradigm. Although a donor phenotype is transmittable via the transfer of gut luminal contents, 'relapse' to the original phenotype is commonly observed, thus indicating an additional host component (Kaila et al., 2004). Furthermore, weight loss was not found to be a gut-transmittable phenotype in human faecal transplant studies, thus further questioning the microbiota as a source of surplus energy (DeWeerd, 2014). The extensive characterisation and description of the intestinal microbiota in different physiologies to date has been insightful. However, moving forward into investigations of the functionality of the microbiota and its interaction with the host will prove more conclusive and necessary for the development of microbiota modulation as a therapeutic.

1.3 GENERAL AIMS OF THE PROJECT

The investigations of this thesis are concerned with the characterisation of the FMO5 KO mouse. Initially the FMO5 KO gross phenotype will be described and investigations will aim to further characterise the age-related changes in the glucose profile and insulin sensitivity of FMO5 KO and WT animals.

Following ageing, the response to a high-fat diet will also be compared in the WT and FMO5 KO and, in the aim of targeting commensal bacteria of the intestine, a low-dose antibiotic treatment is used to determine the role of the intestinal microbiota.

The consequence of FMO5 expression in the intestine will then be considered. The intestinal microbiotas of the WT and FMO5 KO mice will be characterised, along with the expression of FMO5 and an additional protein of interest RELM β . To further investigate the intestine as a potential site of inflammation, the inflammatory profiles of the WT and FMO5 KO animals will also be determined and a role of inflammation in insulin signaling will be discussed.

Each results chapter (Chapters 3 to 5) will introduce the relevant background and research questions of the area of interest and detail the corresponding experimental findings.

Chapter Two: Materials and Methods

2.1 ANIMAL HUSBANDRY

2.1.1 Mice

A wild-type, C57BL/6J (WT), and a *Fmo5*^(-/-) (FMO5 KO) strain that has been backcrossed for 8 generations onto the C57BL/6 strain, were kept in the same animal holding room of a conventional facility and fed a standard chow diet (Harlan Teklad Global 2018); 18 % total protein, 5 % fat and 56 % carbohydrate, except where stated otherwise. The lighting schedule was, lights raised gradually 6 to 7 am, lights on full 7am to 6pm, lights dimmed gradually 6 to 7 pm. FMO5 KO mice were previously created by insertional inactivation of the *Fmo5* gene; Exon 2 was replaced with the neomycin resistance cassette via homologous recombination (Hernandez et al., 2006b).

2.1.2 Blood Collection

Blood samples were taken between 9:30am – 12pm. Topical anaesthetic (EMLA®) was applied to the tail tip and to induce vasodilation, animals were placed in a 37 °C chamber, for a minimum of 15 minutes prior to bleeding. Blood was then collected from the tail tip using EDTA or heparin coated microtubes (Sarstedt, Microvette® CB300). Blood was placed on ice immediately upon collection. Blood was then centrifuged at 4 °C for 10 minutes at 3000 g. The top partition of plasma was then removed and aliquots were stored at -80 °C.

2.1.3 High-Fat Feeding

At 33-weeks of age, WT and FMO5 KO animals were split into cohorts and *ad libitum* fed either a high-fat diet (Modified TestDiet® AIN-93G Rodent Diet 58M1 with 35% kcal Fat as Lard); 22.6 % protein, 16.1 % fat and 48.6% carbohydrate or the standard chow diet (as above). The diet intervention lasted 7 weeks, during which the animals were weighed twice weekly. On day 41 (~week 6) the glucose tolerance test was performed (*see* 2.1.7). After a 7-day recovery period post glucose tolerance testing, plasma was collected (*see* 2.1.2).

2.1.4 Antibiotic Treatment

At 30.5–32.5 weeks of age, treatment groups of WT and FMO5 KO animals were given ampicillin and neomycin in their drinking water (1 g.L⁻¹ and 0.5 g.L⁻¹ respectively). Using sterilised equipment, the antibiotic was dissolved in drinking water and replenished twice weekly with freshly prepared solution. Animals were housed in the same animal room as the control groups (non-antibiotic-treated) and were given free access to the standard chow diet. The antibiotic treatment lasted 4 weeks and the animals were weighed twice weekly. On day 14 of treatment glucose tolerance was measured (*see* 2.1.7). After a 7-day recovery period post glucose tolerance testing, plasma was collected (*see* 2.1.2).

2.1.5 Faecal Sample Collection

For microbiota analysis, faecal samples were collected from the base of the cage using sterile containers. Replica faecal samples were taken from different cages, each housing 3 to 4 mice. Where possible, the content of the stomach was also harvested *ex vivo* for microbiota analysis of particular conditions. Upon collection, the slurry was placed immediately on ice.

For protein analysis, freshly voided faecal pellets were collected from individual animals and placed immediately on ice. Where possible, the content of the colon was also harvested *ex vivo* for protein measurements in particular conditions. Upon collection, the slurry was placed immediately on ice.

Samples were collected from male WT and FMO5 KO mice aged 7-, 10-, 15- and 30-weeks old, and after a period of high-fat diet feeding or antibiotic treatment. Samples were stored at -80 °C.

2.1.6 Glucose Tolerance Test

Mice were fasted overnight (15 hours) and weighed the following morning. 15 minutes prior to the procedure, topical anaesthetic (EMLA®) was applied to the base of the tail of each animal.

Basal Blood Glucose

Using a sterile blade, a small incision was made within the anaesthetised area nicking the tail vein. From the bleed, a drop of blood was applied to a glucose test strip (Bayer, CONTOUR® NEXT Test Strips) connected to a glucometer (Bayer, CONTOUR® XT Meter).

Glucose Test

Glucose doses were calculated to 2g/Kg of body weight and administered via intraperitoneal injection. A 20 % (w/v) glucose solution (Baxter) was used for injection (10 µL administered per g of body weight).

Time Course Measurements

Subsequent blood glucose measurements were taken at 15, 30, 60, 90 and 120 minutes post glucose injection. This was performed by reopening the initial incision and applying a fresh drop of blood to clean glucose test strips secured to the glucometer.

Area Under the Curve (AUC)

For statistical analysis, AUC was calculated as described previously (Heikkinen et al., 2007):-

$$AUC = \int_{n=1}^{\chi-1} x \left((Tn + 1 - Tn) \left(\frac{|Gt - Gt+1|}{2} + \min(Gt, Gt + 1) - Gt0 \right) \right)$$

G: glucose concentration

t: time

n: time point number

χ : total number of time points

min(Gt,Gt+1): the lower value of two consecutive glucose concentrations

2.1.7 *Insulin Sensitivity Test*

Mice were fasted for 5.5 hours (9 am to 14:30 pm) and then weighed. 15 minutes prior to the procedure, topical anaesthetic (EMLA®) was applied to the base of the tail of each animal.

Basal Blood Glucose

Using a sterile blade, a small incision was made within the anaesthetised area nicking the tail vein. From the bleed, a drop of blood was applied to a glucose test strip (Bayer, CONTOUR® NEXT Test Strips) connected to a glucometer (Bayer, CONTOUR® XT Meter).

Insulin sensitivity Test

Insulin doses were then calculated to 0.25 IU/Kg of body weight and administered via intraperitoneal injection. 1000 IU/mL insulin (Actrapid®) was diluted 1:1000 in sterile 0.9 % (w/v) NaCl (Sigma-Aldrich®). The working 1 IU/mL insulin solution was used for injection (2.5 µL administered per g of body weight).

Time Course Measurements

Subsequent blood glucose measurements were taken at 15, 30, 45, 60, 75 and 90 minutes post insulin injection. This was performed by reopening the initial incision and applying a fresh drop of blood to clean glucose test strips secured to the glucometer. Percentage values of baseline glucose were then calculated for each time point: -

$$\% \text{ Baseline Glucose} = \left(\frac{Gt}{Gt0} \right) \times 100$$

G: glucose concentration

t: time

Inverse Area Under the Curve (iAUC)

For statistical analysis, inverse AUC was calculated as described previously (Heikkinen et al., 2007):-

$$\text{AUC} = \int_{n=1}^{x-1} x \left((Tn + 1 - Tn) \left(\frac{|Gt - Gt+1|}{2} + Gt0 - \max(Gt, Gt + 1) \right) \right)$$

G: glucose concentration

t: time

n: time point number

χ : total number of time points

$\max(G_t, G_{t+1})$: the higher value of two consecutive glucose concentrations

2.1.8 Tissue Insulin Sensitivity Test

Animals were fasted for 5.5 hours (9 am to 14:30 pm) and weighed. Insulin doses were then calculated to 0.5 U/Kg of body weight and administered via intraperitoneal injection. At exactly 10 minutes post insulin injection, individual animals were culled by dislocation of the neck. Using clean instruments, the animal was dissected and epididymal fat samples were collected. Tissues were collected in the same order from each animal and always within 5 minutes post cull. Tissue was washed in ice-cold, sterile phosphate buffered saline and excess liquid was carefully blotted on tissue paper. Tissue samples were snap-frozen on dry ice and stored at -80 °C for further analysis.

2.1.9 Animal Dissection and Tissue Collection

Animals were culled by a Schedule 1 procedure according to Home Office regulations. At their experimental end, mice were exposed to carbon dioxide and death was confirmed with dislocation of the neck. For tissue harvest, when a more immediate method is required, cervical dislocation was employed. Mice were culled between 9:30am and 12pm. Clean instruments were then used to dissect and record the internal anatomy of the animal. In high-fat diet investigations, photographic records were taken.

2.1.9.1 Tissues For Western Blot Protein Analysis and RNA Quantification

Dependent on requirement, liver, muscle and epididymal fat, was collected following standard dissection instructions. Tissue was washed in ice-cold, sterile phosphate buffered saline (PBS) (10 mM Na_2HPO_4 , 2 mM KH_2PO_4 , 2.7 mM KCl and 137 mM NaCl, pH 7.4) and excess liquid was carefully blotted on tissue paper. In some cases, tissues were weighed. For protein analysis, tissue was snap-frozen on dry ice and stored at -80 °C. For RNA analysis, tissue was immersed in *RNAlater*® (Sigma) and stored at -80 °C.

2.1.9.2 Tissues For Immunohistological and Immunohistochemical Analyses

For immunohistological and immunohistochemical analysis, a skin sample and sections of the gastrointestinal (GI) tract were harvested. Following cull and dissection, a small patch of skin from the inguinal region of the mouse was taken, mounted on 3 MM chromatography blotting paper (Whatman™) and immersed in 10 % (v/v) neutral buffered formalin (Leica Biosystems). The entire GI tract (from stomach to anus) was then removed from the abdomen and sectioned. Making a cut at the start of the duodenum, the stomach was first isolated. Using a needled syringe, the tissue was inflated with 10 % (v/v) neutral buffered formalin before being placed directly into 10 % (v/v) neutral buffered formalin. The small intestine was then liberated, by making a further cut above the cecum. Three sections of equal length; denoted top (duodenum), middle (jejunum) and bottom (ileum), were partitioned and a transverse section from each partition was taken and placed directly into 10 % (v/v) neutral buffered formalin. Making a cut just after the cecum of the remaining tract isolates the colon. A transverse section of the colon was placed directly into 10 % (v/v) neutral buffered formalin.

To assess morphological and histochemical differences along the length of the digestive tract, Swiss rolls were then prepared from the duodenum and ileum portions of the small intestine and colon as previously described (Moolenbeek and Ruitenbergh, 1981; Park et al., 1987). The mesentery was first stripped and each segment was then slit open longitudinally and washed with PBS. Faecal contents were removed by gently sweeping the mucosa with a clean instrument. Fine-pointed forceps were used to pinch the caudal end of the segment and, with the mucosa remaining on the outside, the tissue was wound around the forceps and itself. Sufficient tension was used to prevent the butterflyed lumen re-adhering to itself, hence maintaining the outer edge flat. The strip of tissue remained aligned during rolling, further ensuring the complete spiral structure in later sectioning. Once fully rolled, a needle was used to impale the entire structure and liberate the roll from the forceps. Together, this was fixed in 10 % (v/v) neutral buffered formalin.

2.2 PLASMA MEASUREMENTS AND BIOCHEMICAL ANALYSES

2.2.1 Glucose

Plasma glucose was measured by applying a drop of blood to a glucose test strip (Bayer, CONTOUR® NEXT Test Strips) connected to a glucometer (Bayer, CONTOUR® XT Meter).

2.2.2 Insulin

Plasma insulin was quantified using an enzyme-linked immunosorbant assay (ELISA) (Millipore, Rat / Mouse Insulin Elisa). Manufacturer's instructions were followed. Plasma was applied to a microtiter plate pre-coated with a monoclonal antibody to mouse insulin, allowing plasma insulin to be captured and immobilised on the plate. After washing, a second detection antibody was added to the plate, linking the immobilised complex to horseradish peroxidase. Following the addition of a chromogenic substrate, horseradish peroxidase catalyses a colorimetric reaction which can be measured photometrically. Absorbance at 450 nm is therefore proportional to the amount of detected insulin. Concentrations of unknown samples are interpolated from a standard curve of absorbance values from solutions of known concentration.

2.2.3 Lipopolysaccharide (LPS)

Plasma LPS (or endotoxin) was measured at Lonza Endotoxin Service Europe. The Limulus Amebocyte Lysate (LAL) test was used for endotoxin quantification. Endotoxin, from the outer membrane of gram-negative bacteria, converts a proenzyme of LAL into an active enzyme. The active enzyme will then catalyse the release of p-nitroaniline from a synthetic substrate, producing a yellow colour. Enzyme activation, hence endotoxin concentration, can therefore be quantified photometrically.

Plasma samples were heat inactivated for 10 minutes at 72 °C and diluted 1:40 in endotoxin free water (Lonza). Diluted plasma samples were mixed with LAL and incubated with the substrate. Resultant absorbance at 410 nm is proportional to the amount of endotoxin in the original sample. Endotoxin concentrations of unknown

samples were interpolated from a standard curve, generated from absorbance values of known concentrations.

2.2.4 *Resistin Like Molecule β (RELM β)*

Plasma levels of resistin like molecule β (RELM β) were measured using an enzyme-linked immunosorbant assay (ELISA) (MyBiosource, Mouse Resistin Like β ELISA). Plasma samples were diluted 1:10 in phosphate buffered saline (PBS) (137 mM NaCl, 2.7 KCl, 10 mM Na₂HPO₄, 1.8 mM KH₂PO₄) and manufacturer's instructions were followed. The diluted plasma was applied to a plate pre-coated with a RELM β antibody. After washing, a second detection antibody was then applied to the plate, linking horseradish peroxidase to the immobilised antigen-antibody complex. Following the addition of the enzyme substrate, a colour change occurs proportional to the amount of immobilised enzyme, hence antigen present. Concentrations of unknown samples are then interpolated from a standard curve, generated by samples of known concentration.

2.2.5 *Tumour Necrosis Factor α (TNF α)*

TNF α was quantified using an ELISA (Enzo, TNF α mouse EIA kit). Plasma was diluted 1:8 in the assay buffer provided and manufacturer's instructions were followed. Diluted plasma was applied to a microtiter plate pre-coated with a monoclonal antibody to mouse TNF α . After washing, a second anti- TNF α antibody is applied to wells, binding the captured TNF α . A detection antibody conjugated to horseradish peroxidase is then incubated, linking the immobilised complex to a colourmetric reaction. Addition of enzyme substrate results in a colour change, proportional to the amount of TNF α present, which can be measured at 450 nm. Concentrations of samples are interpolated from a standard curve, generated by standards of known TNF α concentration.

2.2.6 *Lipid Profiling*

An Olympus Diagnostic Systems AU400 Automated Clinical Chemistry Analyzer, equipped with an ion selective electrode, was used to measure plasma lipids. Plasma samples were analysed at the Medical Research Council Mammalian Genomics Unit in Harwell, Oxfordshire as described previously (Hough et al., 2002). Levels of total

cholesterol, HDL cholesterol, LDL cholesterol, triglycerides, free fatty acids and glycerol were quantified.

2.3 *INTESTINAL MICROBIOTA ANALYSIS*

Despite the highly conserved sequence of the 16S rRNA gene in bacteria, it contains nine variable regions that can be utilised in comparative sequence analysis to classify microbial species (Ludwig and Schleifer, 1994; Zoetendal et al., 2008; Hamady and Knight, 2009; Rajendhran and Gunasekaran, 2011). In conjunction with the rich databases available, 16S rRNA sequences isolated from faecal matter can therefore be used to assay the microbial diversity of the gastrointestinal tract of the mouse.

2.3.1 *Isolation of Faecal DNA*

DNA was isolated from faecal samples using a commercially available kit (Isolate Faecal DNA Kit, Bioline). Three faecal pellets (~150 mg), harvested from the same cage, were used for each sample and duplicate or triplicate samples were performed per condition. For stomach content analysis, samples from 3 individual animals were pooled and 140 mg of slurry was used. Manufacturer's instructions were followed. As samples had been frozen prior to processing, sufficient homogenisation required an additional 30 minutes of shaking, after addition of lysis buffer. Homogenates were centrifuged and a spin column was used to filter the lysate supernatant. The flow through was applied to a separate column to bind DNA. Bound DNA was then washed before being eluted. The DNA solution was then re-filtered using a spin column and heated at 80 °C for 20 minutes to denature any DNases present. DNA Extraction was confirmed with a 0.8 % agarose gel electrophoresis and samples were then stored at 4 °C.

2.3.2 *Selection of Primers*

Using available, online tools such as the Probe Match function of the Ribosomal Database Project (RDP) (<http://rdp.cme.msu.edu/probematch/search.jsp>) (Cole et al., 2009) and Blast (<http://blast.ncbi.nlm.nih.gov/Blast.cgi>), all currently available universal bacterial 16S rRNA primers were ranked on their coverage. Queries, using

both forward and reverse primers, were conducted to identify the pair that would amplify the most bacterial 16S rRNA genes sequences and specifically only amplify this gene. In conjunction with a literature search for compatibility information, forward primer 8FE (5'-AGAGTTTGATCCTGGCTCAG-3') and reverse primer 1387FE (5'-GGGCGGTGTGTACAAGGC-3') were selected and synthesized by MWG.

2.3.3 Polymerase Chain Reaction (PCR) Amplification of 16S rRNA Gene Sequences

The bacterial 16S rRNA gene sequences were specifically amplified using the universal 16S rRNA primer pair 8FE and 1387FE. PCR conditions consisted of a 5-minute 'hot start' at 95 °C. This was followed by 30 cycles; 95 °C for 1 minute, 51 °C for 1 minute and 72 °C for 1 minute, and a final elongation at 72 °C for 5 minutes. 5 pmoles of each primer and approximately 16ng of isolated DNA (*see* 2.3.1) was used per 25 µL reaction. Each reaction included 2.5 µL dNTPS (10 mM), 0.25 µL BioTaq polymerase (5 U.µL⁻¹), 0.75 µL of MgCl₂ (50 mM) and 2.5 µL of 10X NH₄ buffer. DNA amplification was confirmed with a 1 % agarose gel electrophoresis and the samples were stored at -20 °C.

2.3.4 Ligation of 16S rRNA Gene Sequences

PCR products (*see* 2.4.3) were ligated into the pGEM-T vector system (Promega) and the manufacturer's instructions were followed. 3 µL of amplified DNA (~100 ng) was added to the ligation reaction, containing 1 µL of vector (50 ng.µL⁻¹), to achieve an insert: vector ratio of 2:1. The reaction was left at room temperature for 30 minutes and then overnight (16 hours) at 4 °C. Samples were then stored at -20 °C.

2.3.5 Preparation of Chemically Competent Cells

10 mL of Luria Broth (LB) with MgCl₂ (1 % w/v tryptone, 0.5 % w/v yeast extract, 1 % w/v NaCl, 20mM MgCl₂, pH 7.5) was inoculated with a single colony of *Escherichia coli* DH5α. Cultures were grown overnight, shaking at 37 °C. The 10 mL culture was then reinoculated into 500 mL LB with MgCl₂ and left shaking at 37

°C. When an OD₆₀₀ of 0.3-0.4 was reached (~2-3 hours), cultures were cooled on ice for 30 minutes and kept at 4 °C for all subsequent steps. Cells were centrifuged at 10,000 g for 10 minutes at 4 °C. The supernatant was discarded and the resultant pellet resuspended in 100 mL of 75 mM ice-cold CaCl₂. The cell suspension was then centrifuged again at 10,000 g for 10 minutes at 4 °C. The supernatant was discarded and the resultant pellet resuspended in 12.5 mL of 75 mM ice-cold CaCl₂. The cell suspension was transferred to chilled microcentrifuge tubes and aliquots were snap-frozen in a dry ice-ethanol bath and stored at -80 °C until required.

2.3.6 Transformation of Chemically Competent Cells

5 µL of the ligated DNA product (*see* 2.3.4) was added to chilled microcentrifuge tubes. 20 ng of pUC19 DNA was also added to a positive control tube. An aliquot of chemically competent cells (*see* 2.3.5) was thawed on ice and 50 µL of the cell suspension was added to each DNA tube, followed by a gentle mix. Reactions were left on ice for 20 minutes and then heat shocked at 42 °C for 50 seconds. This was followed by a further 2-minute incubation on ice, after which the sample was transferred into 500 µL super optimal broth with catabolite repression (SOC) (2% w/v tryptone, 0.5% w/v yeast extract, 0.5 % w/v NaCl, 10 mM MgCl₂, 2.5 mM KCl, 20 mM glucose) at room temperature. Cultures were left to recover at 37 °C with shaking for 1 hour. After recovery, cells were plated on LB-Agar (1 % w/v tryptone, 0.5 % w/v yeast extract, 1 % w/v NaCl, 1.5 % w/v agar, pH 7.5) containing ampicillin (100 µg.mL⁻¹), X-gal (40 µg.mL⁻¹) and IPTG (0.1 mM). Plates were grown overnight (16 hours) at 37 °C.

2.3.7 Preparation of Electrocompetent Cells

A single colony of *Escherichia coli* JM109 was inoculated into 5mL of LB medium (1 % w/v tryptone, 1 % w/v NaCl, 0.5 % w/v yeast extract, pH 7.5) and grown overnight at 37 °C with shaking. 1 mL of culture was reinoculated into 200 mL LB and grown at 37 °C with shaking until an OD₆₀₀ of 0.5 was reached (~4 hours). Cells were then chilled for 30 minutes on ice. Cells were kept at 4 °C for all subsequent steps. Cells were centrifuged at 5500 g for 10 minutes at 4 °C and the supernatant was discarded.

The pellet was resuspended in a small volume of ice-cold water, mixed with 200 mL of ice-cold water and chilled for 10 minutes. The cells were centrifuged at 15,000 g for 10 minutes at 4 °C. The supernatant was immediately discarded and the pellet was resuspended in the residual liquid. Another 200 mL of ice-cold water was added and the cells were chilled for 10 minutes before being centrifuged for at 15,000 g for 10 minutes at 4 °C. The supernatant was discarded immediately and the pellet was resuspended in the residual liquid. The cells were resuspended in an equivalent amount of ice-cold 10 % glycerol, aliquoted into pre-chilled microcentrifuge tubes and frozen in a dry ice-ethanol bath. Cell aliquots were then stored at -80 °C until required.

2.3.8 Transformation of Electrocompetent Cells

An aliquot of electrocompetent cells (*see* 2.3.7) was thawed on ice. 7 µL of ligated DNA product (*see* 2.3.4) was added to 100 µL of electrocompetent cells on ice. For a positive control, 40 pg of pUC19 DNA was also added to 100 µL of electrocompetent cells. DNA-cell suspensions were then transferred to individual pre-chilled electroporation cuvettes (BioRad, gap width 2mm). Once placed in the sample chamber of the electroporator (BioRad, Gene Pulser™), a pulse was applied (2.5 kV, resistance: 200 ohms, capacitance: 25 µFD). Cells were then immediately transferred to 600 µL SOC at room temperature and incubated without shaking at 37 °C for 1 hour. Cells were plated on LB-Agar (1 % w/v tryptone, 0.5 % w/v yeast extract, 1 % w/v NaCl, 1.5 % w/v agar, pH 7.5) containing ampicillin (100 µg.mL⁻¹), X-gal (40 µg.mL⁻¹) and IPTG (0.1 mM). Plates were grown overnight (16 hours) at 37 °C.

2.3.9 Selection of Successful Transformants

Growth plates from transformation procedures (*see* 2.3.6 and 2.3.8) were used to screen for successful transformants. The pGEM-T vector contains the ampicillin resistance gene (Figure 2.1). Therefore, LB-agar containing ampicillin will only allow growth of bacteria which have been transformed with pGEM-T.

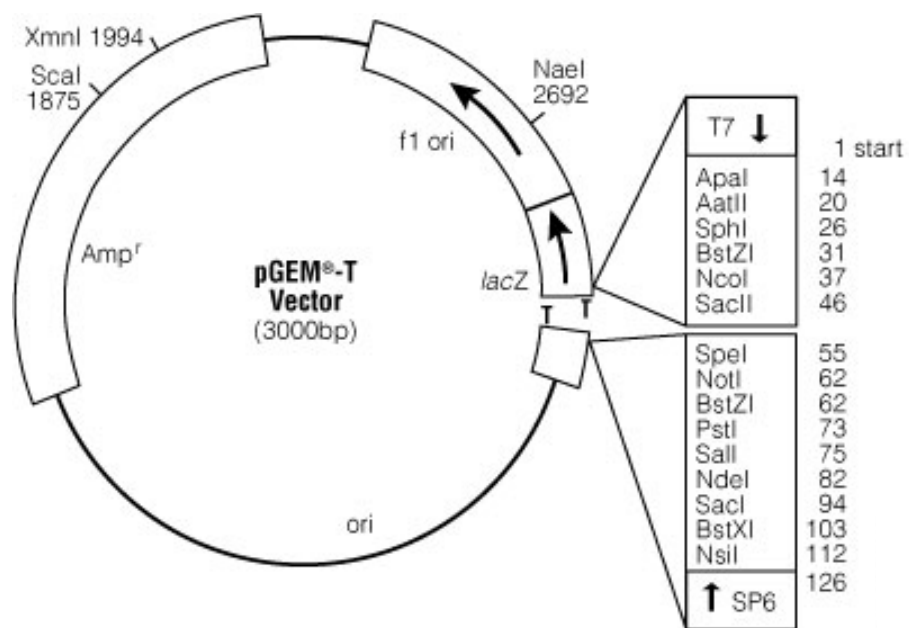


Figure 2.1 – pGEMT vector. The vector contains the ampicillin resistance gene (*Amp^r*). The β-galactosidase gene (*lacZ*), under the control of the *lac* operon, is interrupted by the multiple cloning site. (Taken from pGEM®-T and pGEM®-T Easy Vector Systems Technical Manual, Promega)

The ligation reaction (*see* 2.3.4) does not result in a homogeneous solution of positive ligations (vector containing insert); the vector may self ligate with no insert. Therefore it is necessary to screen for transformants which have specifically taken up plasmids containing inserts.

The vector contains the β -galactosidase gene under the control of the *lac* operon. The multiple cloning site of pGEM-T is however situated within the gene sequence. Ligation of an insert into the vector will subsequently interrupt the gene. Therefore, due to the presence of IPTG; an inducer of the *lac* operon, and X-gal; a substrate of β -galactosidase in the growth medium, we are also able to identify bacteria which have been transformed with an empty vector.

X-gal is cleaved by β -galactosidase, producing galactose and 5-bromo-4-chloro-3-hydroxyindole. 5-bromo-4-chloro-3-hydroxyindole immediately dimerises, resulting in a blue product. A blue colony on the growth plate therefore indicates transformation of the pGEM-T plasmid with uninterrupted β -galactosidase expression, hence no insert. Conversely, white colonies indicate clones, which have taken up the pGEM-T vector without functional β -galactosidase, hence containing an insert.

White colonies were therefore picked and stabbed into 96-well microtiter plates of LB-agar containing ampicillin ($100 \mu\text{g.mL}^{-1}$). Plates were incubated overnight (16 hours) at 37°C . Plates were then further processed at LGC Genomics. An automated service of plasmid extraction and Sanger sequencing of insert DNA provided us with sequence reads of around 1200 bp for each isolate. Single read sequencing was performed with the pGEM1 primer (5'-CGACTCACTATAGGGCGAATTGGG-3').

2.3.10 Phylogeny Classification

Sequence alignments were performed for all isolates using the Ribosomal Database Project (RDP) (<http://rdp.cme.msu.edu>). Sequence sets from each condition were compared to the RDP library of known 16S rRNA gene sequences and classifications above an 80 % confidence threshold were recorded.

2.4 WESTERN BLOT ANALYSIS

Gel electrophoresis allows the separation of proteins according to their molecular weight. Biological samples are loaded into polyacrylamide gels and application of a current results in the migration of proteins, through the gel matrix, proportional to protein size. Separated proteins can then be transferred onto membranes, which are probed with antibodies against proteins of interest. Western blot analysis was used to compare the presence, abundance and oligomeric state of different protein targets in various biological samples.

2.4.1 Sample Collection Protein Isolation

WT and FMO5 KO mice of different ages, or following different treatments, were culled and appropriate tissues were collected as described above (*see* 2.1.9 and 2.1.10). Faecal samples and the contents of the colon were also collected from WT and FMO5 KO mice of different ages, or following different treatments (2.1.5). Tissues and faecal samples were stored at -80 °C.

2.4.1.1 Liver

Liver samples were placed on ice and, using clean implements, 5-10 mg of tissue was weighed and immersed immediately in 1mL aliquots of ice-cold Triton lysis buffer (1% Triton X-100, 140 mM NaCl, 10 mM Tris pH8, 1 mM EDTA, 1 mM PMSF) containing Halt™ Protease and Phosphatase Inhibitor Cocktail (Thermo Scientific). A 5 mm stainless steel bead was placed into each sample and tubes were loaded into the Tissue Lyser II (Qiagen). Samples were homogenised at 25 Hz for 30 seconds, left to cool on ice for 1 minute and homogenised for a further 30 seconds at 25 Hz. To ensure complete homogenisation, samples were rotated on a spinning wheel at 4 °C for 15 minutes.

Homogenates were then spun in a microcentrifuge for 20 minutes at 12,000 g, 4 °C. The supernatant was transferred into a clean microcentrifuge tube and the pellet was discarded.

2.4.1.2 *Epididymal Adipose Tissue*

Epididymal adipose tissue samples were placed on ice and clean implements were used to weigh 10 mg of tissue. Weighed tissue was immediately immersed in 1 mL aliquots of ice-cold Triton lysis buffer (1% Triton X-100, 140 mM NaCl, 10 mM Tris pH8, 1 mM EDTA, 1 mM PMSF) containing Halt™ Protease and Phosphatase Inhibitor Cocktail (Thermo Scientific). A 5 mm stainless steel bead was placed into each sample and tubes were loaded into the Tissue Lyser II (Qiagen). Samples were homogenised at 25 Hz for 30 seconds, left to cool on ice for 1 minute and homogenised for a further 30 seconds at 25 Hz. To ensure complete homogenisation, samples were rotated on a spinning wheel at 4 °C for 15 minutes.

Homogenates were then spun in a microcentrifuge for 20 minutes at 12,000 g, 4 °C. Due to the origin of the sample, the homogenate is rich in lipid, with a thick layer visible at top of the supernatant. To obtain the supernatant, whilst avoiding the fat layer, a needle attached to a syringe was used to carefully transfer the protein fraction to a clean microcentrifuge tube. During transfer, inclusion of a small amount of fat is inevitable. Therefore, to further dilute out the fat from the sample, two more spins were conducted. Samples were spun for 5 minutes at 12,000 g, 4 °C to separate the lipid layer and a needled syringe was again used to transfer the supernatant whilst avoiding the fat. This was repeated for a total of two times, after which a 5-minute spin formed no visible lipid layer.

2.4.1.3 *Faecal and Colonic Samples*

Faecal or colonic samples were placed on ice and 30-60 mg of matter was immersed in 1 mL aliquots of ice-cold Triton lysis buffer (1% Triton X-100, 140 mM NaCl, 10 mM Tris pH8, 1 mM EDTA, 1 mM PMSF) containing Halt™ Protease and Phosphatase Inhibitor Cocktail (Thermo Scientific). A 5 mm stainless steel bead was placed into each sample and tubes were loaded into the Tissue Lyser II (Qiagen). Samples were homogenised at 25 Hz for 30 seconds, left to cool on ice for 1 minute and homogenised for a further 30 seconds at 25 Hz. To ensure complete homogenisation, samples were rotated on a spinning wheel at 4 °C for 40 minutes.

Homogenates were then spun in a microcentrifuge for 20 minutes at 12,000 g, 4 °C. As the resultant pellet was very soft and prone to resuspend, the supernatant was quickly transferred into a clean microcentrifuge tube and the pellet was discarded.

2.4.2 Protein Precipitation

When probing for certain targets in biological samples, it was necessary to first precipitate the protein. Pelleted protein can then be resuspended in a small volume of compatible buffer, resulting in a more concentrated solution of the original proteins present.

After protein isolation (*see* 2.4.1), the equivalent volume of ice-cold 20 % trichloroacetic acid was added to homogenates to a final concentration of 10 % (v/v). Samples were incubated at 4 °C for 10 minutes and centrifuged for 5 minutes at 14,000 g, 4 °C. The supernatant was removed and discarded, leaving the protein pellet intact. The pellet was then washed in 200 µL ice-cold acetone, tubes were vortexed for 10 seconds so as to disturb, but not dissolve, the pellet. Samples were then centrifuged for 5 minutes at 14,000 g, 4 °C. Taking precaution to not disturb the resultant pellet, the supernatant was removed and discarded. A further acetone wash was conducted; 200 µL ice-cold acetone was added and the tubes were briefly vortexed before a 5 minute centrifuge at 14,000 g, 4 °C. Samples were then heated at 95 °C for 5 minutes to evaporate the majority of the acetone, whilst not completely drying the pellet. When all that remained was a wet pellet (~ 10 µL residual acetone), 50 µL of resuspension buffer (6 M urea, 0.5 % SDS, 50 mM TrisHCL pH6.8, 5 mM EDTA) was added. To resuspend the pellet, the samples were heated for 10 minutes at 95 °C and briefly vortexed and centrifuged. A further 7-minute heat, followed by a vortex resulted in resuspension.

2.4.3 Protein Determination by BCA assay

The bicinchoninic acid (BCA) assay couples the reduction of Cu^{2+} to Cu^{1+} by protein, with the specific colorimetric detection of the cuprous cation (Cu^{1+}) by BCA. BCA is a chromogenic compound: chelation of reduced copper atoms produces a colour change, which can be measured photometrically at 562 nm. Absorbance at 562 nm is therefore linearly related to the protein concentration of the sample. A set of bovine serum albumin standards, of known concentrations, is used to generate a standard curve from which the concentration of unknown samples can be interpolated.

The Pierce® BCA Protein Assay Kit (Thermo Scientific) was used for measurement and the manufacturer's instructions were followed. Standards and samples to be measured were applied to a microtiter plate in duplicate. A solution containing

bicinchoninic acid and cupric sulphate was then added to all reactions and the plate was incubated at 37 °C for 30 minutes. Absorbance was read at 562 nm and the concentrations of the unknowns were calculated.

2.4.4 Protein Determination by Coomassie Protein Assay

For protein determination of samples originating from adipose tissue, the BCA assay (*see* 2.4.3) was found to be inappropriate. Although care was taken to eliminate the maximum amount of lipid possible, residual fat in the samples interfered with the method of detection resulting in variable and invalid protein concentration readings. Instead, a coomassie-based assay was used for adipose tissue homogenates.

The Pierce Coomassie Protein Assay (Thermo Scientific) is a stable solution of the Bradford assay reagent, used to measure protein concentration at 595 nm. The Bradford assay reagent, acidic Coomassie Brilliant Blue G-250, changes maximum absorbance from 465 nm to 595 nm upon binding to protein. A set of bovine serum albumin standards, of known concentrations, is used to generate a standard curve from which the concentration of unknown samples can be interpolated.

1 mL of the coomassie reagent was dispensed into the required number of cuvettes. 1 µL of standard or sample was dispensed into each cuvette and the reactions were mixed by inversion. Absorbance was read at 595 nm and the concentrations of the unknowns were determined.

2.4.5 Sample Preparation for Electrophoresis

Correct sample volumes required for a defined amount of protein were calculated using results of the BCA (*see* 2.4.3) or Coomassie Protein Assay (*see* 2.4.4). Sample volumes were then normalised using distilled, deionised water, and mixed with 4X sample buffer to a final concentration of 1X. Samples were heated for 6 minutes at 95 °C.

All samples prepared for electrophoresis were denatured and, depending on the protein target, either reduced or non-reduced. For reducing conditions the samples were mixed with a 4X sample buffer containing a reducing agent (200 mM Tris pH 6.8, 40 % (v/v) glycerol, 8 % (w/v) SDS, 1 % (w/v) bromophenol blue, 400 mM DTT) and for non-reducing conditions 4X sample buffer without reducing agent was

used (200 mM Tris pH 6.8, 40 % (v/v) glycerol, 8 % (w/v) SDS, 1 % (w/v) bromophenol blue).

2.4.6 Electrophoresis

The Mini-PROTEAN® Tetra Cell System from BioRad was used for sodium dodecyl sulphate polyacrylamide gel electrophoresis (SDS-PAGE). Proteins were separated by the mini-vertical electrophoresis system and the manufacturer's instructions were followed. Briefly, precast gels (Mini-PROTEAN® TGX™ gels, BioRad) were securely fixed into the inner cell and immersed in running buffer (0.1 % (w/v) SDS, 25 mM Tris, 192 mM glycine). The bottom of the tank was also filled with running buffer, ensuring electrodes are too immersed in buffer. Precision Plus Protein™ Dual Colour Standards (BioRad) and MagicMark™ XP Western Protein Standard (Invitrogen) were loaded to allow visual and chemiluminescent detection of protein size respectively. Prepared samples (*see* 2.4.5) were then loaded into the appropriate wells. Application of the tank lid locks the mini-cell and connects the system to a power pack. The gel was run at 150 V for 50 minutes. Depending on the size of the target protein, different percentage gels were selected. For proteins larger than 30 kDa, 10 % precast gels were used, however for the separation of smaller proteins (<20 kDa), samples were run on 4- 12 % gradient gels.

2.4.7 Protein Transfer

The presence of SDS in sample and running buffers during electrophoresis imparts a negative charge to separated proteins. Charged, immobilised proteins can therefore be transferred from the gel to a membrane with the application of an electric current.

The Trans-Blot® Turbo™ Transfer System (BioRad) was used for transfer. The gel to be analysed was freed from the electrophoresis equipment and the manufacturer's instructions were followed. A Trans-Blot® Turbo™ Transfer pack was loaded into the cassette; a nitrocellulose membrane on top of soaked filter paper was placed into the Trans-Blot® cell and the gel was carefully placed on top, ensuring complete contact with the membrane and no bubbles. A further layer of soaked filter paper was placed on top, the cassette was closed and loaded into the transfer system. The transfer was run at 1.3 A, 25 V for 7 minutes.

2.4.8 *Blocking of the Membrane*

Membranes have a high affinity for protein binding. Therefore it is necessary to first block non-specific interactions between the membrane and detection antibodies. This is achieved by incubating the membrane in a dilute solution of protein, which will cover the unbound membrane however leave transferred proteins unmasked.

Without letting the membrane dry, immediately after transfer, the membrane was placed in blocking buffer. Depending on the following method of detection, the membrane was blocked in the appropriate buffer.

2.4.8.1 *Bovine Serum Albumin*

For chemiluminescent detection of proteins with polyclonal antibodies raised against proteins, membranes were blocked with bovine serum albumin (BSA). A 5 % (w/v) solution of BSA was prepared in Tris-buffered saline (TBS) (150 mM NaCl, 10 mM Tris-Cl pH 7.5) with 0.1% Tween20 (TBS-T). In a clean vessel, the membrane was immersed in 5 % (w/v) BSA and incubated for 1 hour at room temperature.

2.4.8.2 *Non- Fat Dried Milk*

For chemiluminescent detection of RELM β with the polyclonal antibody raised against the peptide sequence (Abcam® ab11429), 5 % (w/v) BSA was found to be insufficient and membranes were instead blocked with non-fat dried milk (NFDM). A 5 % (w/v) solution of NFDM was prepared in TBS-T and the membrane was incubated for 1 hour at room temperature.

2.4.8.3 *Odyssey® Blocking Buffer*

For fluorescent detection of proteins with antibodies conjugated to fluorophores, a commercially available blocking buffer, Odyssey® Blocking Buffer (LI-COR), was used. The membrane was immersed in solution and incubated for 1 hour at room temperature.

2.4.9 Incubation with Primary Antibody

After sufficient blocking, the membrane was washed in TBS-T. In a clean vessel, the membrane was immersed in TBS-T and rocked at room temperature for 5 minutes. Three quick rinses in TBS-T followed and this was repeated twice, for a total of three washes. Using manufacturer's instructions for guidance, primary antibody was diluted in the specific blocking buffer used in the previous step (*see* 2.4.8). In accordance with manufacturer's instruction, for dilution of the primary antibody, the Odyssey® Blocking Buffer was supplemented with 0.1 % Tween20.

Antigen (Manufacturer, Catalogue No.)	Sample Analysed	Dilution
Complement Component 3 (Calbiochem®, 204869)	Epididymal adipose tissue	1:1,000
Enolase (Santa Cruz Biotechnology®, sc-15343)	Epididymal adipose tissue	1:200
FMO5 (Proteintech™, 16864-1-AP)	Faecal sample	1:1,500
FMO5 (Proteintech™, 16864-1-AP)	Liver	1:4,500
Phospho-Akt (Ser473) (Cell Signalling Technology®, 9271)	Epididymal adipose tissue	1:1000
RELMβ (Abcam®, ab11429)	Colon contents	1:10,000
RELMβ (Abcam®, ab11429)	Faecal sample	1:10,000
RELMβ (QED Bioscience, 20805)	Colon contents	1:15,000
RELMβ (QED Bioscience, 20805)	Faecal sample	1:1,500

Membranes were immersed in the appropriate dilution of primary antibody and incubated overnight (16 hours) at 4 °C with gentle rocking.

2.4.10 Incubations with Secondary Antibody

Following primary antibody incubation, the membranes were first washed to remove any unbound antibody. The membrane was immersed in TBS-T and rocked at room temperature for 10 minutes. Three quick rinses in TBS-T followed and this was repeated twice, for a total of three washes.

All primary antibodies used were raised in rabbit. Therefore, dependent on the method of detection to follow, either fluorescently labeled or horseradish peroxidase conjugated anti-rabbit secondary antibodies were used.

2.4.10.1 Fluorescent Secondary Antibody

An anti-rabbit antibody coupled to a fluorescent dye (Alexa Fluor® 790 Goat Anti-Rabbit IgG (H+L), Invitrogen) was diluted 1:5000 in Odyssey® Blocking Buffer supplemented with 0.1% Tween20. Membranes were immersed in secondary antibody and incubated for 1 hour at room temperature with rocking.

2.4.10.2 Horseradish Peroxidase Conjugated Antibody

An anti-rabbit antibody conjugated to horseradish peroxidase (HRP) (Donkey Anti-Rabbit IgG H+L (HRP), Abcam) was diluted 1:15,000 in TBS-T. Membranes were immersed in secondary antibody and incubated for 1 hour at room temperature with rocking.

2.4.11 Detection Methods

After incubation with secondary antibody, the membranes were washed to remove any unbound antibody. The membrane was immersed in TBS-T and rocked at room temperature for 10 minutes. Three quick rinses in TBS-T followed and this was repeated twice, for a total of three washes.

2.4.11.1 Fluorescent Antibody Detection

A fluorescent dye label allows the rapid detection of an antibody-antigen complex on the membrane. After washing the blot was scanned, at the appropriate wavelength, using the LiCor® Odyssey® Fc Dual-Mode Imaging System.

2.4.11.2 Enhanced Chemiluminescence

For detection of HRP antibody conjugates, enhanced chemiluminescence (ECL) was used. Enzyme immobilised to the membrane, mediated by the antigen-antibody complex, catalyses the oxidation of luminol emitting light at 428 nm. The addition of an enhancer further amplifies the light emitted and this enables detection of antigen-antibody interactions on the membrane.

Equivalent volumes of ECL reagent 1 (1.25 mM luminol, 2 mM 4-iodophenylboronic acid, 100 mM Tris-HCL pH 8.5) and ECL reagent 2 (5.3 mM H₂O₂, 100 mM Tris-HCL pH 8.5) were mixed. Enough solution was used to cover the membrane evenly and the reaction was left to develop for 1 minute, protected from light. The blot was then exposed and the image captured using the LiCor® Odyssey® Fc Dual-Mode Imaging System.

2.5 HISTOLOGY AND IMMUNOHISTOCHEMISTRY

2.5.1 Embedding and Cutting

Fixed tissues (*see* 2.1.10) were sent to the Medical Research Council Anatomical Pathology Group in Harwell, where they were embedded and cut. The Shandon Pathcentre™ tissue processor was used to embed tissues. A programme gave five changes of graded alcohol over 6 hours, four changes of SubX (Leica Biosystems) clearing over 5.5 hours and four changes of wax over 4 hours. Sections were then cut on a Shandon™ Finesse™ Microtome™ at 3 µm and collected from a water bath onto plain slides. Slides were dried overnight at 37 °C.

2.5.2 Hematoxylin and Eosin Staining

Nucleic acid stain hematoxylin and protein stain eosin are used together to investigate cell and tissue morphology, staining the nucleus blue and cytoplasm pink respectively. Hematoxylin and eosin staining was conducted at the Medical Research Council Anatomical Pathology Group, Harwell. Slides were stained on a Sakura® Tissue-Tek® DRS™ Slide Stainer using Shandon™ Gill™ 3 Hematoxylin and Shandon™ Eosin Y.

2.5.3 Alcian Blue Staining

Alcian blue stains acidic mucin of secretory granules and is therefore used as a goblet cell specific dye. Alcian blue staining was conducted at the Department of Histopathology, University College London Hospital. Sections were dewaxed through xylene and graded alcohols and stained with 1% (w/v) Alcian Blue for 10 minutes. Slides were washed in water, counterstained with 0.5 % (v/v) Neutral Red and dehydrated through graded alcohols and xylene.

2.5.4 Immunohistochemistry

Immunohistochemistry allows the tissue- and cell- specific detection of proteins. Antibodies applied to a fixed section of tissue will bind to their specific antigen, and the antibody-interaction is visualised by conjugating the complex to a colorimetric,

enzyme-catalysed reaction. Immunohistochemistry of sliced and mounted sections of the murine skin and gut was performed at UCL Advanced Diagnostics.

Sections underwent automated dewaxing and endogenous peroxidase activity was blocked using 3-4% (v/v) hydrogen peroxide. Heat/enzyme induced epitope retrieval is described for each protein of interest below. Diluted antibodies, also described below, were then applied to the slides and incubated at ambient temperature for 15 minutes. Signal visualization was performed using Bond™ Polymer Refine Detection Kit (Leica Biosystems) with Bond™ DAB Enhancer (Leica Biosystems). Cell nuclei were counterstained with hematoxylin (Leica Biosystems) Leica Bond-III and Leica Bond Max automated systems (Leica Biosystems) were used.

Antibody (Manufacturer, Catalogue No.)	Antigen Retrieval	Dilution	Diluent
FMO5 (ProteinTech™, 16864-1-AP)	Bond™ Epitope Retrieval Solution 1 (Leica Biosystems): 30 minutes, 100 °C	1:100	Antibody Diluent, Background Reducing (Dako)
RELM β (Abcam, ab11429)	Bond™ Epitope Retrieval Solution 1: 10 minutes, ambient temperature	1:400	Bond™ Primary Antibody Diluent (Leica Biosystems)

2.5.5 Slide Scanning

Slides were scanned using the Axio Scan.Z1 (ZEISS) with a 20 X magnification.

2.5.6 Goblet Cell Quantification

Photomicrographs of alcian blue stained sections of the colon (*see* 2.5.3) were used to quantify colonic crypt length and number of goblet cells per crypt. Using a method previously described, regions of interest containing at least three contiguous crypts were selected and six regions were sampled per photomicrograph. Three crypts per region of interest were analysed. For each crypt, crypt length was measured and number of goblet cells (alcian blue stained bodies) per crypt was counted (de Oliveira

Mello et al., 2012). For both WT and FMO5 KO, three photomicrographs, each from different animals, were used for quantification.

2.6 STATISTICAL ANALYSIS

Data is expressed as mean \pm standard error of the mean (SEM). Statistical significance was determined using Student's t-test. The following symbols were used throughout all figures and text to indicate the significance value:

* = $p < 0.05$, ** = $p < 0.01$, *** = $p < 0.001$, **** = $p < 0.0001$.

Chapter 3: The FMO5 KO Mouse

3.1 INTRODUCTION

3.1.1 Mouse Knockout Models

To further investigate the role of FMOs in both xenobiotic and endogenous metabolism, it is necessary to utilise knockout mouse lines lacking the specific isoforms. There are no known specific inhibitors of family members and antibodies only weakly inhibit catalytic activity. In addition, the thermal sensitivity of the enzyme family, and the difficulty in measuring enzyme products, makes determining the particular activity of FMOs problematic (Shephard and Phillips, 2010).

A mouse model was first created with the aim of humanising the mouse liver and lung, by deleting *Fmo1* and *Fmo2* respectively (Hernandez et al., 2006a). Using *Cre/LoxP* technology, *Fmo1*, *Fmo2* and *Fmo4* were deleted from chromosome 1, creating a *Fmo1,2,4^(-/-)* mouse (FMO1,2,4 KO). Due to the attenuation of *Fmo3* expression during development in males, the male knockout mice are subsequently null for all FMOs known to be involved in drug metabolism and this mouse model has helped us better understand the role of the specific FMOs in drug metabolism. In particular, the FMO1,2,4 KO model revealed the importance of FMO1 in the metabolism of an anti-depressant, imipramine. The mice showed exaggerated and prolonged effects to the drug, maintaining higher plasma concentrations of the parent compound with a reduction in appearance of the *N*-oxide (Hernandez et al., 2009).

This mouse line also has revealed a dual functionality of FMO1; further characterisation of the FMO1,2,4 KO mouse has shown FMO1 to participate in endogenous, as well as xenobiotic, metabolism. When compared to the WT controls, the knockout animal weighs less, is leaner and has less fat. Specifically, an increased capacity for exercise and higher levels of fatty acid oxidation in soleus muscle results in less fat stored in the knockout. Together with a higher resting energy expenditure, due to the activation of a futile cycle in white adipose tissue, this results in an enhanced total energy expenditure in the knockout, which is not accompanied by an increase in calorific intake. Unlike FMO2 and FMO4, FMO1 is highly expressed in the metabolic tissues investigated, therefore the altered phenotype of the knockout is likely to be due to the absence of specifically FMO1. FMO1 can subsequently be

considered as a regulator of energy homeostasis, as well as a drug metabolising enzyme (Veeravalli et al., 2014).

3.1.2 The *FMO5* Knockout Mouse

Employing a slightly different method of homologous recombination, a mouse model deficient in *Fmo5* (FMO5 KO) was also generated. Using a linearized vector, exon two of the *Fmo5* gene was replaced with the neomycin resistance gene (*neo^r*). Embryonic stem cells from the 129 mouse strain (yellow coat) were injected with a targeting construct consisting of *neo^r* flanked by exon 1 and 3 of the *Fmo5* gene, with the thymidine kinase (*tk*) gene downstream of exon 3. If homologous recombination with exon 1 and 3 of the *Fmo5* gene locus occurs, the clones will have replaced exon 2 of the gene with *neo^r*, without incorporating the *tk* gene. These clones will therefore be resistant to neomycin (*neo^r*+) and resistant to ganciclovir (*tk*-) (Hernandez et al., 2006b). Successful clones were selected, injected into C57BL/6 (black coat) blastocysts and blastocysts were injected into foster mothers. Black and brown spotted coat colour indicates chimeric offspring, with DNA from both the C57BL/6 blastocyst and 129 embryonic stem cell (Hernandez et al., 2006c). Genotyping was confirmed by PCR of the *Fmo5* allele and heterozygous mice were back-crossed with the wild-type C57BL/6 animals for eight generations. Male and female mice heterozygous for the mutation were then bred to produce a congenic *Fmo5* knockout line and mice homozygous for the altered allele (Figure 3.1).

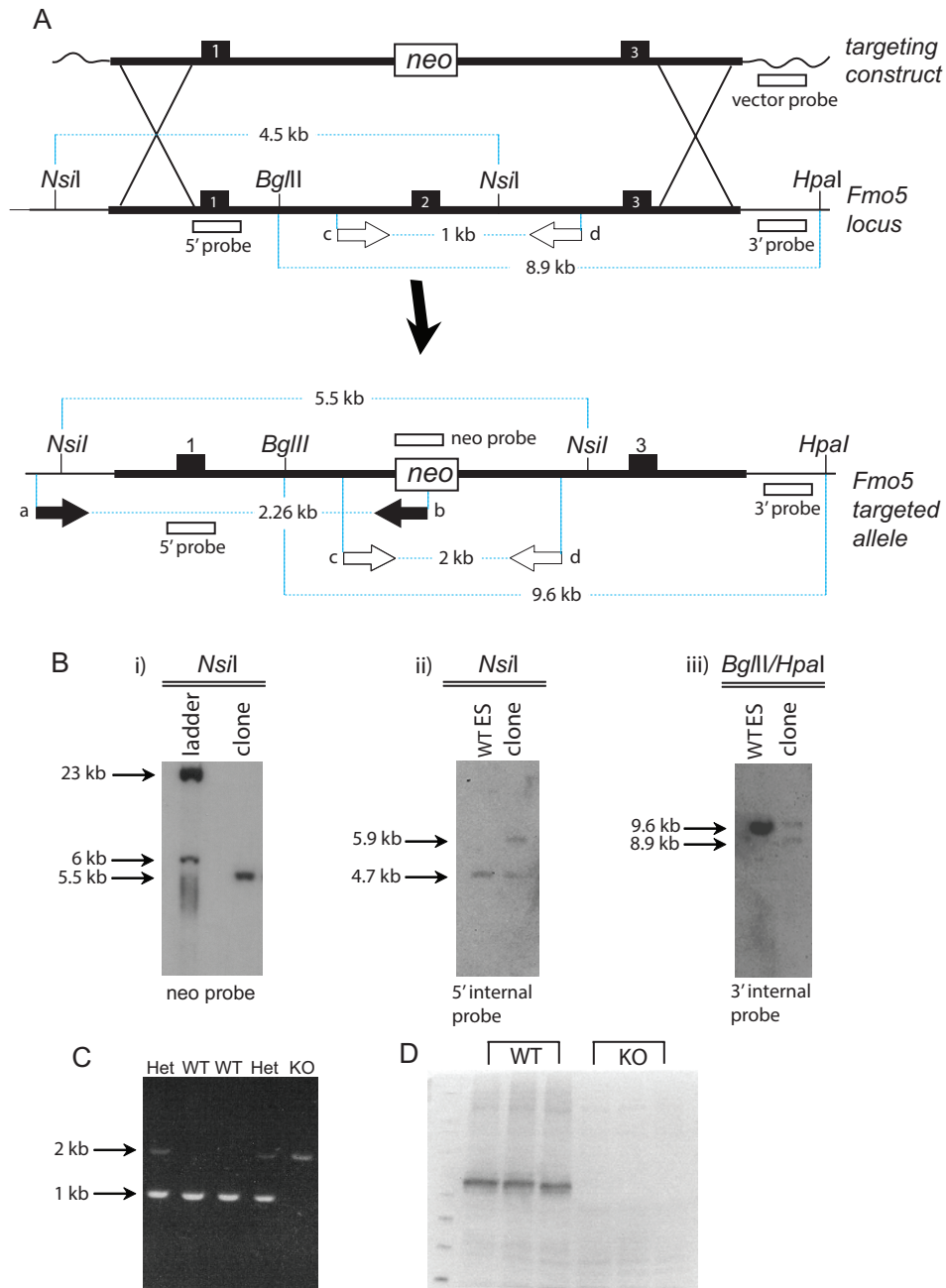


Figure 3.1 – Generation of the FMO5 KO mouse. **A** – Recombination between homologous regions (thick black lines) of the targeting construct and the *Fmo5* locus leads to the generation of a targeted *Fmo5* allele, in which exon 2 is replaced by the *neo*^r cassette. Black arrows: Primers used for screening of G418^r ES clones. White arrows: Primers used for identifying WT and targeted alleles. Probes and restriction sites used for Southern blot genotyping are also indicated. **B** – Southern blot analysis with i) a *neo*^r specific probe, ii) a 5'-internal probe and iii) 3'-external probe verify the correct integration of the targeted allele. **C** – Mice were genotyped by PCR analysis of tail DNA with primers c and d (see **A**). Het, Heterozygous knockout; WT, wild-type; KO, homozygous knockout. **D** – Western blot analysis of protein isolated from liver of wild-type (WT) and homozygous knockout (KO) mice. The KO do not express FMO5 (Hernandez et al., 2006b).

Similar to the FMO1,2,4 KO in the characterisation of FMO1, the FMO5 KO has also implicated a role of FMO5 in endogenous metabolism (Gonzalez Malagon 2011). When compared to the WT, the inactivation of *Fmo5* results in an attenuation of age-related weight gain (Figure 3.2). The use of knockout mouse lines has therefore revealed unsuspected roles of both these isoforms in energy metabolism.

Studies by Gonzalez Malagon revealed up until 20 weeks of age, weight gain in the WT and FMO5 KO is comparable. From 20-weeks however, even though the KO consume more chow per g of body weight and are not more active than the WT, weight gain in the FMO5 KO is reduced (Figure 3.2-A). The weight phenotype becomes more pronounced by 30 weeks of age, where a significant difference in weight of the two animals is observed (Figure 3.2-B).

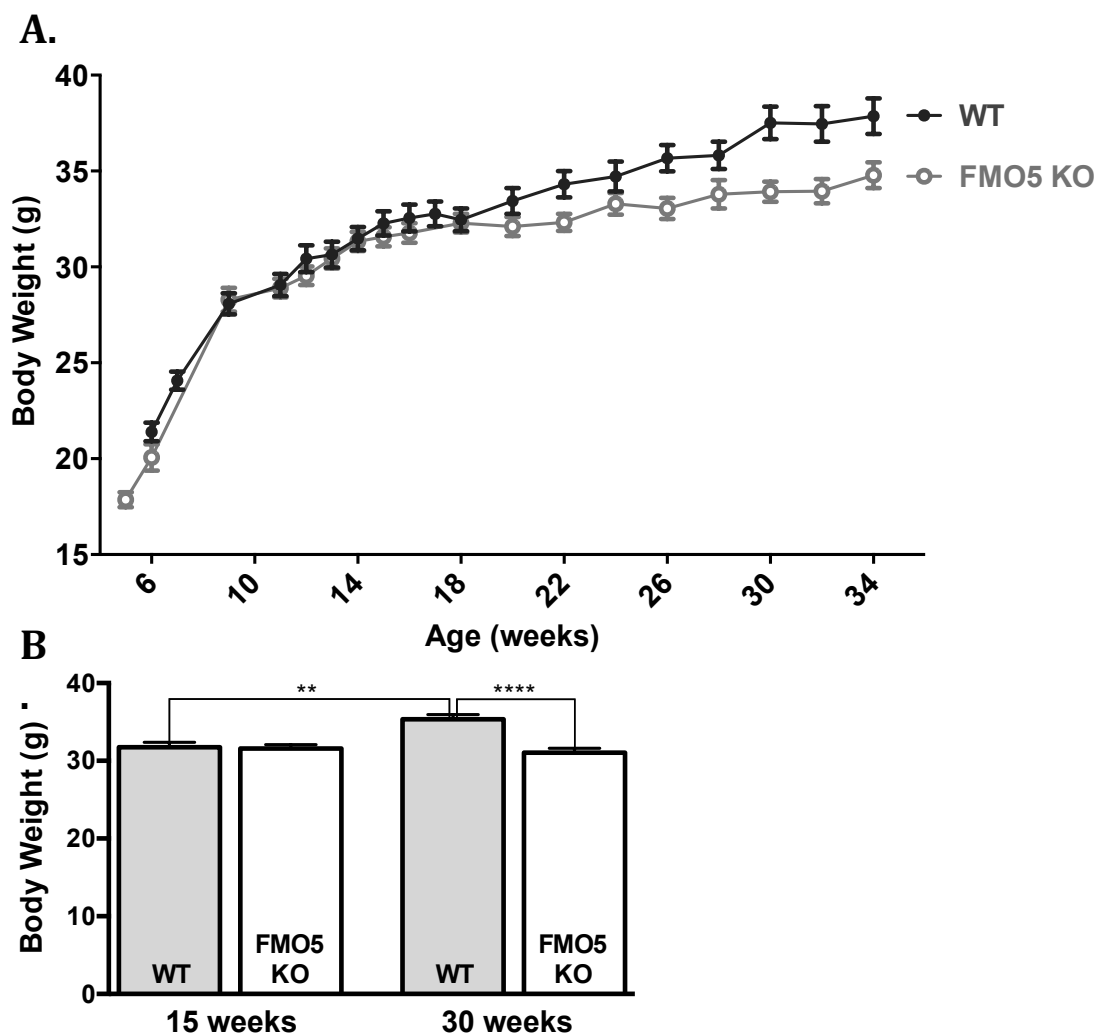


Figure 3.2 – Difference in age-related weight gain. A. WT (n=8) and FMO5 KO (n=7) male mice, fed a standard chow diet *ad libitum*, were weighed once a week for 30 weeks. Data is expressed as mean \pm SEM. B. Body weight comparison of 15-week (WT, n=10; FMO5, n=7) and 30-week (WT, n=27; FMO5 n=24) old male mice fed a standard chow diet *ad libitum*. Data is expressed as mean \pm SEM (**: $p < 0.01$, ****: $p < 0.0001$).

The older FMO5 KO mice were also found to have less fat relative to their total body weight at 30-weeks, with reductions in all fat depot sizes when compared with WT mice. Histological analysis of white adipose tissue revealed the decrease in fat depot size of the FMO5 KO could be attributed to a decrease in adipocyte cell volume. The discovery of this difference in weight and fat storage in the FMO5 KO mice led to further investigations of energy metabolism in these mice.

Similar to the difference in weight, plasma glucose was also found to be different in the 30-week WT and FMO5 KO animals, whereas levels are comparable at 15 weeks of age (Figure 3.3). Between time points 15- and 30-weeks, the WT plasma glucose is significantly increased. However, the plasma glucose of the KO does not change with age, this therefore results in a significant difference between the WT and FMO5 KO at 30 weeks.

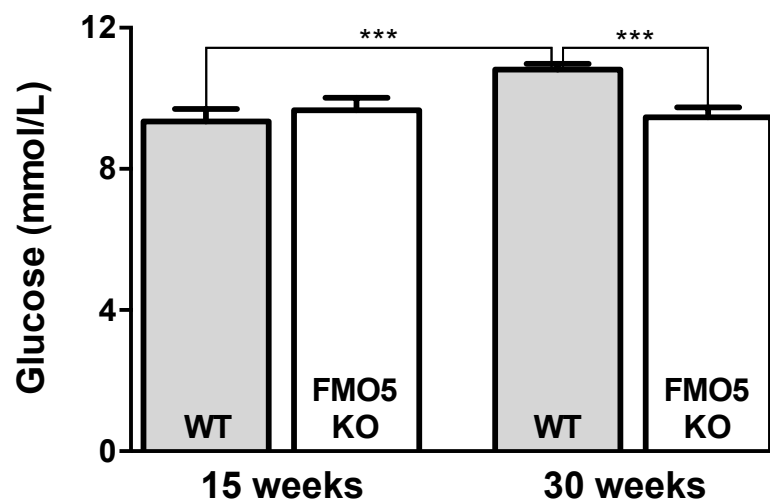


Figure 3.3 – Differences in plasma glucose at 15 and 30 weeks. Plasma glucose was measured between 9-11 am in fed 15-week (WT, n=18; FMO5 KO, n=23) and 30-week (WT, n=22; FMO5 KO, n=21) old male mice. Data is expressed as mean \pm SEM (***: $p < 0.001$).

Another key difference observed in the FMO5 KO mouse is lower plasma cholesterol as early as 15 weeks (Figure 3.4). This change, precedes the difference in weight and glucose observed at 30-weeks of age in the FMO5 KO mice. By the age of 30-weeks, the FMO5 KO mouse therefore presents with significantly lower weight gain, plasma glucose, total, HDL and LDL cholesterol.

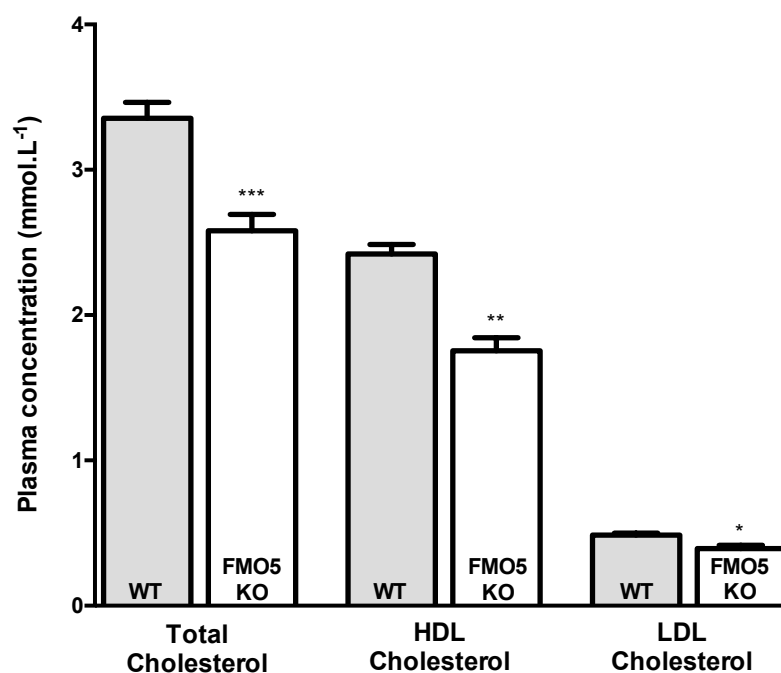


Figure 3.4 – Plasma cholesterol measurements of 15-week old mice. Total (WT, n = 6; FMO5 KO, n = 10), HDL (WT, n = 8; FMO5 KO, n = 10) and LDL (WT, n = 3; FMO5 KO, n = 8) cholesterol was measured in fed 15-week old male mice. Data is expressed as mean \pm SEM (*: $p < 0.05$, **: $p < 0.01$, ***: $p < 0.001$).

At 30-weeks of age total energy expenditure, measured by oxygen consumption, was found to be significantly higher in the FMO5 KO when compared to the WT in both the light (WT, 0.416 ± 0.005 kcal.day⁻¹.g⁻¹; FMO5 KO, $0.458 \pm$ kcal.day⁻¹.g⁻¹) and dark (WT, 0.448 ± 0.006 kcal.day⁻¹.g⁻¹; FMO5 KO, 0.500 ± 0.006 kcal.day⁻¹.g⁻¹) phase ($p < 0.0001$). A higher energy expenditure of the KO animal suggests the oxidation of fuel substrates is continuously higher. Furthermore, the resting energy expenditure (a measure of basal metabolic rate plus energy expended in processing food) was found to be higher in the KO (0.321 ± 0.009 kcal.day⁻¹.g⁻¹) when compared to the WT animal (0.283 ± 0.007 kcal.day⁻¹.g⁻¹) at this age ($p < 0.01$).

The respiratory exchange ratio (RER) is a measure of the relative contributions of carbohydrate and fat oxidation to total energy expenditure. During the light period, RER measurements indicate the animals have a similar utilisation of fuel (WT, 0.950 ± 0.006 ; FMO5 KO, 0.943 ± 0.007). During the dark phase (active period), the average RER value remains the same for the WT, however the RER value of the FMO5 KO increases to 0.989 ± 0.006 . This value is significantly higher than the RER value of the FMO5 KO in the light phase ($p < 0.001$), and the WT average RER during the dark phase ($p < 0.001$). These measurements therefore indicate the FMO5 KO animal uses more carbohydrate than the WT in the active period (Gonzalez Malagon 2011).

The differences recorded by Gonzalez Malagon et. al in weight, plasma glucose and plasma cholesterol in the WT and FMO5 KO mouse are apparent in both male and female cohorts. My analysis herein will therefore focus solely on the male WT and FMO5 KO mouse.

3.2 *EXPERIMENTAL QUESTIONS AND AIMS*

- I. The phenotype suggests that the FMO5 KO mice will be more insulin sensitive than WT mice. Aim I was to further characterise the glucose phenotype observed in the WT and FMO5 KO animals with ageing. Measurement of plasma insulin, glucose tolerance and insulin sensitivity at different ages of the two mouse lines will further elucidate the changes in the phenotype with age.

- II. To investigate the influence of a high-fat diet in the WT and FMO5 KO animals. Measurement of weight, glucose and insulin levels and glucose tolerance in animals subjected to a high-fat diet will identify any differences in diet-induced changes in glucose homeostasis and weight gain.

- III. To examine of the role of the intestinal microbiota in the glucose profile of the WT and FMO5 KO animal. Use of a low-dose course of antibiotics to reduce the bacterial load in the intestine, will clarify the influence of the microbiota in glucose homeostasis.

3.3 RESULTS

3.3.1 *The Glucose Phenotype of the FMO5 KO mice in Ageing*

3.3.1.1 *Glucose Tolerance Test*

The glucose tolerance test is a measure of how effectively an individual can clear glucose from the blood. By injecting an animal with a defined, exogenous amount of glucose, the subsequent rise in blood glucose can be measured. By then taking blood glucose measurements at incremental time points post glucose bolus, the ability of the individual to return glucose levels back to baseline can be assessed. The test was first performed on 15 week-old animals.

In agreement with the plasma glucose measurements at this age (*see* Figure 3.3), the glucose tolerance of 15-week old WT and FMO5 KO animals is also similar (Figure 3.5-A). There was no difference in AUC values of the WT ($596.3 \pm 105.7 \text{ mmol.L}^{-1}.\text{min}^{-1}$, n=5) and FMO5 KO ($526.5 \pm 40.6 \text{ mmol.L}^{-1}.\text{min}^{-1}$, n=7) animals tested.

The test was then performed on 30-week old WT and FMO5 KO animals (Figure 3.5-B). At this age point, there is a measurable difference in glucose tolerance. The glucose bolus results in a higher and more sustained glucose peak in the WT animal. Furthermore, the FMO5 KO is able to clear glucose faster, and to a much greater extent, than the WT. The WT animal fails to return to basal blood glucose in the 120-minute time course. Together, this results in a significant difference between the AUC values of the WT ($1278.3 \pm 124.7 \text{ mmol.L}^{-1}.\text{min}^{-1}$, n=5) and the FMO5 KO ($594.0 \pm 124.5 \text{ mmol.L}^{-1}.\text{min}^{-1}$, n=5) animals ($p < 0.01$).

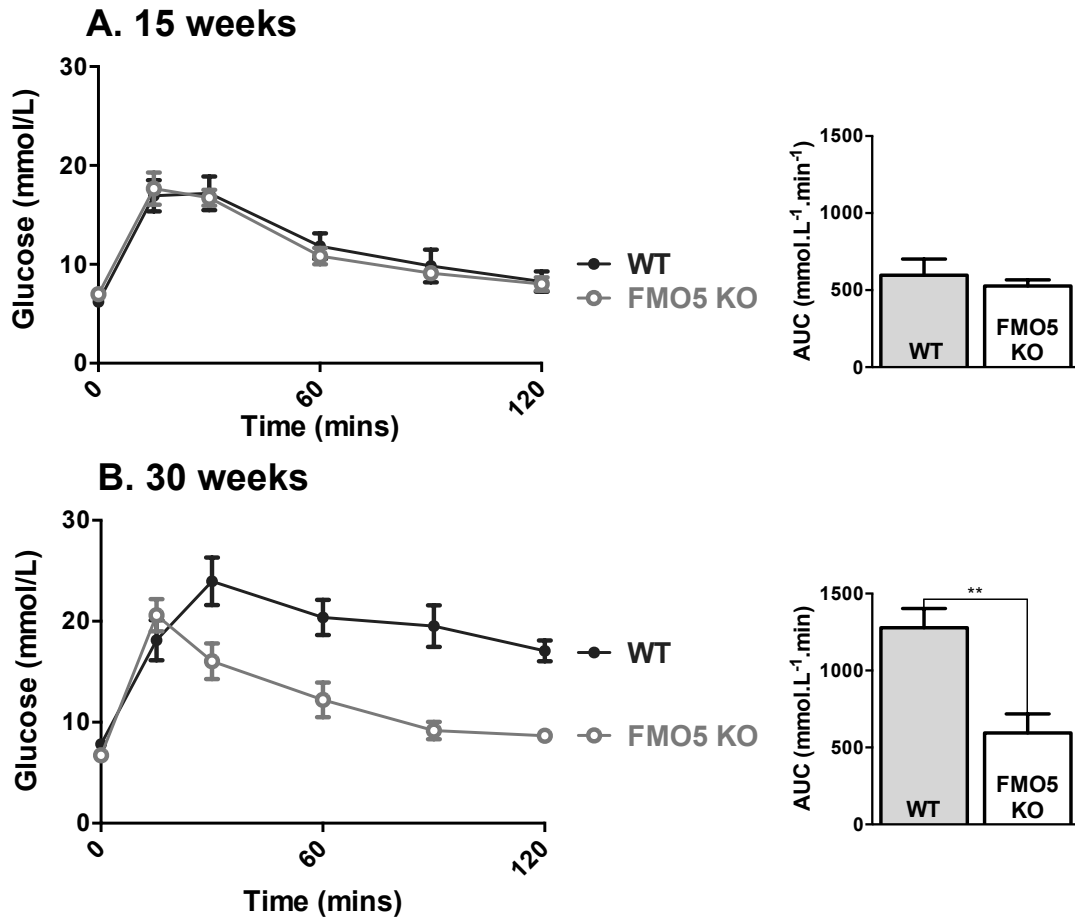


Figure 3.5 – Glucose tolerance of 15- and 30- week old animals. Glucose tolerance was measured in **A.** 15-week (WT, n=6; FMO5 KO, n=5) and **B.** 30-week (WT, n=4; FMO5 KO, n=4) old male mice. Left – Plasma glucose levels following a glucose bolus. Right – Area under the curve (AUC) analysis. Data is expressed as mean \pm SEM (**: $p < 0.01$).

The difference in glucose tolerance reported at 30 weeks, and absent in 15-week old animals, is due to changes in the WT AUC values with age (15 week, 596.3 ± 105.7 mmol.L⁻¹.min⁻¹; 30 week, 1278.3 ± 124.7 mmol.L⁻¹.min⁻¹) ($p < 0.01$), whilst FMO5 KO values remain unchanged (15 week, 526.5 ± 40.60 mmol.L⁻¹.min⁻¹; 30 week, 594.0 ± 124.5 mmol.L⁻¹.min⁻¹). This is consistent with the phenotype observed in plasma glucose; the difference between genotypes appearing at 30 weeks is due specifically to an increase in plasma glucose and glucose tolerance in the WT, whereas KO values remain unchanged. Therefore, both plasma glucose and glucose tolerance worsens with age in the WT animal, however the FMO5 KO is able to retain the healthier profile; lower blood glucose and a better glucose tolerance, through ageing.

3.3.1.2 Plasma Insulin Measurement

Insulin is a hormone released by pancreatic beta cells in response to elevated blood glucose. Amongst other roles, this signal then drives glucose uptake in tissues such as adipose tissue and muscle. Measurement of plasma insulin is used to indicate any changes in the hormone function in states of perturbed glucose homeostasis. Plasma insulin of WT and FMO5 KO animals was measured by ELISA. Measurements were conducted at both 15 and 30 weeks (Figure 3.6).

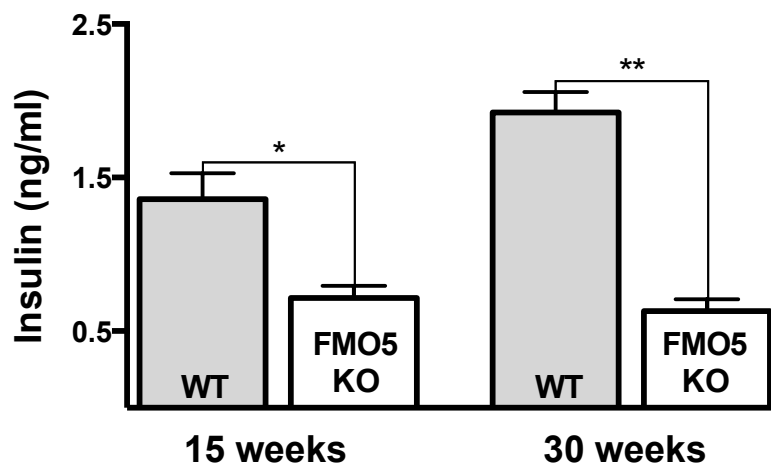


Figure 3.6 – Plasma insulin of 15- and 30-week old animals. Plasma insulin was measured between 9-11 am in fed 15-week (WT, n=4; FMO5 KO, n=4) and 30-week (WT, n=3; FMO5 KO, n=3) old male mice. Data is expressed as mean ± SEM (*: $p < 0.05$, **: $p < 0.01$).

Contrary to blood glucose and glucose tolerance measurements, as early as 15 weeks there is a significant difference in plasma insulin of the WT ($1.36 \pm 0.17 \text{ ng.ml}^{-1}$, n=4) and FMO5 KO ($0.72 \pm 0.08 \text{ ng.ml}^{-1}$, n=4) animals ($p < 0.05$). This difference becomes more pronounced, and significant, at 30 weeks of age (WT: $1.92 \pm 0.13 \text{ ng.ml}^{-1}$ n=3, FMO5 KO: $0.63 \pm 0.08 \text{ ng.ml}^{-1}$, n=3) ($p < 0.01$). In a similar pattern observed in the glucose parameters tested, the greater difference in plasma insulin at 30 weeks is due to an increase in the WT animal in ageing (15 week, $1.36 \pm 0.17 \text{ ng.ml}^{-1}$; 30 week, $1.92 \pm 0.13 \text{ ng.ml}^{-1}$), whilst the FMO5 KO levels remain unchanged (15 week, $0.72 \pm 0.08 \text{ ng.ml}^{-1}$; 30 week, $0.72 \pm 0.08 \text{ ng.ml}^{-1}$).

At 15 weeks, the KO animals have lower circulating levels of insulin whereas there is no difference in the plasma glucose measurements of the two animals. This suggests the knockout animal is more insulin sensitive; they need lower levels of the hormone

to maintain glycaemia. At 30 weeks, even though circulating insulin remains higher in the WT when compared to the FMO5 KO, WT animals now also present with higher levels of plasma glucose and worsened glucose tolerance. Therefore, along with having a greater insulin sensitivity from young, the FMO5 KO mouse appears to be resistant to the age-related decline in insulin sensitivity seen in the WT.

3.3.1.3 Insulin Sensitivity Test

To further define the insulin sensitivity of the WT and FMO5 KO animal, the insulin sensitivity test was performed. Insulin sensitivity of an individual can be experimentally determined by injecting a defined amount of exogenous insulin. Measuring the decline in plasma glucose at incremental time points following the injection gives a measure of the hormone's function. As early as 10 weeks of age, the FMO5 KO animal is more insulin sensitive than the WT (Figure 3.7).

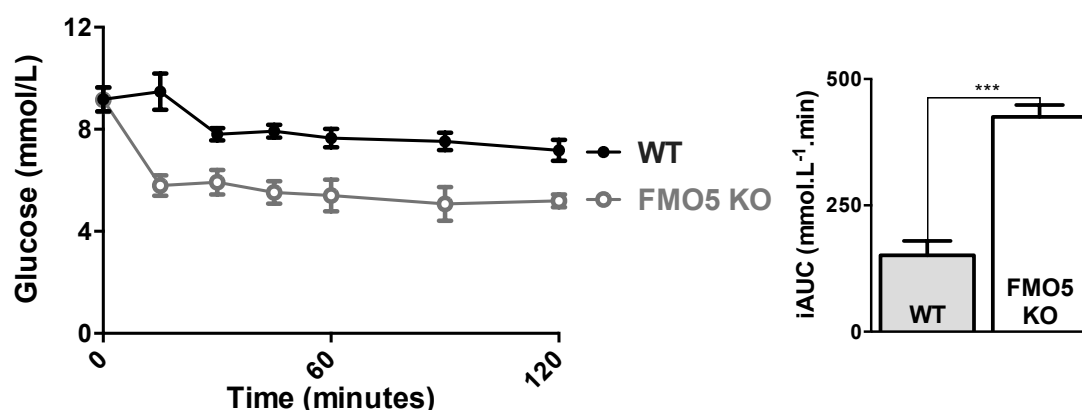


Figure 3.7 –Insulin sensitivity of 10-week old animals. A. Insulin sensitivity was measured in 10-week old male mice (WT, n=4; FMO5 KO, n=4). Left – Plasma glucose following an insulin bolus. Right – Inverse area under the curve (iAUC) analysis. Data is expressed as mean \pm SEM (***: $p < 0.001$).

The 10-week old FMO5 KO animal has a greater response to the same dose of insulin; over the 120-minute time course the animals cleared glucose faster, and to a greater extent than the WT. Subsequently, iAUC values of FMO5 KO animals tested ($425.1 \pm 23.7 \text{ mmol.L}^{-1}.\text{min}^{-1}$, n=4) are significantly greater than that of the WT ($151.1 \pm 28.5 \text{ mmol.L}^{-1}.\text{min}^{-1}$, n=4) ($p < 0.001$). Measurements were also conducted in 15- and 30-week old animals (data not shown) and the insulin sensitivity of the FMO5 KO remains higher than that of the WT throughout ageing.

At 10 weeks of age, the WT and FMO5 KO animals show no difference in weight, plasma insulin, glucose and cholesterol (Figure 3.8). Therefore, preceding all other observed phenotypes, the first measured difference in the FMO5 KO animal is an enhanced insulin sensitivity; inactivation of the *Fmo5* gene results in a greater response to an exogenous dose of insulin. The absence of FMO5 protein further protects the animal from an age-related decline in insulin sensitivity seen in the WT. An elevation in plasma glucose and worsening of glucose tolerance observed in ageing of the WT is not evident in the FMO5 KO, which may therefore explain the attenuation in age-related weight gain.

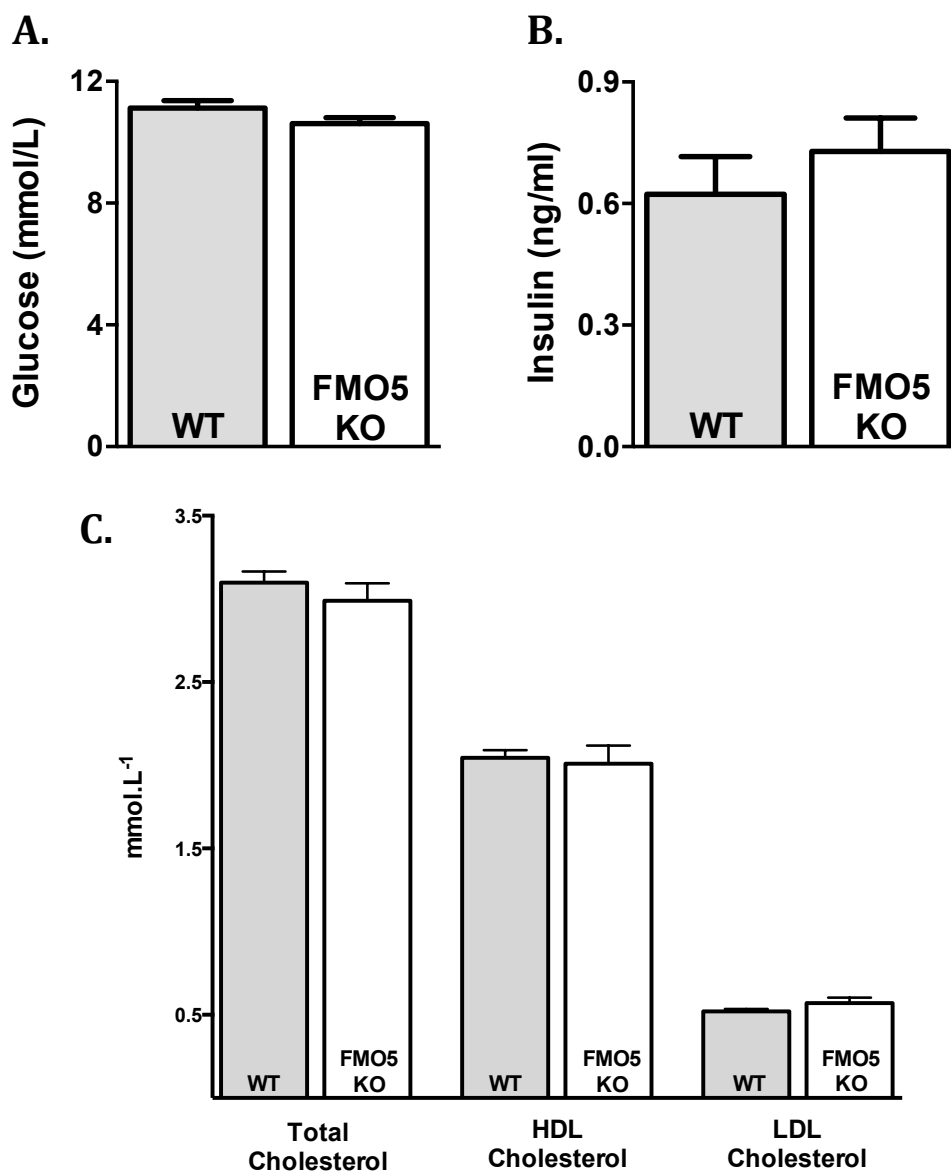


Figure 3.8 – Plasma measurements of 10-week old mice - A. Plasma glucose (WT, n=23; FMO5, n=27), **B.** Plasma insulin (WT, n=4; FMO5, n=4) and **C.** Plasma cholesterol (WT, n=11; FMO5 KO, n=8) was measured between 9-11 am in 10-week old male mice.

In addition, as the differences seen in cholesterol also occur secondary to the difference in insulin sensitivity of the animals, it is tempting to speculate the higher levels of cholesterol in the WT is a consequence of the changes in insulin, whether it be the loss of sensitivity or increase in circulating levels. A wealth of human studies has provided evidence for disturbances in insulin signaling conferring a detrimental influence on cholesterol metabolism. Whole-body cholesterol homeostasis is achieved by the well-governed interplay of endogenous cholesterol synthesis, intestinal absorption and cholesterol clearance (Taverne et al., 2013). Insulin levels, insulin resistance and diabetes are positively associated with an increase in cholesterol synthesis and consequent decrease in intestinal absorption (Simonen et al., 2002a; Pihlajamäki et al., 2004; Gylling et al., 2010; Hoenig and Sellke, 2010; Simonen et al., 2011; Paramsothy et al., 2011). Higher fasting glucose levels alone were sufficient to disrupt the balance of synthesis and absorption (Stranberg et al., 1996; Gylling et al., 2010), and coronary heart disease events are shown to have a greater dependency on insulin resistance and diabetes than baseline HDL cholesterol and triglycerides (Robins et al., 2003).

Currently the mechanism of this cross talk remains unclear. It has been postulated hepatic insulin resistance and/or accompanying hyperinsulinaemia may activate the transcription factor sterol regulatory element binding protein 2 (SREBP-2) resulting in the upregulation of cholesterol synthesis genes, or intestinal insulin resistance would modify transporter expression hence decreasing cholesterol transport (Stranberg et al., 1996; Gylling et al., 2010; Simonen et al., 2011). However, Pihlajamäki et al. suggest the observed decrease in absorption is likely to be merely secondary to the insulin-mediated increase in cholesterol synthesis (Pihlajamäki et al., 2004). An alternative explanation is insulin resistant adipocytes secrete more free fatty acids, which would increase hepatic very low density lipoprotein production, however whether this is capable of concomitantly inducing cholesterol production remains unclear (Simonen et al., 2002a; Pihlajamäki et al., 2004).

Body weight (Simonen et al., 2002b) and specifically visceral fat (Peltola et al., 2006) are also considered catalysts for unregulated cholesterol metabolism. Several of the studies mentioned above state the relationship between insulin resistance and perturbed cholesterol metabolism is obesity independent by virtue of body weight and

BMI measurements, however the measurement of abdominal or visceral adiposity and its contribution is lacking. The role of abdominal fat in the aetiology of insulin resistance is indisputable and it may in fact be a common component of the insulin resistance states used to describe the correlation with cholesterol metabolism in these studies. Therefore, the specific delineation of insulin resistance and obesity in cholesterol homeostasis remains elusive as the latter often accompanies the former. Interestingly however, in comparisons of the WT and FMO5 KO mouse, we observe a difference in insulin sensitivity followed by an increase in cholesterol, prior to any difference in body weight and visceral fat.

3.3.2 The FMO5 KO Animal is Resistant to High-fat Diet Induced Weight Gain

3.3.2.1 Body Weight Analysis

In light of the FMO5 KO mice, fed a standard chow diet, exhibiting reduced weight gain post 20 weeks of age (see Figure 3.2), the effect of a high-fat diet on these animals was investigated (Figure 3.9). At 33 weeks of age, WT and FMO5 KO animals were fed either a standard chow or a high-fat diet.

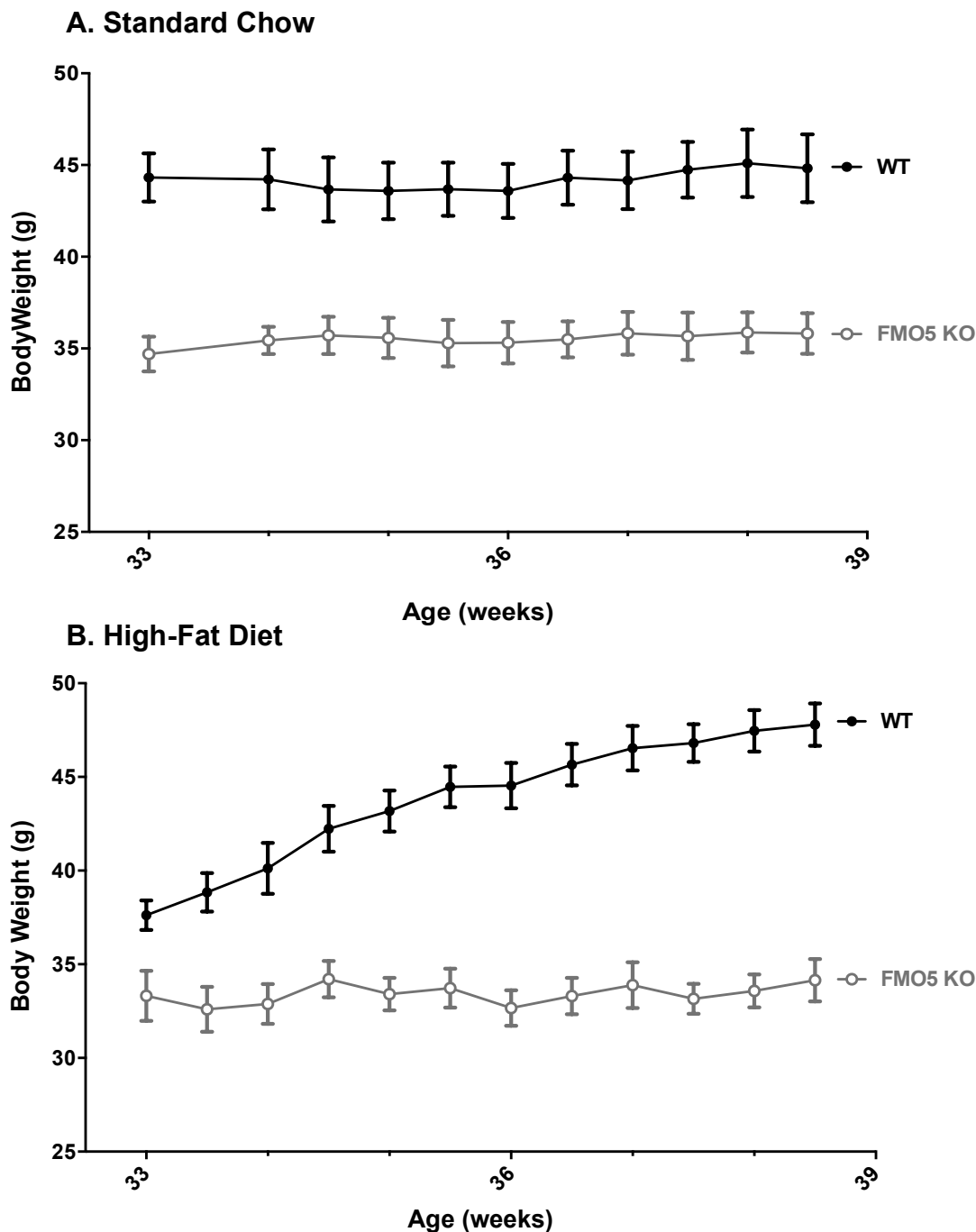


Figure 3.9 – Body weight measurements of mice fed standard chow (A) or a high-fat diet (B). Male mice were fed either a standard chow (WT, n=4; FMO5, n=4) (A) or a high-fat diet (WT, n=7; FMO5, n=7) (B). Mice were placed on the high-fat diet from 33- to 39-weeks of age. Animals were weighed twice weekly during the 6 week diet intervention. Data is expressed as mean \pm SEM.

When fed a standard chow diet, neither cohort of animals gained a significant amount of weight between 33 and 39 weeks of age (figure 3.9-A). When fed a high-fat diet, the weight of the FMO5 KO animal also remains stable; they did not respond to the change in diet. However, high-fat feeding resulted in a substantial increase in body weight in the WT animal (figure 3.9-B). Over the 6-week diet intervention the WT mouse gained, on average, 8.6 ± 0.4 g; over 20 % of their original starting body weight. This resulted in a remarkable disparity in the body weight of the WT and FMO5 KO animal at the end of the study (WT, 46.2 ± 0.9 g, n=7; FMO5 KO, 33.7 ± 1 g, n=7) ($p < 0.0001$); with a difference of more than 25 %. Therefore, as well as curtailing weight gain in the older mouse, absence of FMO5 also protects the mouse from diet-induced weight gain.

3.3.2.2 Plasma Glucose Measurement

Plasma glucose was measured in WT and FMO5 KO animals following the 6-week high-fat feeding period (Figure 3.10). High concentration of lipids in the blood (lipaemia), resulting from the high-fat diet, can interfere with biochemical analyses. Animals were therefore starved overnight prior to blood collection. For comparison, both WT and FMO5 KO animals fed both the standard chow and high-fat diet were starved overnight.

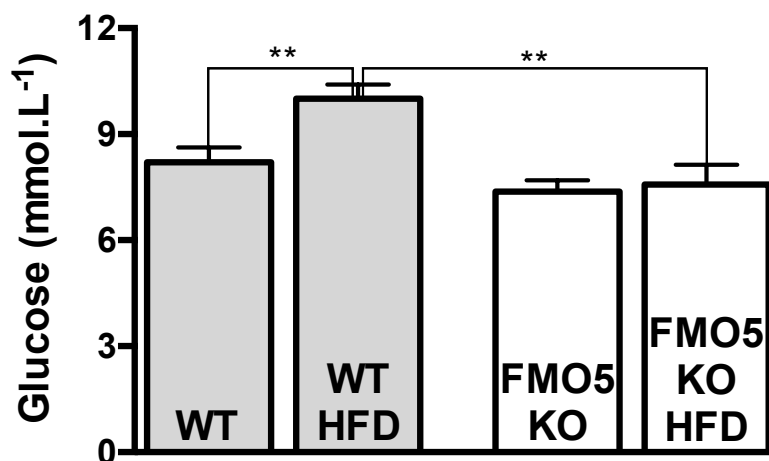


Figure 3.10 – Plasma glucose of mice fed a standard chow or high-fat diet (HFD). Plasma glucose was measured between 9-11 am in overnight-starved male mice fed a standard chow (WT, n=10; FMO5 KO, n=10) or a high-fat diet (WT HFD, n=9; FMO5 KO HFD, n=7). Data is expressed as mean \pm SEM (**: $p < 0.01$).

WT animals fed a high-fat diet (WT HFD) had significantly higher starved plasma glucose than those fed standard chow (WT) (WT, $8.21 \pm 0.42 \text{ mmol.L}^{-1}$, n=10; WT HFD, $10.01 \pm 0.40 \text{ mmol.L}^{-1}$, n=9) ($p < 0.01$). Plasma glucose concentration of FMO5 KO mice fed either the standard chow (FMO5 KO) or high-fat diet (FMO5 KO HFD) was however similar (FMO5 KO, $7.38 \pm 0.32 \text{ mmol.L}^{-1}$, n=10; FMO5 KO HFD, $7.57 \pm 0.56 \text{ mmol.L}^{-1}$, n=7). Subsequently, there is a significant difference in the starved plasma glucose values of the WT and FMO5 KO animals fed a high-fat diet (WT HFD, $10.01 \pm 0.40 \text{ mmol.L}^{-1}$; FMO5 KO HFD, $7.57 \pm 0.56 \text{ mmol.L}^{-1}$) ($p < 0.01$). Therefore, as well as protecting the animal from diet-induced weight gain, the absence of FMO5 also prevents elevations in blood glucose in response to high-fat feeding.

3.3.2.3 *Glucose Tolerance Measurement*

To further investigate the diet-induced changes in glucose metabolism, the glucose tolerance test was performed on WT and FMO5 KO animals fed either the standard chow or high-fat diet (Figure 3.11).

Accompanying the rise in plasma glucose, WT animals fed the high-fat diet (WT HFD) had impaired glucose tolerance compared with mice fed standard chow (WT). A higher, and more sustained, glucose peak resulted in a significant difference in calculated AUC values (WT, $1278.3 \pm 124.7 \text{ mmol.L}^{-1}.\text{min}^{-1}$, n=5; WT HFD, $1901.4 \pm 97.0 \text{ mmol.L}^{-1}.\text{min}^{-1}$, n=4) ($p < 0.01$). The glucose tolerance of the FMO5 KO mice however, was similar on the standard chow (FMO5 KO) and high-fat diets (FMO5 KO HFD) (FMO5 KO, $594.0 \pm 124.5 \text{ mmol.L}^{-1}.\text{min}^{-1}$, n=5; FMO5 KO HFD, $811.7 \pm 88.8 \text{ mmol.L}^{-1}.\text{min}^{-1}$, n=4). A pronounced difference is therefore observed in the glucose tolerance of WT and FMO5 KO animals fed a high-fat diet (WT HFD, $1901.4 \pm 97.0 \text{ mmol.L}^{-1}.\text{min}^{-1}$, n=4; FMO5 KO HFD, $811.7 \pm 88.8 \text{ mmol.L}^{-1}.\text{min}^{-1}$, n=4) ($p < 0.001$).

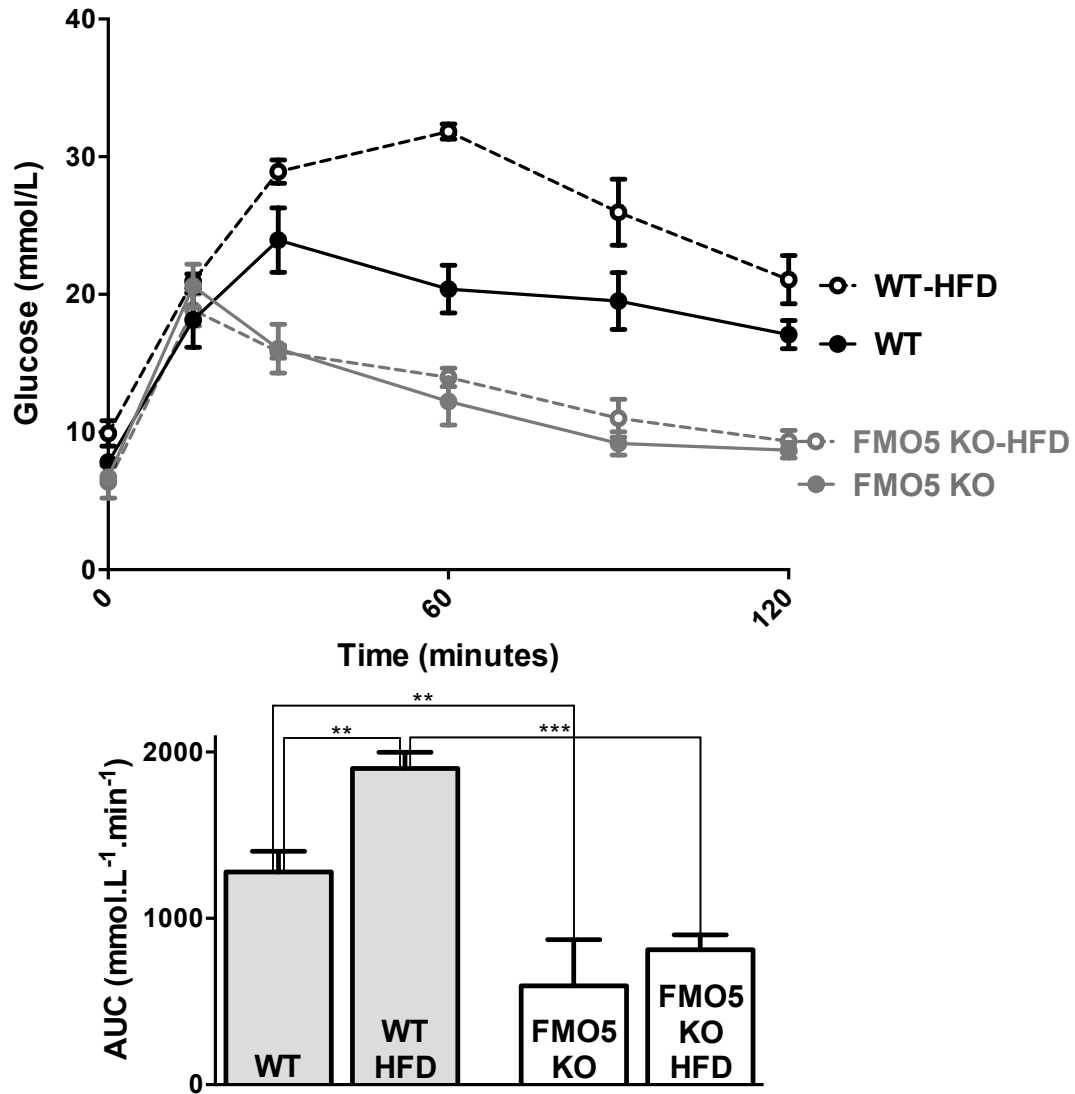


Figure 3.11 –Glucose tolerance of animals fed a standard chow or high-fat diet (HFD). Glucose tolerance was measured in male mice fed standard chow (WT, n=5; FMO5 KO, n=5) or a high-fat diet (WT HFD, n=4; FMO5 KO HFD, n=4). Above – Plasma glucose levels following a glucose bolus. Below – Area under the curve (AUC) analysis. Data is expressed as mean ± SEM (**: $p < 0.01$, ***: $p < 0.001$).

3.3.2.4 Plasma Insulin Measurement

The effect of high-fat feeding on plasma insulin levels was also determined (Figure 3.12). Insulin was measured in plasma of high-fat diet fed animals, which had not been starved, and compared to those fed standard chow.

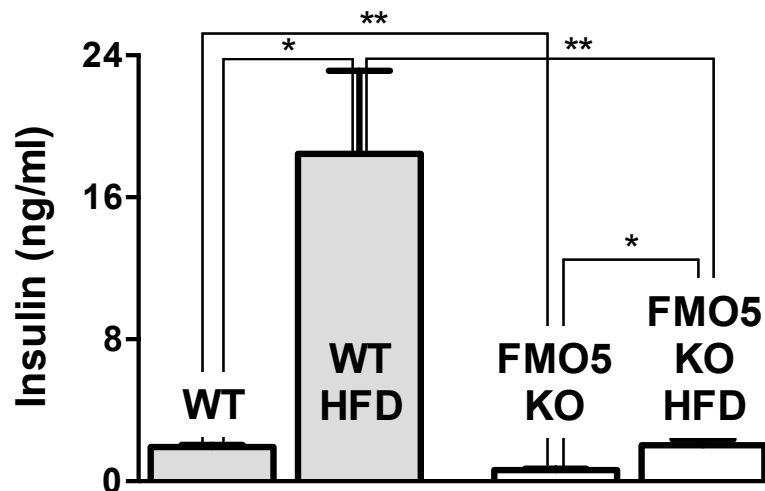


Figure 3.12 – Plasma insulin of animals fed standard chow or a high-fat diet. Plasma insulin was measured between 9-11 am in male mice fed standard chow (WT, n=3; FMO5 KO, n=3) or a high-fat diet (WT HFD, n=3; FMO5 KO HFD, n=4). Data is expressed as mean ± SEM (*: $p < 0.05$, **: $p < 0.01$).

The high-fat diet (HFD) resulted in a great increase in plasma insulin levels in the WT mice (WT, $1.92 \pm 0.13 \text{ ng.ml}^{-1}$, n=3; WT HFD, $18.45 \pm 0.13 \text{ ng.ml}^{-1}$, n=3) ($p < 0.05$). After high-fat feeding, the WT insulin level exceeds 10 ng/ml; the value of the highest point of the standard curve permissible with the chosen method of ELISA quantification. These values are therefore not precise, but instead in excess of 10 ng/ml. The insulin concentration value of $>10 \text{ ng.ml}^{-1}$ indicates a greater than five-fold increase in plasma insulin is needed to regulate glycaemia in the high-fat fed WT mice. The plasma insulin concentration of the FMO5 KO animal is also elevated in high-fat feeding (FMO5 KO, $0.63 \pm 0.08 \text{ ng.ml}^{-1}$ n=3; FMO5 KO HFD, $2.03 \pm 0.33 \text{ ng.ml}^{-1}$, n=4) ($p < 0.05$). The increase is however much lower when compared to that seen in the high-fat fed WT mouse and, in high-fat feeding, levels are still significantly lower in the FMO5 KO mouse (WT HFD, $18.45 \pm 0.13 \text{ ng.ml}^{-1}$, n=3; FMO5 KO HFD, $2.03 \pm 0.33 \text{ ng.ml}^{-1}$, n=4;) ($p < 0.01$),

High-fat feeding results in further loss of glycaemic control in the WT animal due to the development of insulin resistance. In spite of raised circulating insulin, the animal is no longer responding to the hormone effectively and has higher starved plasma glucose than WT mice fed a standard chow. Conversely, the knockout animal is protected. During high-fat feeding, the FMO5 KO mouse maintains glucose homeostasis due to a sustained, higher insulin sensitivity compared to the WT.

3.3.2.5 *Plasma Cholesterol Measurement*

Measurements of plasma cholesterol also indicate the protective effect of the absence of FMO5 when mice are fed a high-fat diet (Figure 3.13). Measurements were conducted in plasma of starved animals to avoid lipaemia interference with the assays in high-fat diet treated cohorts.

As discussed above, as early as 15 weeks, total, HDL and LDL cholesterol is lower in the FMO5 KO (*see* Figure 3.4). However, when measurements are conducted in plasma of starved animals to avoid lipaemia interference, there is no difference in values of total, HDL and LDL cholesterol in the WT and FMO5 KO animals fed a standard chow diet. Yet, when compared to animals fed standard chow (WT), WT animals fed a high-fat diet (WT HFD) have significantly higher total cholesterol (WT, $3.78 \pm 0.08 \text{ mmol.L}^{-1}$, n=4; WT HFD: $5.53 \pm 0.18 \text{ mmol.L}^{-1}$ n=4) ($p < 0.0001$), HDL cholesterol (WT, $2.77 \pm 0.08 \text{ mmol.L}^{-1}$, n=4; WT HFD, $4.03 \pm 0.15 \text{ mmol.L}^{-1}$, n=5) ($p < 0.001$) and LDL cholesterol (WT, $0.59 \pm 0.01 \text{ mmol.L}^{-1}$, n=4; WT HFD, $0.91 \pm 0.05 \text{ mmol.L}^{-1}$, n=5) ($p < 0.001$). The plasma cholesterol levels of the FMO5 KO mice however remain unchanged in high-fat feeding.

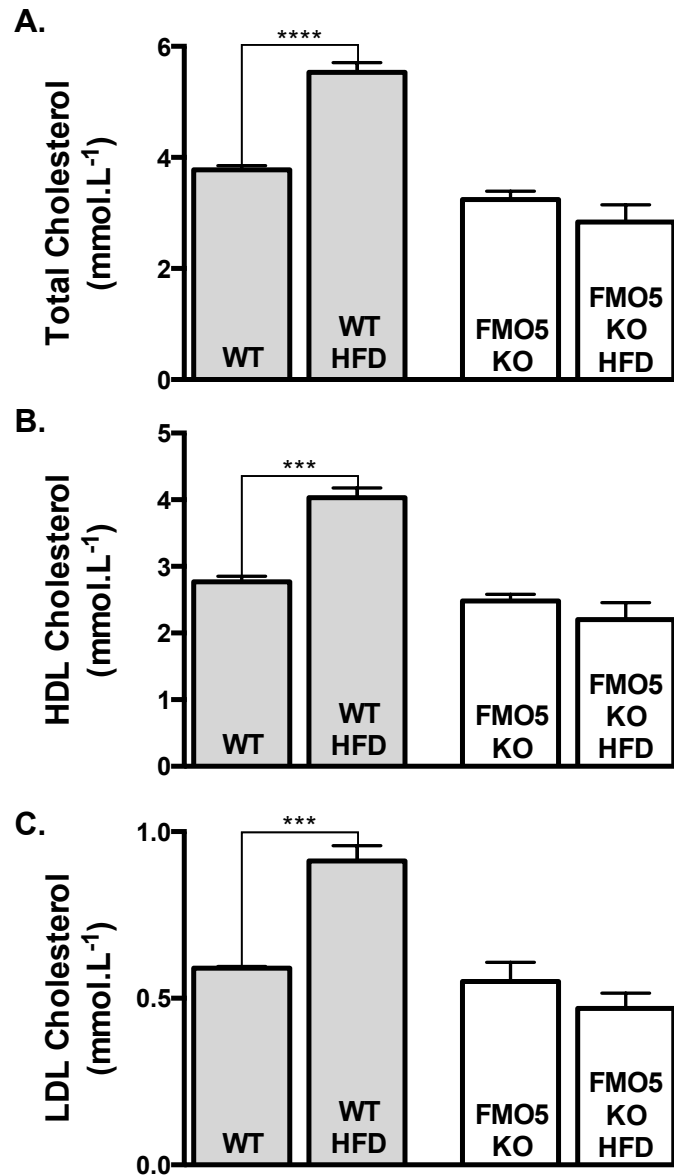


Figure 3.13 – Plasma cholesterol measurements of animals fed a standard chow or high-fat diet (HFD). Total, HDL and LDL cholesterol was measured in overnight-starved male mice fed a standard chow (WT, n=4; FMO5, n=4) or high-fat diet (WT HFD, n=5; FMO5 KO HFD, n=4). Data is expressed as mean \pm SEM (***: $p < 0.001$, ****: $p < 0.0001$).

The WT animal has shown the canonical response to a high-fat diet; a loss in the control of glycaemia due to insulin resistance, increase in plasma cholesterol and excessive weight gain. The absence of FMO5, however, results in a protective phenotype. Throughout the period of high-fat diet feeding, the FMO5 KO mouse remains lean with unaltered glucose and cholesterol profiles and only a small increase in plasma insulin. We propose this to be due to the heightened insulin sensitivity of the FMO5 KO.

3.3.3 *The Effect of an Antibiotic Treatment in the WT and FMO5 KO Animal*

The gut microbiota is considered an environmental factor, capable of modulating host insulin signaling and energy storage (Bäckhed et al., 2004). To explore a role of the intestinal bacteria in the differing phenotypes of the WT and FMO5 KO animal, both mouse lines were subjected to a 4-week antibiotic treatment. Low doses of ampicillin (gram negative) and neomycin (gram positive) antibiotics were co-administered in drinking water, with the aim of reducing the bacterial load of the intestine. These antibiotics were selected based on previous reports of treatment targeting the intestinal microbiota alone. A sustained, low dose treatment ensures poor absorption of the antibiotics from the gut and avoids a systemic, off-target effect in the animal (Vijay-Kumar et al., 2007; Cani et al., 2008a; Membrez et al., 2008). In agreement with previous observations of antibiotic treated animals (Vijay-Kumar et al., 2007), WT and FMO5 KO mice that underwent treatment presented with an enlarged cecum. This is indicative of an elimination of the intestinal microbiota. Furthermore, in plasma analysis of antibiotic treated animals, circulating bacterial metabolites were reduced when compared to control treated animals (data not shown).

3.3.3.1 *Plasma Glucose Measurement*

After 2 weeks of treatment, plasma glucose was measured in WT and FMO5 KO animals treated with antibiotics (Figure 3.14). Antibiotic treated WT animals (WT AB) have significantly lower plasma glucose compared to untreated WT mice (WT) (WT, $10.82 \pm 0.16 \text{ mmol.L}^{-1}$, n=22; WT AB, $7.78 \pm 0.41 \text{ mmol.L}^{-1}$, n=4) ($p < 0.0001$). Plasma glucose of FMO5 KO mice treated with antibiotics (FMO5 KO AB) was found to be slightly lower than untreated animals (FMO5 KO) (FMO5 KO: $9.46 \pm 0.28 \text{ mmol.L}^{-1}$ n=21, FMO5 KO AB: $8.30 \pm 0.45 \text{ mmol.L}^{-1}$ n=6), however the reduction was not as great as that seen in the WT and was not significant. Antibiotic treatment, and a reduced microbial load in the intestine, reduces plasma glucose in the WT. Levels of treated WT animals are subsequently similar to those of FMO5 KO animals, which are comparatively unaffected in treatment.

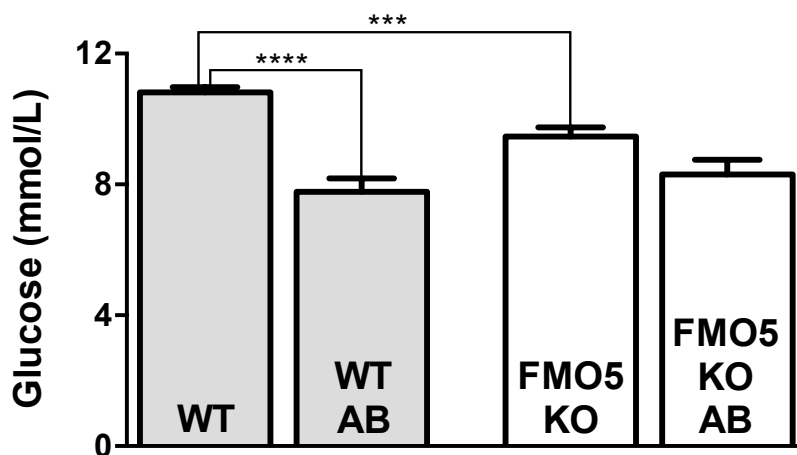


Fig. 3.14 – Plasma glucose of control and antibiotic treated (AB) animals. Plasma glucose was measured between 9-11 am in 30-week old control treated (WT, n=3; FMO5 KO, n=3) and antibiotic treated (WT AB, n=3; FMO5 KO AB, n=3) male mice. Data is expressed as mean \pm SEM (***: $p < 0.001$, ****: $p < 0.0001$).

3.3.3.2 Glucose Tolerance Test

To further analyse glucose homeostasis in response to antibiotic treatment, the glucose tolerance of the treated animals was also measured (Figure 3.15). Antibiotic treatment improves glucose tolerance of WT animals. Treatment resulted in a smaller glucose peak, and faster and more efficient clearance of blood glucose. Together, this results in significantly lower calculated AUC values of treated WT animals (WT AB, $331.0 \pm 17.5 \text{ mmol.L}^{-1}.\text{min}^{-1}$, n=3) compared to untreated controls (WT, $1278.3 \pm 124.7 \text{ mmol.L}^{-1}.\text{min}^{-1}$, n=5;) ($p < 0.05$). No difference in glucose tolerance was observed in antibiotic treatment of FMO5 KO animals (FMO5 KO, $594.0 \pm 124.5 \text{ mmol.L}^{-1}.\text{min}^{-1}$, n=5; FMO5 KO AB, $501.5 \pm 55.2 \text{ mmol.L}^{-1}.\text{min}^{-1}$, n=5). Therefore, a reduction of the intestinal microbiota in response to antibiotic treatment results in improved glucose tolerance of WT animals, and a tolerance that is similar to the untreated FMO5 KO animals. Strikingly however, the glucose tolerance of antibiotic-treated FMO5 KO animals is the same as that of non-antibiotic treated animals.

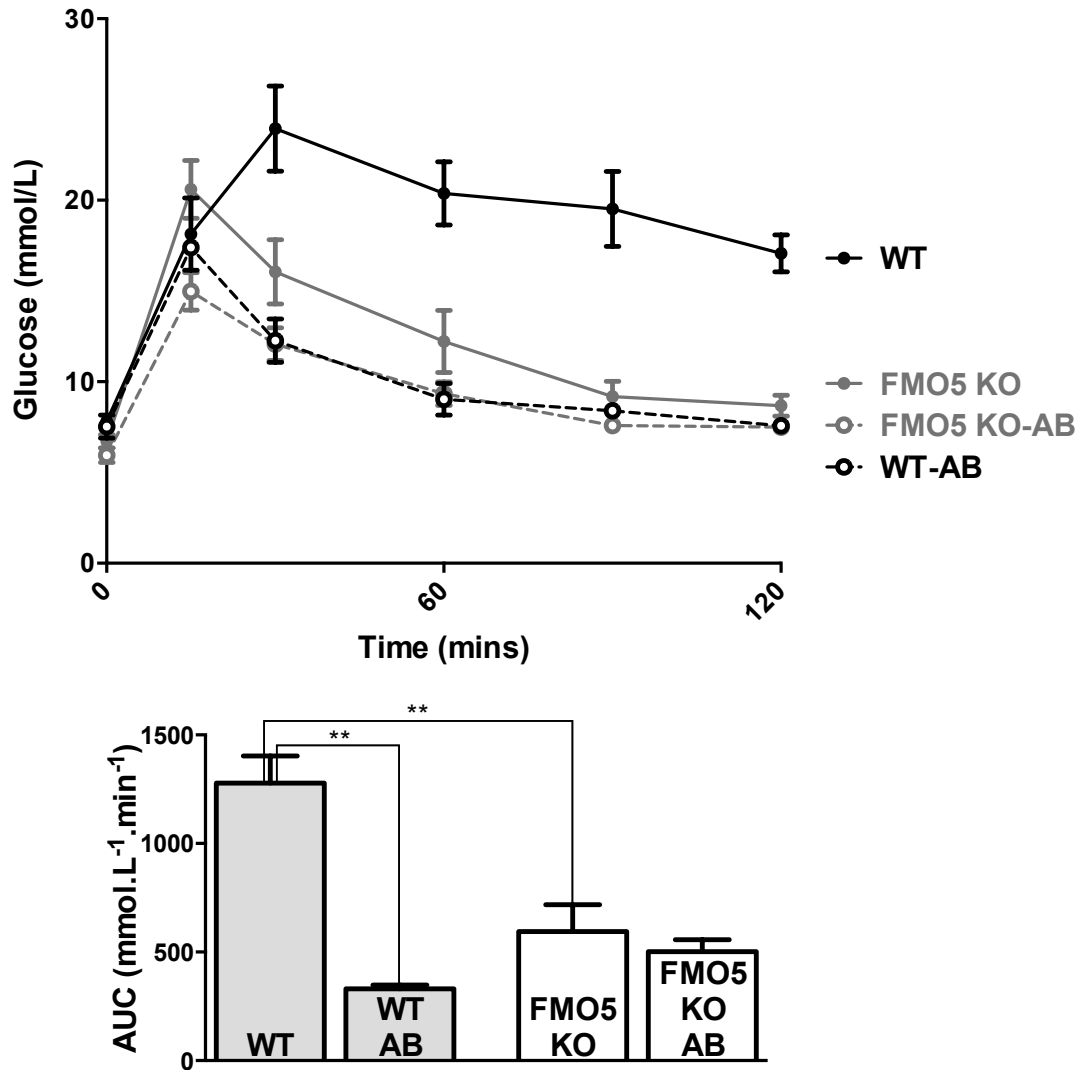


Figure 3.15 –Glucose tolerance of control and antibiotic treated (AB) animals. Glucose tolerance was measured in 30-week old control treated (WT, n=5; FMO5 KO, n=5) or antibiotic treated (WT AB, n=3; FMO5 KO AB, n=5) male mice. Above – plasma glucose levels following a glucose bolus. Below – Area under the curve (AUC) analysis. Data is represented as mean \pm SEM (**: $p < 0.01$).

3.3.3.3 Plasma Insulin Measurement

Plasma insulin was also measured following the antibiotic treatment (Figure 3.16). Similar to the effect on plasma glucose, antibiotic treatment also reduces plasma insulin in the WT animal (WT, $1.92 \pm 0.13 \text{ ng.ml}^{-1}$, $n=3$; WT AB, $0.31 \pm 0.08 \text{ ng.ml}^{-1}$, $n=3$) ($p<0.001$). There was however no difference in plasma insulin after antibiotic treatment of the FMO5 KO animal (FMO5 KO, $0.63 \pm 0.07 \text{ ng.ml}^{-1}$, $n=3$; FMO5 KO AB, $0.55 \pm 0.13 \text{ ng.ml}^{-1}$, $n=3$). These results demonstrate that microbiota modulation, through treatment with antibiotics, reduces circulating insulin in the WT animals. However, this is not the case in the FMO5 KO animal. Along with plasma glucose and glucose tolerance, plasma insulin of the antibiotic-treated WT animals therefore becomes similar to that of the FMO5 KO.

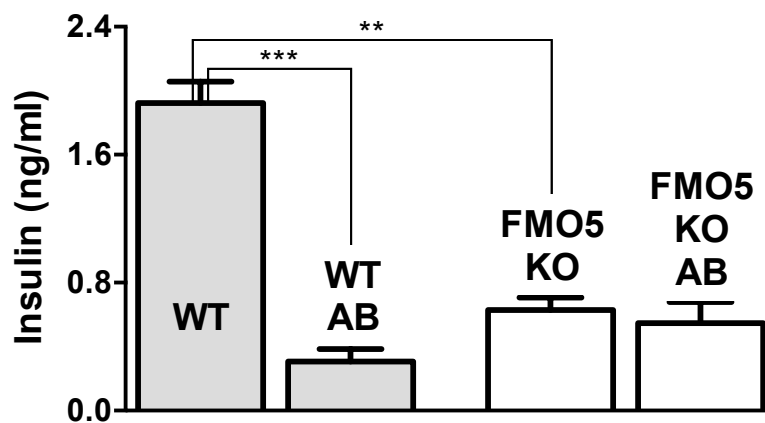


Figure 3.16 – Plasma insulin of control and antibiotic treated (AB) animals. Plasma insulin was measured between 9-11 am in 30-week old control treated (WT, $n=3$; FMO5 KO, $n=3$) and antibiotic treated (WT AB, $n=3$; FMO5 KO AB, $n=3$) male mice. Data is expressed as mean \pm SEM (**: $p<0.01$, ***: $p<0.001$).

3.4 CONCLUSIONS

Inactivation of *Fmo5* results in a heightened insulin sensitivity from young and protection from the age-related decline in insulin signaling. The FMO5 KO therefore remains leaner in old age and has improved parameters of glucose homeostasis and cholesterol metabolism. Furthermore, the KO are protected from the diet-induced obesity and disruptions in glucose homeostasis observed in WT animals upon high-fat feeding.

In response to microbiota modulation, there is an improvement in insulin sensitivity of the WT animal. A sustained, low-dose antibiotic treatment designed to specifically target the intestinal microbiota has reduced circulating insulin and improved glucose homeostasis of the WT. As a consequence, the glucose profile of the antibiotic-treated WT now resembles that of the FMO5 KO animal. The improved metabolic phenotype of specifically the WT animal in antibiotic treatment is in support of previous studies of germ-free and conventionally raised animals, indicating the intestinal microbiota's influence in insulin signaling (*see* 1.2.2). The failure of treatment to produce a comparable response in the FMO5 KO points towards a role of this protein in the host response to the commensal bacteria of the intestine. The phenotype of the untreated KO is similar to a germ-free WT; in the absence of FMO5 the animal is "pseudo germ-free".

***Chapter 4 – The Intestine and the Commensal
Microbiota***

Modulation of the intestinal microbiota had a great effect on the metabolic phenotype of the WT animal. The same treatment did not however result in any consequence in the FMO5 KO. This led investigations into the intestine of the WT and FMO5 KO animals. Previous investigations into the function of FMO5 have focused on its primary site of expression; the liver (Janmohamed et al., 2004; Zhang and Cashman, 2005). However, FMO5 is also expressed in the digestive tract, where its role is also unclear.

4.1 INTRODUCTION

4.1.1 Intestinal Epithelial Cells

The role of the intestine is the digestion and absorption of ingested food. The intestine is also the major site of bacterial colonisation of the human; with over a 100 trillion microorganisms present, it is one of the most extensively populated microbial communities on earth (Ley et al., 2006a). The other essential role of the intestine is therefore the elimination of microbes and microbial products along with undigested dietary components. Intestinal epithelial cells (IECs) constitute the interface between the host and this luminal environment; they serve as the first line of defense against potential pathogens. Not only a physical barrier, allowing the selective absorption of nutrients and denial of antigenic compounds, IECs are also a vital component of the innate immunity of the intestine. They are able to recognise pathogens, activate the host immune system and secrete antimicrobials and cytokines accordingly. A protective mucus layer, intercellular tight junctions and the adaptive and innate immune system of the host synergistically regulate the integrity of IECs. Therefore, the precise interaction between the commensal bacteria of the intestine, the mucus layer, the epithelia and host immunity is fundamental in maintaining intestinal homeostasis. Disruptions or dysregulation in this cross talk leads to a compromise of the protective barrier, with increased permeability having the potential to lead to chronic inflammation and systemic deleterious consequences in the host (Strober et al., 2002; Kim and Ho, 2010; Pastorelli et al., 2013).

4.1.2 The Intestinal Microbiota

4.1.2.1 Intestinal Microbiota and Inflammation

The persistence and proximity of the intestinal microbiota to the mucosal barrier almost makes them self-antigens in the digestive tract. Consequently, the appropriate reaction of the host immune response in the intestine could be considered a form of autoimmunity. The presence of the microbiota is indeed the stimulus for intestinal inflammation and specific species (or an altered population) appear to be more important than others. Consequently, microbial classification of the intestinal lumen has undergone extensive investigation in pathophysiologies such as inflammatory bowel disease (IBD) and Crohn's disease. However, these inflammatory disorders are more likely to be a result of the inappropriate activation of the host immune system rather than dysbiosis itself. Both IBD and Crohn's disease are a result of several genetic abnormalities, both presenting as a loss in tolerance to commensal bacteria required for the functional integrity of the intestine (Specian and Oliver, 1991; Kim and Ho, 2010; Hooper and Macpherson, 2010; Pastorelli et al., 2013).

Correct recognition of commensal bacteria is therefore required for intestinal homeostasis. IECs expressing toll like receptors (TLRs) have been shown to be of critical importance. Deletion of TLR5 led to the development of spontaneous colitis in mice due to a higher microbial burden in the intestine (Vijay-Kumar et al., 2007). This specific knockout also went on to develop a phenotype resembling human metabolic syndrome (higher body mass, hyperglycaemia and insulin resistance), indicating the possible role of intestinal inflammation in systemic metabolic phenotypes (Vijay-Kumar et al., 2010).

Several genetic polymorphisms of TLRs have been associated with inflammatory disorders and further mouse knockout studies have strengthened the link between defective TLR function and intestinal infection (Pastorelli et al., 2013). However, reduced TLR5 function is also suggested to be protective. Heterozygote carriers of a TLR5 polymorphism, resulting in a premature stop codon, have reduced TLR5 activity which results in a dampened response to the bacterial antigen flagellin, and was also negatively associated with the incidence of Crohn's disease (Gewirtz, 2006). Therefore, although it is clear detection of the microbiota is vital, in this example

where an individual is not completely deficient in TLR5 function, a perhaps “less active” immune response can be beneficial.

4.1.2.2 *Dysbiosis in Metabolic Disorders*

Along with a hand in the instigation of inflammation, the intestinal microbiota has also been linked with the incidence of obesity in an individual. Dysbiosis, specifically the increase in Firmicutes and concomitant decrease in Bacteroidetes phyla, has been reported in both obese animals and humans (Ley et al., 2005; Turnbaugh et al., 2009a). This change is reversed when obese subjects were subjected to a low calorie diet. Following weight loss, the obese subjects’ microbiota began to resemble that of a lean subject (Ley et al., 2006b). What remains unclear however, is whether changes in the microbiota composition is a cause or simply an effect of an obesogenic state. In fact, extensive studies have, perhaps unsurprisingly, indicated the extent to which the diet can affect the microbiota (Turnbaugh et al., 2009b; Hildebrandt et al., 2009; Koropatkin et al., 2012; Tachon et al., 2012; Sahasakul et al., 2012), and the speed of response of the host to dietary changes (Burcelin et al., 2011; Angelakis et al., 2012).

Nevertheless, the population of bacteria residing in the gut became to be regarded as an important factor in the cause and contribution of obesity. The microbiota was considered as a modulator of how an individual is able to harvest energy from their diet (Turnbaugh et al., 2006). Indeed, changes in metabolism upon conventionalisation illustrate how the presence of the microbiota alone is a powerful influence (*see* 1.2.2). However, given it is host cells of the intestine which recognise the commensal bacteria, it is now regarded as a much more complicated paradigm. In fact, again it is the host-genetic component, influencing how these intestinal cells function, which is now regarded as paramount in intestinal homeostasis and subsequent energy storage. Discussed herein is one such intestinal cell lineage, the goblet cell.

4.1.3 Goblet Cells

Along with absorptive enterocytes, Paneth cells and enteroendocrine cells, goblet cells make up the intestinal mucosal epithelium. Goblet cells function to secrete bioactive molecules into the lumen of the intestine and goblet cell differentiation is a hallmark of intestinal inflammation. Goblet cells originate from stem cells in the lower regions of colonic crypts and very rapidly begin to synthesise mucins. Mature goblet cells are located on the upper region of the crypt, where they are polarized and specialised in unidirectional secretion of mucin granules. Upon secretion, along with other factors, mucins form the mucus layer; a physical separation between the apical IEC membrane and the luminal bacteria. This layer serves as a lubricant; allowing the passage of organisms and molecules down the digestive tract, and as a molecular sieve; the penetrative capacity of a molecule is governed by its molecular weight (Nimmerfall and Rosenthaler, 1980; Smithson et al., 1981; Specian and Oliver, 1991).

The mucin matrix serves as a diffusion gradient of IEC-secreted factors and the mucus layer can be further divided into two distinct zones. Antimicrobials secreted by IECs are high in concentration close to the apical epithelial cell surface, creating a relatively sterile environment. The outer layer, devoid of antimicrobials, is however rich in bacteria as mucin oligosaccharides provide a site of adherence and a source of energy for invading microbes. This ‘mucosal trapping’, along with the secretion of IgA, is thought to limit the association of bacteria with the epithelial cell membrane, hence preventing bacterial invasion of host tissue. It is apparent that defects in this mucosal protection allows bacterial penetration and consequent inflammation; IBD patients have more bacteria associated with the epithelial cell surface (Roze et al., 1982; Hooper and Macpherson, 2010).

A necessary balance of synthesis, secretion and degradation of the mucus layer is achieved by bacterial breakdown and the mechanical force of peristalsis. However, quantitative and qualitative changes are seen in mucus production in certain pathologies. Normally, many mucin granules lie beneath the apical membrane of a goblet cell, and the baseline mucus layer is maintained by the continuous exocytosis of just one granule. However when challenged physically or chemically, the goblet cell is able to rapidly secrete its entire granule mass. Mucin is then quickly

resynthesized and the cell is refilled with granules during an acute phase of infection (Specian and Oliver, 1991; Kim and Ho, 2010). However, in chronic infection, hence sustained increased secretion of mucins, goblet cells are depleted and the mucus barrier is weakened due to altered synthesis and impaired secretion of mucins (Kim and Ho, 2010).

MUC2 is the main structural component of the mucus layer. It is clear mucins of the mucus layer have a critical role in epithelial protection, as knockouts and genetic polymorphisms in the *MUC2* gene lead to spontaneous colitis due to a poorer barrier function of the intestinal lumen (Van der Sluis et al., 2006; Heazlewood et al., 2008). However, mucin overproduction can also be pathogenic. A mouse line defective in IEC signaling (*Pofut1*^{-/-}) exhibits goblet cell hyperplasia and hypertrophy leading to the overproduction of mucus. As early as four weeks, these mice display colonic inflammation thought to be a result of a change in the bacteria associated with the colonic mucosa (Guilmeau et al. 2008).

Therefore, mucins appear to be tightly regulated in the homeostasis of the epithelial barrier, with pathologies being associated with both under and over production. This is further confounded by goblet cell ablation experiments. Unexpectedly, mice with a 60% reduction of goblet cells in the large intestine were protected from intestinal injury. Despite goblet cell depletion, MUC2 expression was comparable to the control mice, suggesting a compensatory overproduction of MUC2 (Itoh et al., 1999; Van der Sluis et al., 2006; Guilmeau et al., 2008; Heazlewood et al., 2008). The protection mediated by fewer goblet cells therefore indicates the significance of other goblet cell secreted factors in the protection from inflammation. A goblet cell secreted factor that has been extensively studied in intestinal homeostasis is resistin like molecule β .

4.1.4 Resistin Like Molecule β

Murine resistin is an adipose tissue derived hormone, which antagonises the action of insulin in the liver (Steppan et al., 2001a; Youn et al., 2004). The expression of resistin in human adipose tissue is much lower and the biological relevance of the

human orthologue however remains unclear (Yang et al., 2003). More recently, a family of resistin-like molecules (RELMs), or molecules found in inflammatory zones (FIZZ), were concomitantly characterised in the mouse. Subsequently, resistin and the three structurally related RELMs, RELM α , RELM β and RELM γ , constitute a family of proteins with isoform specific tissue expression.

Murine RELM α (FIZZ1) mRNA was located to several tissues including white adipose tissue and the lungs, where it is induced upon epithelial injury. RELM β (FIZZ2) was however found exclusively in goblet cells of the murine digestive tract, most abundant in the colon and to a lesser extent in the small intestine. RELM γ (FIZZ3) was expressed in the white adipose tissue of many of the organs tested. RELM proteins are secreted and, unlike the family founder resistin, are all induced in type 2 infection. Human orthologues of RELM α and RELM γ have not been identified, however human and mouse RELM β are very highly conserved and display similar expression profiles. Subsequently RELM β has received much more attention in the investigation of colonisation and infection of the gastrointestinal tract, in which it is shown to be apically secreted into the lumen exclusively by colonic goblet cells (Holcomb et al., 2000; Stepan et al., 2001b; Yang et al., 2003; He et al., 2003; Shojima et al., 2005; Hogan et al., 2006).

RELMs contain an N-terminal signal sequence, a variable middle portion and a highly conserved C-terminal region containing 10 invariantly spaced cysteine residues. Like resistin, human and murine RELM β also contain an additional cysteine residue in the N-terminal domain. Whilst the 10 conserved cysteine residues are thought to mediate intramolecular disulphide bonds, the 11th residue mediates the formation of dimers of resistin and RELM β , identified both *in vitro* and *in vivo*. The biological significance of dimer formation is unknown, however studies of resistin indicate the monomer is the bioactive form. The conservation in vertebrates and absence in lower organisms of RELM β suggest its expression in the intestine is a result of host-defense evolution against gastrointestinal infections (Banerjee and Lazar, 2001; Patel, 2004; Artis et al., 2004; Nair et al., 2006).

4.1.4.1 *RELM β in Parasitic Infection*

Gastrointestinal (GI) nematode parasites pose a threat to health, infecting more than one billion people worldwide, and burden the economy in areas of infected livestock. Infection is characterised by goblet cell hyperplasia and a heightened helper T cell-2 (Th2) cytokine response required for worm expulsion (Cliffe and Grencis, 2004).

Whilst Th2 cytokines are considered to have an anti-inflammatory role, Th1 cytokines are associated with proinflammatory effects and perpetuating the autoimmune response. The two distinct sets of cytokines are reciprocally regulated dependent on the type of immune assault and ideally, a correct balance of Th1 and Th2 activation will result in the appropriate response when challenged. In a specific example of parasite infection, Th2 cytokines are required for the expulsion of *Trichuris muris* and resistance to infection. However, Th1 cytokines such as INF γ , are associated with chronic infection and the development of severe intestinal inflammation (Cliffe and Grencis, 2004; Zaph et al., 2007). Different levels of infection of this parasite produce polarised immune responses, hence giving rise to resistant or susceptible phenotypes. At low levels of infection, *Trichuris muris* promotes a Th1 mediated response leading to chronic infection, whereas at higher levels of infection, the release of Th2 cytokines results in worm expulsion. *Trichuris muris* infection has therefore been employed as an experimental system to investigate the two host responses to intestinal infection.

RELM β was originally shown to be coincident with the production of Th2 cytokines IL-4 and IL-13 during parasitic infection and in studies of the RELM β knockout (RELM β KO) mouse, the protein was shown to be required for parasite expulsion (Artis et al., 2004; Herbert et al., 2009). Conversely, when investigating ‘low-dose’ infection, the RELM β KO mouse was protected against intestinal inflammation. Infected RELM β KO mice had lower levels of Th1 proinflammatory cytokines TNF α and INF γ and subsequently less intestinal inflammation than WT controls (Nair et al., 2008). Therefore, along with its identified anti-parasitic effect in the Th2 response, RELM β also has a critical role in the development of severe intestinal inflammation in the chronic Th1 response. This was further explained by the capability of RELM β

to activate macrophages leading to the increased production of $\text{INF}\gamma$ in cellular experiments (Nair et al., 2008).

4.1.4.2 *RELM β in Models of Colonic Injury*

Models of experimentally induced colonic injury further corroborate a role of RELM β in intestinal inflammation. Dextran sulphate sodium (DSS) is a common agent used to induce epithelial injury. Treatment leads to a reduced epithelial barrier function and infiltration of antigenic luminal components into the lamina propria beneath the epithelium. Here, microbial components making contact with the host immune system have the potential to lead to chronic inflammation. The RELM β KO mouse was protected against intestinal inflammation in DSS treatment when compared to a WT control, even though intestinal permeability was present and comparable in both groups. McVay et al. therefore hypothesise that once the epithelial barrier is breached, RELM β is able to permeate and activate host immune cells. In vitro and in vivo experiments revealed macrophages are activated by recombinant RELM β , resulting in the release of inflammatory cytokine TNF- α . In agreement, the RELM β KO mouse has lower colonic levels of TNF- α (McVay et al., 2006).

The protection from DSS treatment in the RELM β KO mouse is further supported by additional investigations by Hogen et al. DSS treatment resulted in a marked increase in RELM β mRNA in the colon of WT mice and in agreement with previous observations, the knockout animals showed less weight loss, diarrhea-rectal bleeding and importantly higher survival rates when treated with the agent. However, an additional observation was made; the permeability of the intestinal membrane, measured by tissue resistance, of untreated mice was higher in the knockout (Hogan et al., 2006). This paradoxically implicates RELM β to have a positive role in normal barrier physiology. Indeed, the animals were more susceptible to inflammation when another agent, trinitrobenzene sulphonate (TNBS) co-administered with ethanol, was used to induce epithelial damage. TNBS functions in a distinct mechanism to DSS and is not accompanied by an increase in RELM β expression (Wirtz et al., 2007). The disparity in the two models of inflammation again presents RELM β as a molecule of conflicting function. In normal physiology, hence 'basal' expression, RELM β is protective and contributes to barrier integrity. However, if induced in models such as

DSS exposure, the protein has a role in disease pathogenesis, contributing to the severity of inflammation.

4.1.4.3 *RELM β in Bacterial Colonisation*

Along with its role in parasitic infection, a relationship between RELM β and the bacterial colonisation of the intestine has also been identified. Commensal bacteria of the intestine has the potential to modify host gene expression and, using germ-free models or antibiotic treatment, has been implicated in several inflammatory disorders of the intestine such as IBD and cystic fibrosis (Norkina et al., 2004a; Wang et al., 2005; Hooper and Macpherson, 2010). RELM β has been characterised as a factor, which is strongly influenced by the presence of the microbiota and the composition of diet, and is also capable of modifying the luminal environment.

He et al. first showed RELM β exists in murine and human stool samples, where it is present as a dimer. RELM β protein expression was markedly reduced in samples from germ-free animals and expression could be recovered by the reintroduction of bacteria into the intestine (conventionalisation). The induction of RELM β expression upon conventionalisation was comparable in severe-combined immunodeficient mice, indicating bacterial mediated RELM β expression is not dependent on the adaptive immune system. Immunohistochemistry instead revealed colonisation of germ-free animals influenced the proliferation and maturation of goblet cells; changing the size, frequency and location of this particular cell lineage and subsequently RELM β expression (He et al., 2003; Wang et al., 2005).

Hildebrandt et al. further confirmed the microbiota-mediated induction of RELM β mRNA and went on to show RELM β protein is robustly induced in stool in response to high-fat feeding. This is supported by colonic mRNA and serum protein measurements conducted by Fujio et al., who also showed feeding alone induces colonic RELM β . Along with increased colonic mRNA, higher levels of epididymal fat were reported after the two-week high-fat diet. Conversely diets high in protein and carbohydrate, diets associated with reduced diabetes incidence and improved waist circumference, led to reduced epididymal fat and lower RELM β expression. Therefore, it is clear RELM β responds to dietary stimuli and levels appear to correlate with changes epididymal fat (Fujio et al., 2008; Hildebrandt et al., 2009).

Analysis of the intestinal bacteria of a RELM β KO mouse also revealed this apically secreted protein modifies the commensal bacteria. When compared to the WT animal, differences in the Bacteroidetes and Firmicutes phyla were reported in the RELM β KO. The same investigation showed the RELM β KO mouse to be protected from diet-induced weight gain (and increase in fat mass) in response to high-fat feeding. When WT and RELM β KO animals were fed a high-fat diet, weight gain was only observed in the WT. Moreover, this protection was mediated independently to changes in the microbial population. In high-fat feeding both animals made the transition to a population well associated with weight gain and increased adiposity, a higher abundance of the Firmicutes phylum with a concomitant decrease in Bacteroidetes (Ley et al., 2005; Turnbaugh et al., 2009a), whereas only the WT controls developed the metabolic phenotype (Hildebrandt et al., 2009).

Collectively these studies implicate RELM β as a microbial sensor in the intestine, susceptible to changes upon conventionalisation and microbial shifts associated with diet. Furthermore, expression is associated with the development of an unfavourable metabolic phenotype in response to dietary changes. However, in the absence of the protein, KO animals do not respond to the high-fat diet and accompanied microbial shift.

Wang et al. went on to show the presence of bacteria specifically upregulates RELM β mRNA in the colon, with levels of family members RELM α and RELM γ remaining unchanged. This is different to parasitic induction of the RELM family, where it is reported all three isoforms are upregulated in the colon and suggests a disparity in bacterial-mediated and infection-induced regulation of RELM β .

4.1.4.4 *RELM β in Other Inflammatory Disorders*

Cystic fibrosis (CF) is a result of mutations in the *CFTR* gene. The CFTR protein controls ion transport across epithelia, hence fluid secretion and the pH of affected organs. CF is consequently characterised by mucus aggregation, due to the poor solubility of secreted mucins and glycoproteins, and inflammation in airways and intestines of sufferers. The cystic fibrosis mouse model presents with an increase in immune cells of the intestine and, along with other genes of the innate immune system, RELM β was shown to be upregulated. Norkina et al. went on to suggest

bacterial overgrowth in the small intestine, mediated by mucus aggregation, could explain intestinal inflammation. Indeed, antibiotic treatment ameliorated the CF phenotype and resulted in a concomitant decrease in RELM β expression (Norkina et al., 2004a; 2004b).

Asthma is another chronic inflammatory disease of the airways. Overproduction of mucus in the mucosa is a hallmark of asthma and other obstructive airway disorders. A marked overexpression of RELM β was reported in the bronchial mucosa of asthmatics, which correlated with impaired lung function and epithelial mucin production. Furthermore, expression was shown to increase with severity of asthma and is further induced upon inhalation challenges (Mishra et al., 2007; Grainge et al., 2012).

In these pathologies ectopic RELM β expression appears to be linked with detrimental over production of mucus. Recently using human colonic cell lines, RELM β was proposed to act as a mucosecretagogue, specifically increasing the production and secretion of mucin MUC2 when applied apically. RELM β mediated MUC2 release was further confirmed by immunohistochemical analysis of colons of mice after receiving intrarectal RELM β infusion (Krimi et al., 2008). This positive regulation of mucin release and mucus formation could very well explain the pathogenicity of the induction of RELM β in disorders of mucosal sites. RELM β over expression at affected sites leads to an overproduction of mucus, which is involved in disease pathogenesis.

A mucosecretory function of RELM β would also explain observations of the RELM β KO mouse. As described previously (*see* 4.1.3), a tight balance of mucin secretion is required, as pathologies are associated with both under and over production. Likewise, a similar control of RELM β expression seems necessary for intestinal homeostasis. In the absence of RELM β , mice have increased permeability of the intestinal epithelium and are more susceptible to certain noxious agents, indicating a requirement for a basal expression of the hormone. However, in conditions of intestinal stress, induction of RELM β participates in disease development. In both DSS treatment and high-fat feeding the RELM β KO mouse is protected from intestinal inflammation and diet-induced weight gain respectively.

4.1.4.5 *RELM β in Insulin Signaling*

As resistin is secreted by adipocytes and reported to inhibit insulin action and adipocyte differentiation, a role of RELM β in insulin signaling has also been investigated. Initially it was demonstrated an intra-arterial bolus of RELM β worsened insulin sensitivity in mice. During pancreatic insulin clamp experiments, lower levels of glucose and higher levels of insulin were required to maintain glycaemia in the RELM β infused animals. An increase in glucose production, resulted by higher levels of glycogenolysis, gluconeogenesis and glucose turnover, indicate an increase in circulating RELM β reduces hepatic insulin sensitivity (Rajala et al., 2003). Although the physiological relevance of the RELM β infusion used in experiments is unclear; as actual RELM β levels entering the portal venous circulation is unknown, these results present an attractive link between a gut-derived hormone and hepatic metabolism.

Kushiyama et al. went on to show hepatic overexpression of RELM β had deleterious consequences in mice challenged with a high-fat diet. Transgenic mice, the livers of which express RELM β , were compared to WT animals in standard chow and high-fat feeding conditions. Only once challenged with a high-fat diet, transgenic animals became glucose intolerant, insulin resistant and displayed insufficient suppression of hepatic gluconeogenesis. This was accompanied by increased serum glucose, insulin and lipids and hepatic triglycerides. In cellular experiments, treatment of cultured hepatocytes with RELM β resulted in activation of JNK, ERK and p38 kinases, all known to inhibit insulin receptor activity, and a subsequent decrease in cellular insulin signaling was observed (Kushiyama et al., 2005). Therefore, although it is clear RELM β has the potential to influence hepatic insulin resistance via MAPKs, the hepatic overexpression of RELM β alone is not sufficient to mediate the progression of systemic insulin resistance; transgenic and control animals in standard chow conditions were comparable. Furthermore the physiological relevance of hepatic overexpression is unclear. The development of insulin resistance is evidently a more complicated event, likely to be influenced by several different extra-hepatic sites.

In a more physiological context, without exogenous doses and overexpression, RELM β and RELM γ were shown to be upregulated in serum of WT (C57BL/6J) mice in response to high-fat feeding. Serum levels were in agreement with an increase in colonic RELM β mRNA and protein, and correlate with body weight and serum

glucose and insulin. This study begins to validate the previously mentioned investigations, indicating RELM β is indeed able to enter circulation from the intestine. However, the disparity in methods of investigation employed makes comparisons of actual levels of resultant circulating RELM β between studies very difficult. RELM β and RELM γ isoforms were also increased in sera and colons of genetically obese (*db/db*) mice. Interestingly, here, RELM β and RELM γ correlated with weight and insulin but not glucose (Shojima et al., 2005). RELM β was therefore proposed as a diagnostic marker for obesity and diabetes, however measurement in human plasma has proved problematic (Neilson et al., 2011).

Krimi et al. have suggested a functional role of RELM β in the jejunum. Experiments using isolated jejunal tissue show a decrease in glucose transport via the Na⁺/glucose cotransporter-1 (SGLT-1) and an increase in the translocation of GLUT2 to the brush border membrane in response to RELM β stimulation (Krimi et al., 2009). The inverse regulation of these two transporters results in the more rapid uptake of glucose in the jejunum tissue, a characteristic response of inflamed tissue due to increased metabolic demand. Although corroborating a role of the protein in inflammation, the relevance of these investigations is again questionable as the jejunum is not the primary site of RELM β expression, and the experiments are conducted *ex vivo* on processed tissue. Moreover, no differences are observed in the plasma glucose of the RELM β KO mouse and elevated RELM β expression is not always associated with elevated serum glucose (Shojima et al., 2005; Hogan et al., 2006).

Whilst the area of research is evidently under debate, we can conclude RELM β has the potential to influence insulin signaling and possibly glucose transport in the instance of inflammation. Indeed, the mechanism of function for RELM β seems to be site specific and therefore the molecule more likely acts as a signal or cytokine, mediating subsequent cellular events, rather than a specific metabolic hormone.

To conclude, a tight balance of RELM β expression in the colon maintains intestinal homeostasis. Basal expression has been indicated to have a positive role in barrier morphology and an anti parasitic function of the protein has been suggested. However, it is also evident the chronic, ectopic or excessive production of such a

factor in sustained infection, high-fat feeding and disease can contribute to the severity of inflammation.

4.2 *EXPERIMENTAL QUESTIONS AND AIMS*

- I. The intestinal microbiota has been proposed as a modulator of host energy storage (*see* 1.2.2). To further characterise the luminal environment of the WT and FMO5 KO animal and its potential role in the metabolic phenotype, the intestinal microbiotas of the two mouse lines, fed either a standard chow or high-fat diet, will be investigated.
- II. To further clarify the expression of FMO5 in the digestive tract, investigations will aim to confirm the presence of the protein and investigate specific localisation in the murine gut. The influence of a high-fat diet in intestinal expression of FMO5 will also be investigated.
- III. Similarities have been observed in the phenotype of the FMO5 KO and RELM β KO mice; both animals are resistant to diet induced obesity. To explore the potential link between the two intestinal proteins, the expression and function of RELM β will be compared between the WT and FMO5 KO animal.
- IV. Furthermore, following the vast improvement in the metabolic phenotype of the WT animal in antibiotic treatment, I will also consider the effect of antibiotic treatment on the expression of proteins of interest, FMO5 and RELM β .

4.3 RESULTS

4.3.1 *A Perturbed Intestinal Microbiota in the FMO5 KO Animal*

A dysbiosis of the intestinal microbiota has been linked with the occurrence of obesity in an individual (Ley et al., 2005; Turnbaugh et al., 2009a). It was proposed a change in the representation of the different phyla, in particular a rise in Firmicutes and decrease in Bacteroidetes, has the potential to alter the capacity of the host to harvest energy from the diet. To investigate a potential role of the intestinal microbiota in the altered energy phenotype of the FMO5 KO, the commensal bacteria of the intestine was profiled in the WT and FMO5 KO animal. DNA was isolated from faecal pellets of WT and FMO5 KO animals, bacterial 16S rRNA genes were selectively amplified, cloned and sequenced. Using the online tool, The Ribosomal Database Project, 16S rRNA sequences were aligned and matched to 16S rRNA sequences of known bacterial origin (Wang et al., 2007; Cole et al., 2009). Initially, the phyla composition was compared between the WT and FMO5 KO microbiota at 7, 10 and 30 weeks of age (Figure 4.1, Table 4.1).

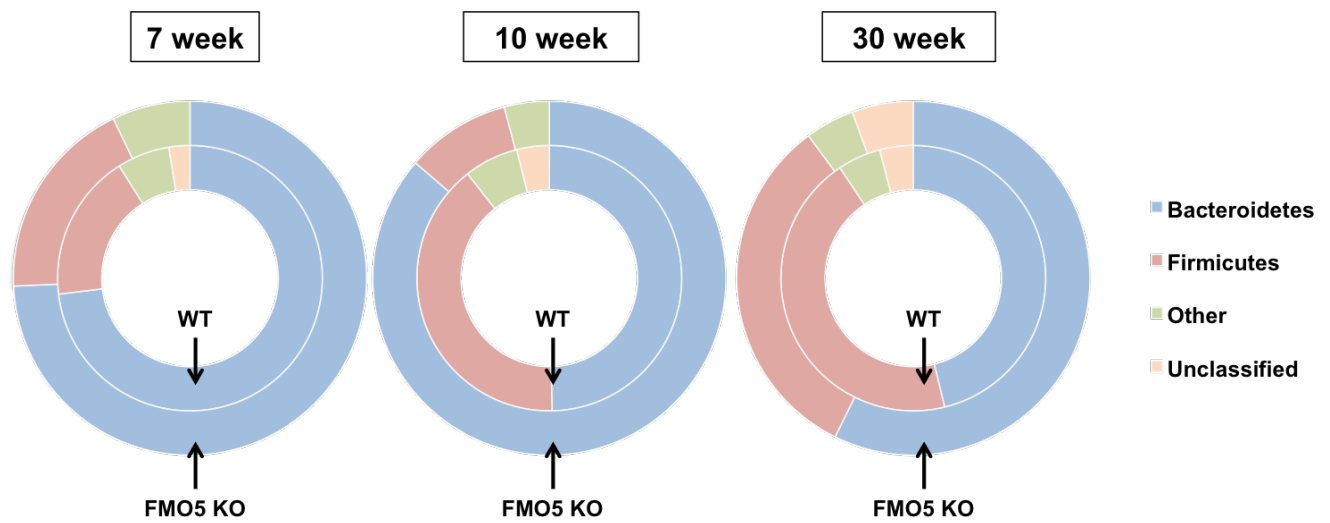


Figure 4.1 – Phyla level analysis of the intestinal microbiota of 7-week, 10-week and 30-week old male WT and FMO5 KO male mice. Sequence reads were pooled from faecal samples of triplicate cages (housing 3-4 mice) for each age point. Analysis was conducted on samples from 7-week (WT, n=79; FMO5 KO; n=70), 10-week (WT, n=156; FMO5 KO, n=73) and 30-week (WT, n=172; FMO5 KO, n=180) old male mice. Data is expressed as a percentage of total sequence reads.

Phylum	Abundance of Phylum (%)					
	7 week		10 week		30 week	
	WT	FMO5 KO	WT	FMO5 KO	WT	FMO5 KO
Bacteroidetes	73	74	50	86	46	57
Firmicutes	18	19	40	10	45	33
Other	6	7	6	4	5	4
Unclassified	3	-	4	-	4	6

Table 4.1 – Phyla level analysis of the intestinal microbiota of 7-week, 10-week and 30-week old WT and FMO5 KO male mice. Sequence reads were pooled from faecal samples of triplicate cages (housing 3-4 mice) for each age point. Analysis was conducted on samples from 7-week (WT, n=79; FMO5 KO; n=70), 10-week (WT, n=156; FMO5 KO, n=73) and 30-week (WT, n=172; FMO5 KO, n=180) old male mice. Data is expressed as percent of total sequence reads.

Five phyla were identified in the digestive tract of the WT and FMO5 animal; Actinobacteria, Proteobacteria, Deferribacteres, Firmicutes and Bacteroidetes. This is in agreement with previous investigations indicating only few bacterial divisions are present in the gastrointestinal tract, with the Bacteroidetes and Firmicutes phyla dominating (Bäckhed et al., 2005; Ley et al., 2006a; Arumugam et al., 2011). As the representation of the three less abundant phyla; Actinobacteria, Proteobacteria, Deferribacteres, remained unchanged between animals and age groups they will be referred to herein as Other and analysis will focus on the abundance of the Bacteroidetes and Firmicutes phyla. Unclassified refers to bacterial sequences that were not assigned at the phyla or family level with >80 % confidence.

In the 7-week old animals, the representation of Bacteroidetes and Firmicutes is similar in both the WT and FMO5 KO animal (Figure 4.1, Table 4.1). However, from 7 to 10 weeks there is a rise in Firmicutes detected in the WT (7 week, 18 %; 10 week, 40 %), which is accompanied by a decrease in Bacteroidetes (7 week, 73 %; 10 week, 50 %). The microbiota of the FMO5 KO however remains comparatively stable between 7 and 10 weeks, which results in a marked difference observed between the two animal lines at 10 weeks. The ratio of Bacteroidetes to Firmicutes shifts further in the WT animals between 10 and 30 weeks; where detected levels of the two phyla almost become equivalent. However, even though there is also a shift in the same direction observed in the FMO5 KO animal between 10 and 30 weeks, Bacteroidetes still outnumber the Firmicutes to a ratio of around 2:1 (Figure 4.1, Table 4.1).

Taking a closer look at the changes in family representation of each phyla, we observe the change in abundance of Firmicutes through ageing is specifically due to a bloom in the Erysipelotrichaceae family (Table 4.2). In the WT animal it is undetectable at 7 weeks, however this family accounts for 26 % of the bacterial composition at 10 weeks. The bloom in the Erysipelotrichaceae family is accompanied by a specific decrease in counts of the Porphyromonadaceae family of the Bacteroidetes phylum (7 week, 56 %; 10 week, 34 %). Furthermore, when considering the less dramatic shift in Bacteroidetes and Firmicutes in the FMO5 KO between 10 and 30 weeks, it is again due to the concomitant rise in Erysipelotrichaceae and fall in Porphyromonadaceae families of the Firmicutes and Bacteroidetes phyla respectively.

Phylum	Family	Abundance of Family (%)					
		7 week		10 week		30 week	
		WT	FMO5 KO	WT	FMO5 KO	WT	FMO5 KO
Bacteroidetes	Rikenellaceae	4	10	2	11	2	3
	Prevotellaceae	5	27	9	5	6	8
	Bacteroidaceae	4	17	0	0	0	4
	Porphyromonadaceae	56	20	34	60	35	34
	Unclassified	4	-	4	10	4	8
Firmicutes	Lachnospiraceae	3	16	9	4	7	6
	Ruminococcaceae	-	-	1	0	2	8
	Lactobacillaceae	-	-	1	0	3	1
	Erysipelotrichaceae	-	-	26	1	28	13
	Unclassified	15	3	1	4	5	4

Table 4.2 – Family level analysis of the intestinal bacteria of 7-week, 10-week and 30-week old WT and FMO5 KO male mice. Sequence reads were pooled from faecal samples of triplicate cages (housing 3-4 mice) for each age point. Analysis was conducted on samples from 7-week (WT, n=79; FMO5 KO; n=70), 10-week (WT, n=156; FMO5 KO, n=73) and 30-week (WT, n=172; FMO5 KO, n=180) old male mice. Data is expressed as a percentage of total sequence reads.

In summary, at 7 weeks the FMO5 KO and WT animals present with similar phyla composition. The levels of Bacteroidetes and Firmicutes in the two sets of mice are comparable, however the Bacteroidetes phylum is slightly more diverse in the FMO5 KO at this age. Through ageing in the WT animal, we report a marked increase in the abundance of the Firmicutes phylum with a reciprocal decrease in Bacteroidetes, a shift well associated with an obesogenic state. Although this shift occurs in the FMO5 KO animal, it is to a much lesser extent and occurs later in ageing. Our

observations are in part agreement with what is currently thought of the microbiota; a higher Firmicutes to Bacteroidetes ratio is observed in the WT animal, who gain more weight with ageing than do the FMO5 KO animals. However, the difference in bacteria representation between WT and FMO5 KO mice is observed as early as 10 weeks, whereas the weight phenotype difference between the two sets of animals does not present until the animals are 20 weeks and older (*see* Figure 3.2).

4.3.2 The Response of the Intestinal Microbiota To High-Fat Feeding

High-fat feeding is a remarkable modulator of the intestinal bacteria. Through diet intervention studies in mice, a high-fat diet has been extensively shown to increase the abundance of Firmicutes and decrease the abundance of Bacteroidetes (Kim et al., 2012; Turnbaugh et al., 2008; Lam et al., 2012; Hildebrandt et al., 2009; Turnbaugh et al., 2009b). The microbial shift is thought to propagate the deleterious affects of high-fat feeding, further worsening the metabolic outcome of the individual.

The FMO5 KO animal is resistant to the canonical metabolic response to high-fat feeding; they remain lean and their plasma glucose and insulin are unaffected (*see* section 3.3.2). To assess a potential role of the microbiota in this protection, the intestinal bacteria of high-fat diet fed WT and FMO5 KO animals was also investigated (Figure 4.2, Table 4.3).

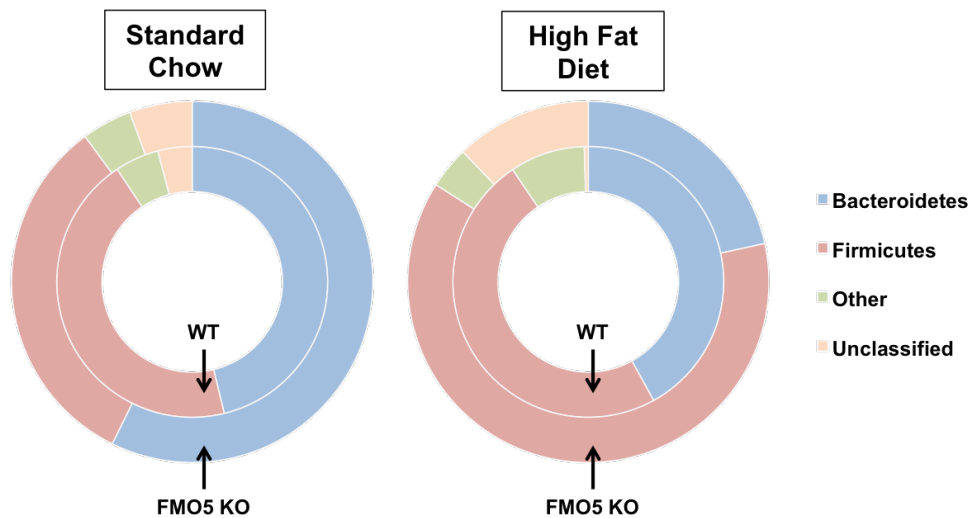


Figure 4.2 – Phyla level analysis of the intestinal microbiota of 30-week WT and FMO5 KO male mice fed a standard chow or a high fat diet. Sequence reads were pooled from faecal samples of triplicate cages (housing 3-4 mice) for standard chow and duplicate cages for high fat diet conditions. Standard chow (WT, n=172; FMO5 KO, n=180). High Fat Diet (WT, n=212; FMO5 KO, n=214). Data is expressed as a percentage of total sequence reads.

Phylum	Abundance of Phylum (%)			
	Standard Chow		High Fat Diet	
	WT	FMO5 KO	WT	FMO5 KO
Bacteroidetes	46	57	42	22
Firmicutes	45	33	49	62
Other	5	4	9	4
Unclassified	4	6	-	12

Table 4.3 – Phyla level analysis of the intestinal microbiota of 30-week old WT and FMO5 KO male mice fed standard chow or a high fat diet. Sequence reads were pooled from faecal samples of triplicate cages (housing 3-4 mice) for standard chow and duplicate cages for high fat diet conditions. Standard chow (WT, n=172; FMO5 KO, n=180). High fat diet (WT, n=212; FMO5 KO, n=214). Data is expressed as percent of total sequence reads.

The microbiota of WT and FMO5 KO respond to the high-fat diet in the expected manner; Firmicutes becomes the most abundant phylum, with an accompanied decrease in Bacteroidetes levels. In fact, the shift in composition is much more severe in the FMO5 KO animal, the Firmicutes now greatly outnumber the Bacteroidetes (Figure 4.2, Table 4.3). Again, the rise in Firmicutes and fall in Bacteroidetes can be specifically attributed to the bloom in the Erysipelotrichaceae family and depletion of the Porphyromonadaceae family respectively (Table 4.4).

Phylum	Family	Abundance of Family (%)			
		Standard Chow		High Fat Diet	
		WT	FMO5 KO	WT	FMO5 KO
Bacteroidetes	Rikenellaceae	2	3	12	3
	Prevotellaceae	6	8	0	0
	Bacteroidaceae	0	4	1	6
	Porphyromonadaceae	35	33	25	4
	Unclassified	4	8	4	9
Firmicutes	Lachnospiraceae	7	6	8	16
	Ruminococcaceae	2	8	6	7
	Lactobacillaceae	3	1	0	0
	Erysipelotrichaceae	28	13	32	36
	Unclassified	5	4	3	3

Table 4.4 – Family level analysis of the intestinal bacteria of 30-week old WT and FMO5 KO male mice fed standard chow or a high fat diet. Sequence reads were pooled from faecal samples of triplicate cages (housing 3-4 mice) for standard chow and duplicate cages for high fat diet conditions. **Standard Chow** – WT; n=172, FMO5 KO; n=180. **High Fat Diet**– WT; n=212, FMO5 KO; n=214. Data is expressed as a percentage of total sequence reads.

Therefore, in high-fat feeding, both animals now harbor an intestinal microbiota that has been linked to excessive weight gain. During the 6-week high-fat feeding experiment, the FMO5 KO animals did not however gain weight (*see* Figure 3.9). Taken together with the original observed microbiota differences at 10 weeks far predating the weight phenotype, the intestinal microbiota profile in both standard chow and high-fat feeding conditions does not correlate with the differences in body weight observed in the WT and FMO5 KO animal.

Our results are not alone in disputing the change in the Bacteroidetes and Firmicutes phyla to be responsible for a change in energy storage of the host. First and foremost, there are contradictory results regarding the change in the Bacteroidetes:Firmicutes ratio between obese and lean subjects; researchers report an obese microbiota exhibits no change at all, and either higher representation of the Firmicutes or Bacteroidetes phyla (Venema, 2010; Harris et al., 2012). Taken with the findings that microbiota monitoring during weight loss also produces polarized results (Ley, 2010), it is clear the relationship is not always universally true and therefore a direct causative link is in dispute. Although microbiota transplant experiments provide a convincing argument; germ-free mice that receive microbiota from obese donors gain more weight than those who receive a transplant from lean animals (Turnbaugh et al., 2006), it has been questioned whether the modest change in energy harvest, mediated by a change in the representation of bacterial genes, would be great enough to elicit an immediate, observable change in the hosts gross phenotype. Furthermore, a microbiome deemed more efficient in energy harvest is not always associated with an increase in weight gain and fat mass (Cani et al., 2008b).

In the studies of the WT and FMO5 KO animal, we have however identified FMO5 as a novel regulator of the intestinal bacteria. WT and FMO5 KO animals housed in the same animal holding room and fed the same standard chow present with different microbiotas. Furthermore, we have shown the effect of a high-fat diet on the microbiota supersedes the genetic influence. The diet intervention remodeled the commensal bacteria so that both WT and FMO5 KO animals present with similar microbiotas. However, in the FMO5 KO the diet induced microbial shift is not accompanied by the once proposed related incidence of excessive weight gain.

In support of our findings, the colonic host protein RELM β also modulates the intestinal microbiota when animals are fed a standard chow. Similar to the FMO5 KO, the RELM β KO presents with a microbiota depleted in Firmicutes and enriched in Bacteroidetes. The switch to a high-fat diet results in the canonical bloom in Firmicutes in both the WT and RELM β KO, however, like the FMO5 KO, the RELM β KO animal is protected from the diet induced obesity that is observed in the WT. Akin to the FMO5 KO, the RELM β KO mouse line is therefore further evidence of high-fat diet modulation of the intestinal microbiota occurring independently to obesity (Hildebrandt et al., 2009). The protection from high-fat diet induced obesity, mediated by the absence of these two host proteins, highlights the complicated cross-talk of host genetics and the microbiota in the response to diet. The hosts recognition, and subsequent reaction to the commensal bacteria and the luminal environment of the gut is now regarded to be just as, if not more, important than the microbiota itself.

4.3.3 *FMO5 is Expressed in the Murine Digestive Tract*

When compared to the WT, the FMO5 KO has an altered intestinal microbiota. Although this disparity does not correlate with the observed metabolic phenotype, this led to further exploration into a role of FMO5 in the intestine. FMO5 expression in the murine digestive tract was initially characterised.

4.3.3.1 *FMO5 detection in faecal contents*

To first confirm the presence of FMO5 in the murine digestive tract, protein isolated from faecal matter of WT animals was probed for FMO5. Protein was isolated from faecal homogenates, acetone-precipitated and electrophoresed before transfer onto a nitrocellulose membrane (Figure 4.3). A band migrating between the 50 and 60 kDa molecular weight marker was present in the WT samples and absent from the faecal matter proteins extracted from FMO5 KO mice.

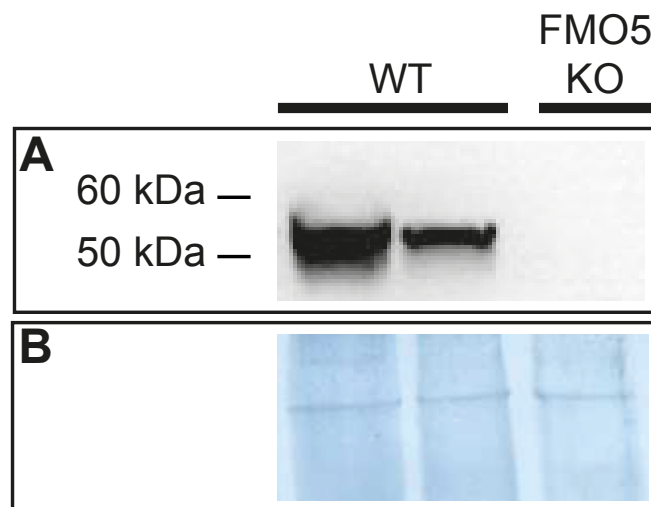


Figure 4.3 – FMO5 expression in the murine digestive tract. Western blot analysis of protein isolated from faecal pellets of WT (n=2) and FMO5 KO (n=1) animals. The membrane was probed for FMO5 (A) and total protein stain amido black was used to confirm equal loading (B).

The detection of FMO5 in faeces indicates the protein is present in the digestive tract of WT mice. The detection of FMO5 could be a result of the protein being secreted into the intestinal lumen. Alternatively, FMO5 expression in epithelial cells, which are sloughed in excretion, would also result in the protein appearing in faeces.

To further clarify the localisation of FMO5, immunohistochemical analysis was conducted on sections of the murine digestive tract (Figure 4.4 – 4.6).

4.3.3.2 *FMO5* expression in stomach mucosa

Immunohistochemistry (IHC) of WT stomach mucosa (Figure 4.4-A and B) suggests FMO5 immunodetection (brown) in both the lamina propria, at the base of the mucosa, and the columnar epithelial cells, at the luminal surface of the tissue. FMO5 KO tissue was stained for a negative control (Figure 4.4-C). KO tissue had similar staining at the base of the lamina propria, indicating this signal is not a result of FMO5 expression and due to non-specific antibody binding. The absence of the columnar epithelium staining in KO tissue would however indicate this is specific to WT tissue, therefore a result of FMO5 expression.

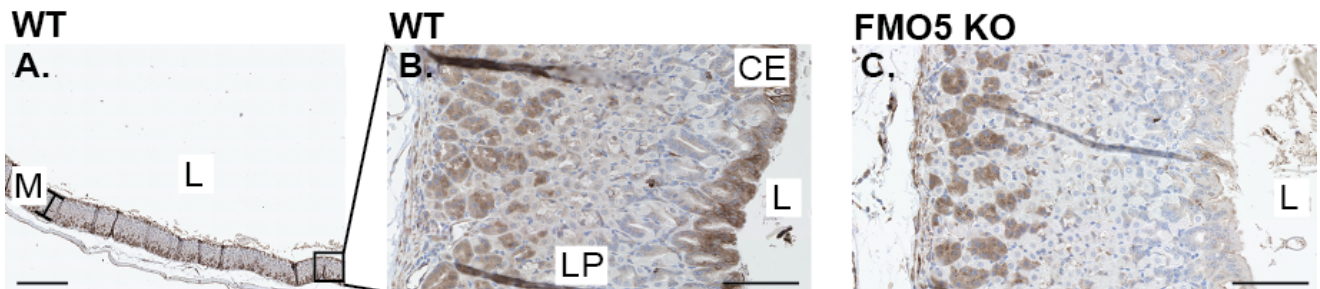


Figure 4.4 – Immunohistochemical detection of FMO5 in stomach mucosa. Butterfly section of WT stomach stained for FMO5 (A). Higher magnifications of WT mucosa (B) and, for negative control, FMO5 KO mucosa (C). Scale bar: A, 500 μm ; B and C, 100 μm . M, mucosa; L, lumen; LP, lamina propria; CE, columnar epithelium. Photomicrographs are a representative of four WT and FMO5 KO male mice.

4.3.3.3 *FMO5* expression in small intestine mucosa

IHC was also performed on transverse sections of WT and *FMO5* KO small intestine (Figure 4.5). Sections of WT duodenum (Figure 4.5-A and D), jejunum (4.5-B and E) and ileum (Figure 4.5-C and F) stained for *FMO5* (brown) also indicate the prevalent expression of the enzyme in the intestinal mucosa.

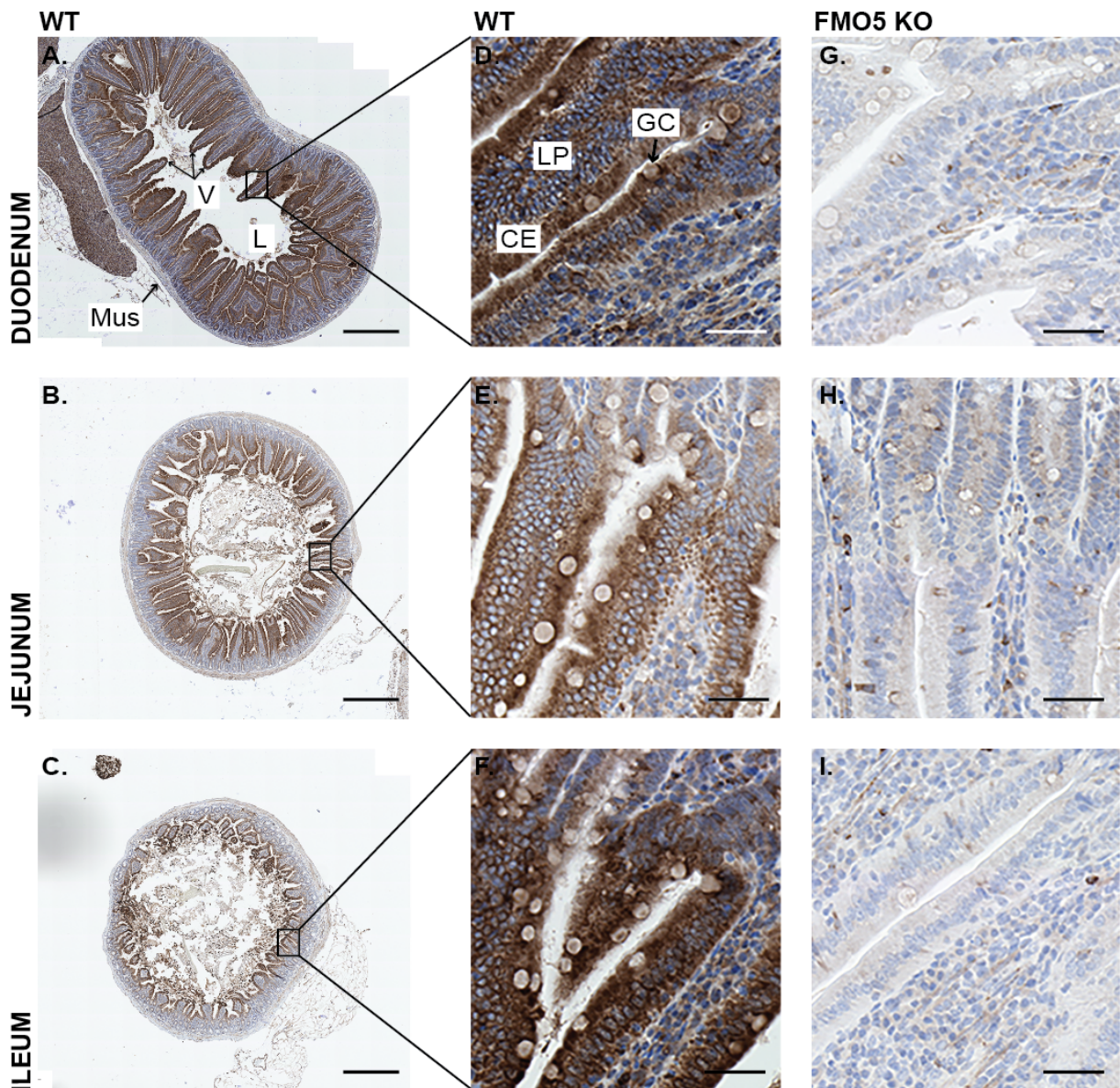


Figure 4.5 – Immunohistochemical detection of *FMO5* in small intestine mucosa. Transverse sections of WT duodenum (A), jejunum (B) and ileum (C) stained for *FMO5*. Higher magnifications of villi from WT duodenum (D), WT jejunum (E) and WT ileum (F) are shown in middle panels. For negative controls, villi of corresponding *FMO5* KO sections are shown in furthest right panels (G, H and I). Scale bar: A - C, 500 μ m; D - I, 100 μ m. Mus, muscle; V, villi; L, lumen; CE, columnar epithelium; LP, lamina propria; GC goblet cell. Photomicrographs are a representative of four WT and *FMO5* KO male mice.

FMO5 is again expressed in the columnar epithelium of the mucosa, at the luminal surface of the tissue. Higher magnifications of the intestinal villi (projections of the mucosa) (Figure 4.5-D, E and F) show the pervasive expression of FMO5 in the epithelial cell layer, including the specialised goblet cell; a cell type discussed in more detail in the introduction to this chapter (*see* 4.1.3). The visible secretory granule, devoid of any staining, distinguishes the goblet cell from other epithelial cells. FMO5 is not expressed in the secretory granule itself, but is detected in the corresponding cell cytoplasm and expression seems most concentrated at the periphery of the granule. Analogous staining of FMO5 KO duodenal (Figure 4.5-G), jejunal (Figure 4.5-H) and ileal tissue (Figure 4.5-I) resulted in no signal, indicating the described staining of WT tissue is FMO5 specific. Swiss rolls of WT intestine also show FMO5 is expressed throughout the length of the small intestine (data not shown).

4.3.3.4 *FMO5 expression in colonic mucosa*

Colonic FMO5 expression was also confirmed with IHC (Figure 4.6). Unlike the villi-projections seen in the small intestine, the mucosa of the colon is arranged in to rows of tubular glands (crypts of Lieberkühn or crypts). The colonic mucosa may also further fold on itself forming a projection distinct to a villus; a mucosal fold. Similar to the mucosa of the small intestine however, FMO5 (brown) is highly expressed at the luminal surface of colonic mucosa (Figure 4.6-A). Further magnification of WT colonic crypts (Figure 4.6-B) shows a gradient of FMO5 expression from the base to the luminal opening of the crypt, and expression of FMO5 is again throughout the columnar epithelium, including the prevalent goblet cells. FMO5 is not packaged within the secretory granule of the goblet cell, however staining is again clear in the cytoplasm and expression appears to be focused surrounding the granules. FMO5 staining was also conducted in FMO5 KO colonic tissue for a negative control (Figure 4.6-C). Staining is only observed in WT tissue and is therefore considered FMO5 specific. Colonic Swiss rolls again reveal FMO5 to be expressed throughout the entire colon

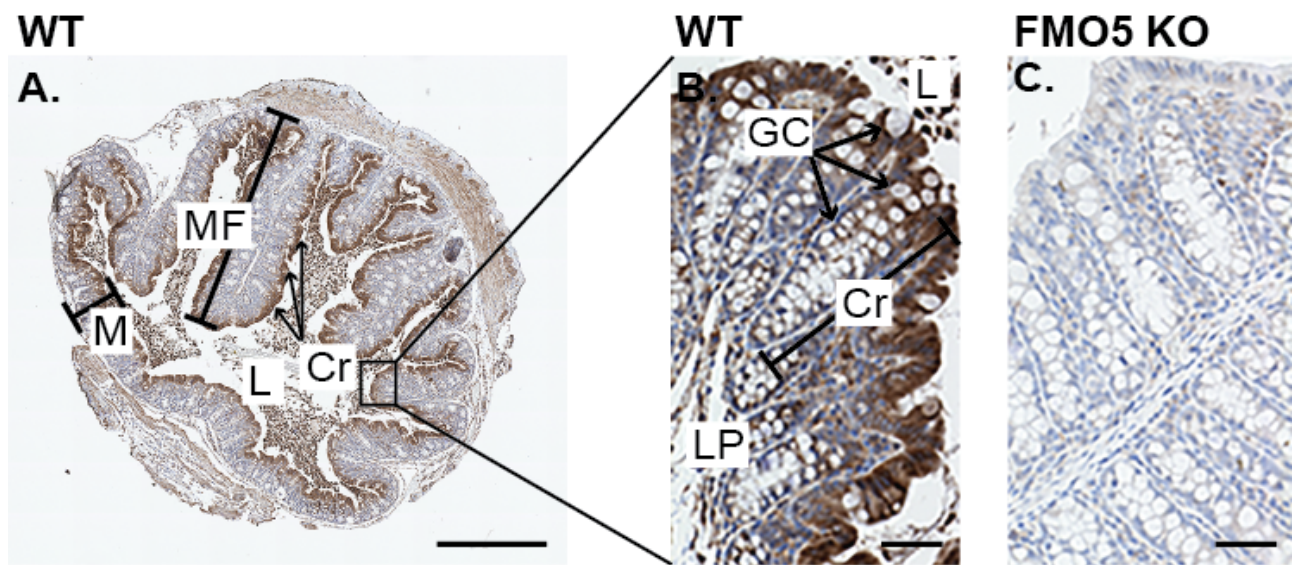


Figure 4.6 – Immunohistochemical detection of FMO5 in mucosal crypts of the colon. Transverse section of WT colon stained for FMO5 (A). Higher magnifications of WT mucosa (B) and, for negative control, FMO5 KO mucosa (C). Scale bar: A, 200 μm ; B and C, 50 μm . MF, mucosal fold; M, mucosa; L, Lumen; GC, goblet cell; Cr, crypt; LP, lamina propria. Photomicrographs are a representative of four WT and FMO5 KO male mice.

4.3.4 *No Gross Morphological Differences in the WT and FMO5 KO Digestive Tract*

Following the detection of FMO5 expression throughout the digestive tract, general histology was conducted to compare the gross morphology of WT and FMO5 KO tissues (Figures 4.7 – 4.9). Nucleic acid stain hematoxylin and protein stain eosin were used together to investigate cell and tissue morphology, staining the nucleus blue and cytoplasm pink respectively.

Hematoxylin and eosin staining of WT and FMO5 KO stomach (Figure 4.7) revealed no difference in mucosal thickness or tissue structure.

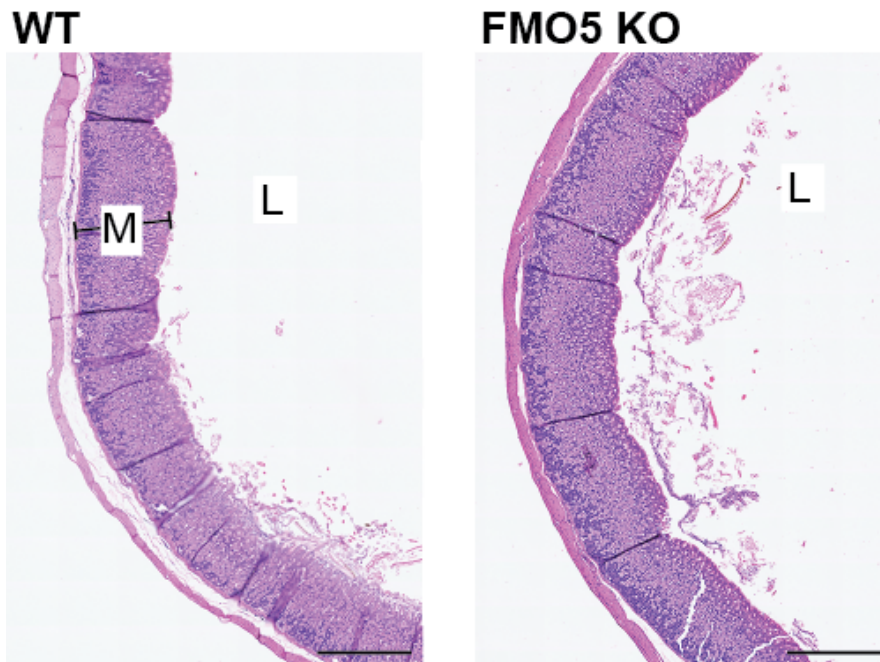


Figure 4.7 – Gross morphology of WT and FMO5 KO stomach. Butterfly sections of WT (A) and FMO5 KO (B) stomach stained with hematoxylin and eosin. Scale bar: 500 μ m. M, mucosa; L, lumen. Photomicrographs are a representative of four WT and FMO5 KO male mice.

Likewise, when comparing hematoxylin and eosin stained sections of WT and FMO5 KO duodenum (Figure 4.8-A and D), jejunum (Figure 4.8-B and E) and ileum (Figure 4.8-C and F) no difference is observed in the muscle layer or luminal arrangement of the small intestine.

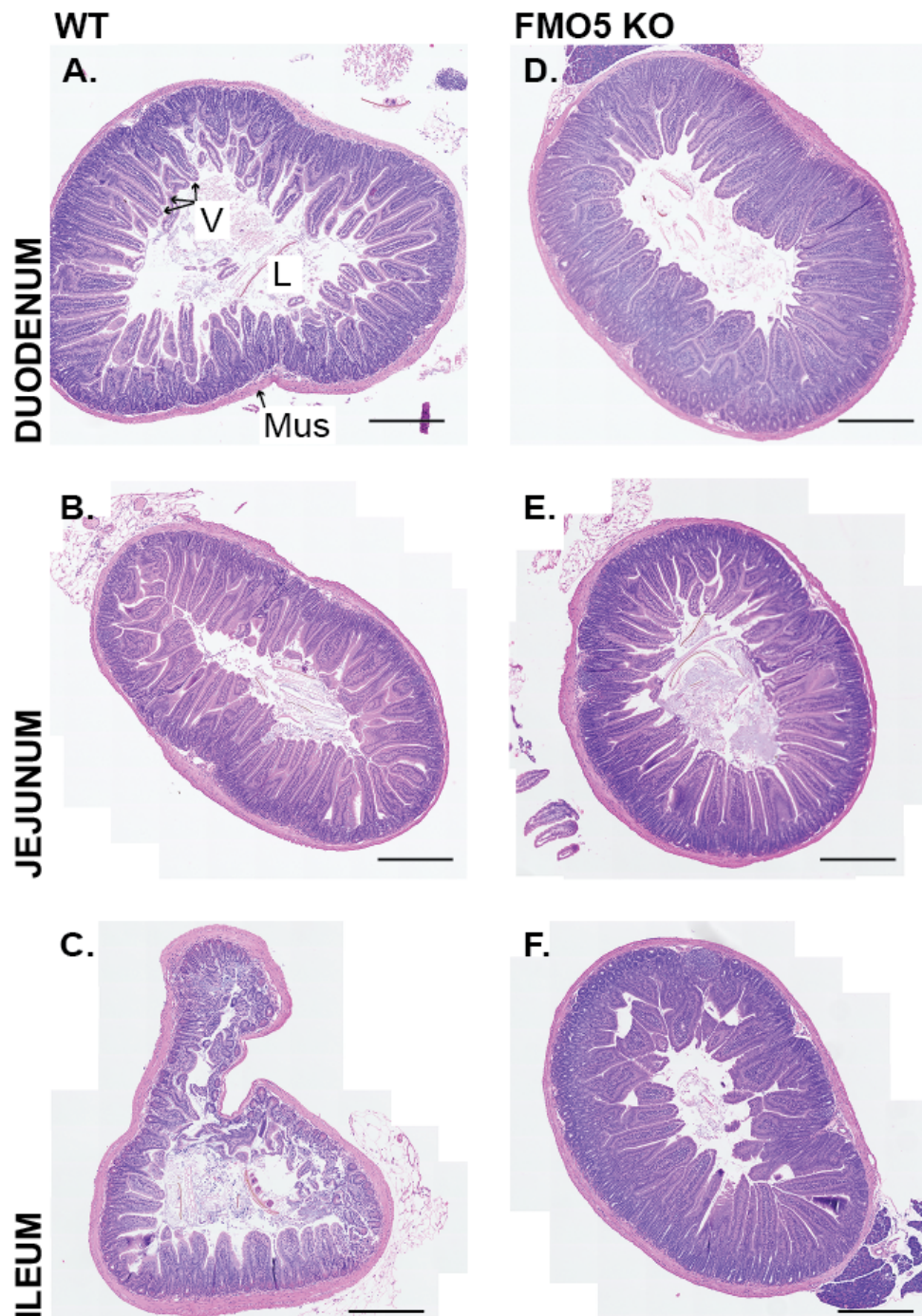


Figure 4.8 – Gross morphology of WT and FMO5 KO small intestine. Transverse sections of WT duodenum (A), WT jejunum (B) and WT ileum (C) and FMO5 KO duodenum (D), FMO5 KO jejunum (E) and FMO5 KO ileum (F) stained with hematoxylin and eosin. Scale bar: 500 μ m. V, villi; L, lumen; Mus, muscle. Photomicrographs are a representative of four WT and FMO5 KO male mice.

Furthermore, staining also shows no difference in the mucosal arrangement or muscle layer thickness of colon tissue of the WT and FMO5 KO mice (Figure 4.9).

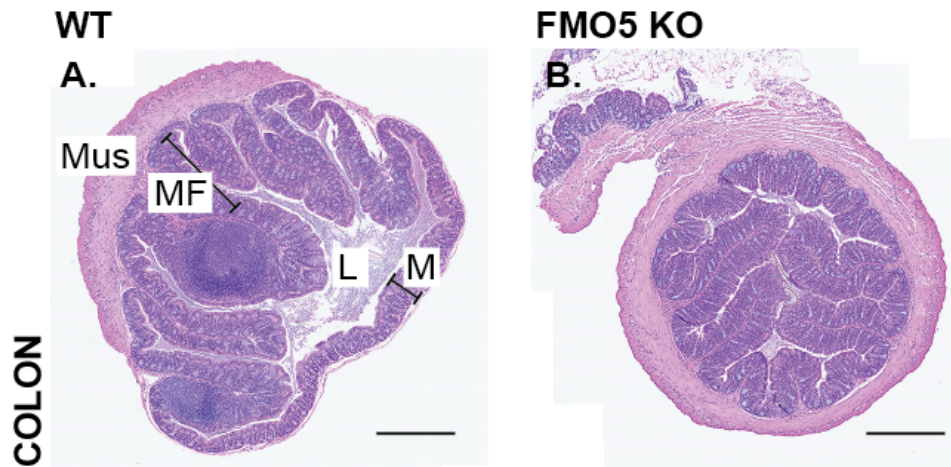


Figure 4.9 – Gross morphology of WT and FMO5 KO colon. Transverse sections of WT (A) and FMO5 KO (B) colon stained with hematoxylin and eosin. Scale bar: 500 μ m. Mus, muscle; MF, mucosal fold; L, lumen; M, mucosa. Photomicrographs are a representative of four WT and FMO5 KO male mice.

Immunohistochemical analysis of WT tissue reveals the prevalent expression of FMO5 throughout the murine digestive tract, in particular epithelial cells at the luminal surface of tissue. However, in comparison of the WT and FMO5 KO tissue, no gross morphological differences are observed in the protein's absence. No epithelial damage or reduction in barrier integrity was recorded for either genotype in any intestinal section.

4.3.5 *FMO5 Expression is Induced in Response to the High-Fat Diet*

The disparity in the metabolic phenotype of the WT and FMO5 KO animal becomes more pronounced in response to a high-fat diet (*see* 3.3.2). High-fat feeding resulted in further weight gain and increases in plasma glucose and plasma insulin in the WT animal, whereas the FMO5 KO remained lean with low plasma glucose and insulin. The worsening of the metabolic phenotype in the WT, and protection in the FMO5 KO, suggests FMO5 may have a role in the response of an animal to their diet. Intestinal expression of FMO5 following high-fat diet feeding was therefore investigated. Protein isolated from faecal samples of WT animals fed either a control or high-fat diet was concentrated by acetone precipitation, electrophoresed and Western blot analysis was performed with an FMO5 antibody.

FMO5 expression in the digestive tract is robustly induced in response to high-fat feeding (Figure 4.10), indeed suggesting an involvement in an animal's response to high-fat feeding. The analysis was conducted in faecal samples, a gross, and non-specific representative of the digestive tract.

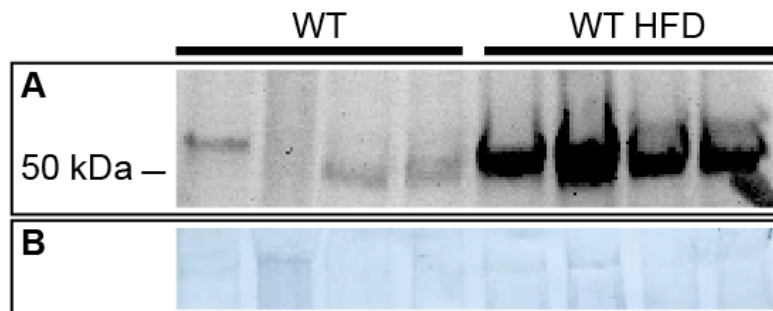


Figure 4.10 – Faecal FMO5 expression following high fat feeding. Western blot analysis of protein isolated from faecal samples of WT animals fed a standard chow (WT, n=4) or a high fat diet (WT-HFD, n=4). The membrane was probed for FMO5 (A) and total protein stain, amido black was used to confirm equal loading (B).

4.3.6 A Disparity in RELM β Expression in the WT and FMO5 KO Animal

This study shows that FMO5 is expressed throughout the murine digestive tract and is induced in high-fat feeding. RELM β is a goblet cell secreted factor described in more detail in the introduction to this chapter (*see* 4.1.4). RELM β is highly expressed in the colon and is also induced in high-fat feeding. Like the FMO5 KO (*see* Figure 3.9), the RELM β KO is protected from diet-induced obesity (Hildebrandt et al., 2009). The common colonic expression of both proteins, and the similarity in the phenotypes of the FMO5 and RELM β KO mice, led to the investigation of the of colonic expression of RELM β in the presence (WT mice) and absence (FMO5 KO mice) of FMO5.

4.3.6.1 Western Blot Analysis of Colon Contents

RELM β expression was initially investigated in the luminal content of the colon. Protein was isolated from colon contents of the WT and FMO5 KO mouse and electrophoresed. Western blot analysis was conducted using an antibody against full-length RELM β (Abcam®) (Figure 4.11).

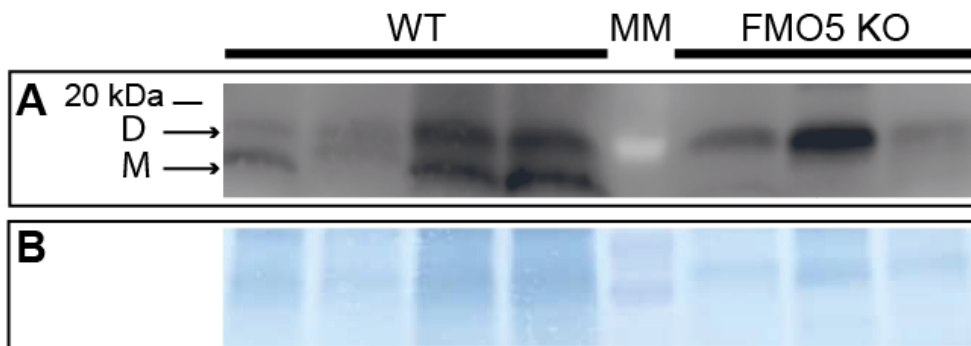


Figure 4.11 – Expression of RELM β in colon contents of WT and FMO5 KO animals. Immunoblot analysis of protein isolated from colon contents of WT (n=4) and FMO5 KO (n=3) male mice. MM: molecular weight marker. The membrane was probed for RELM β (A) and total protein stain amido black was used to check protein loading (B). M, monomer; D, dimer.

RELM β was first shown to exist in stool contents of the murine colon by He et al. (He et al., 2003). The protein exists as a dimer under non-reducing conditions, migrating just above a 17 kDa marker. In both the WT and FMO5 KO samples, we also detect a band, migrating just below the 20 kDa molecular weight marker, likely to correspond to the dimer. In all WT samples analysed, there is also an additional band migrating just below the proposed dimer. In the WT colon, RELM β also appears to exist as a monomer of approximately 8 kDa.

He et al. detected the RELM β monomer (6-8 kDa) when the SDS-PAGE was run under reducing conditions. In my investigations the gel was not run under stringent reducing conditions, this is clear from the presence of the dimer. Although dithiothreitol was used as a reducing agent in the sample buffer used to prepare samples for SDS-PAGE, subsequent observations revealed the agent must also be added to running buffers used in the electrophoresis system due to the small size and high cysteine content of the protein. Regardless, under the ‘partial’ reducing condition used for both WT and FMO5 KO samples, there is disparity in the RELM β species present. In the WT and FMO5 KO colon the dimer is detected, however I also propose the smaller molecular weight species, found exclusively in the WT, to be the monomer.

4.3.6.2 *Immunohistochemistry of Colon Tissue*

Following Western blot analysis of colon contents, immunohistochemistry compared expression of RELM β in WT and FMO5 KO colonic tissue (Figure 4.12). Transverse sections of WT (Figure 4.12-A) and FMO5 KO (Figure 4.12-B) colon stained for RELM β (brown) show protein expression is localised to the crypts of the colonic mucosa. Higher magnifications of WT (Figure 4.12-C) and FMO5 KO crypts (Figure 4.12-D) further show RELM β expression is concentrated in the secretory granules of goblet cells and, similar to colonic staining for FMO5, a gradient of expression from the base of the crypt to the luminal opening is observed. This is in agreement with previous investigations into RELM β expression (He et al., 2003; Hogan et al., 2006; McVay et al., 2006) and the absence of RELM β staining in extra-colonic sections of the intestine further confirms RELM β to be a colon specific protein (data not shown). Immunohistochemistry does not provide information on the dimerisation state of RELM β however, in agreement with the Western blot analysis of colon contents, both

the WT and FMO5 KO produce RELM β . Furthermore, localisation of the colonic hormone is unchanged in the genotypes.

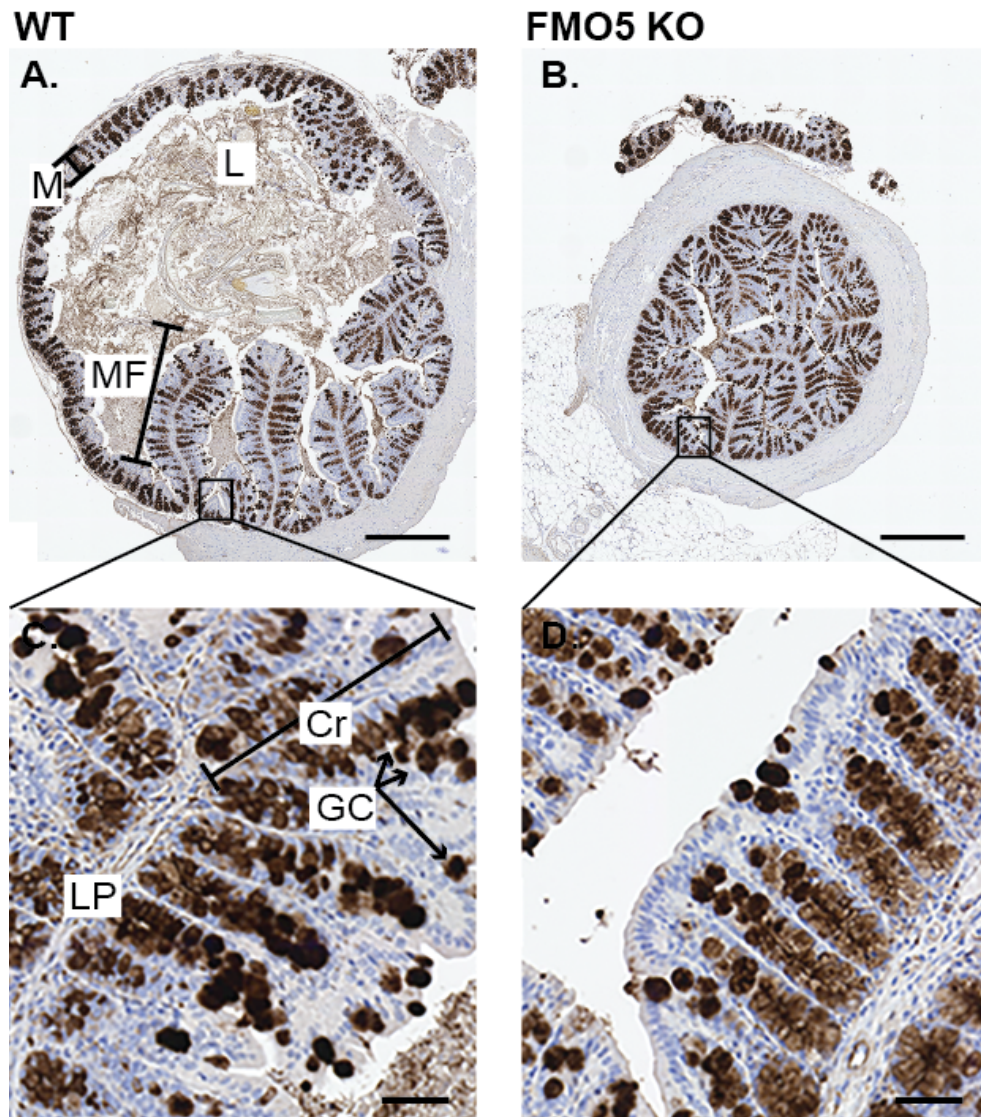


Figure 4.12 – Goblet cell expression of RELM β in WT and FMO5 KO colon. Transverse sections of WT (A) and FMO5 KO (B) colon stained for RELM β . Higher magnifications of WT mucosa (C) and FMO5 mucosa (D) are shown below. Scale bar: A and B, 500 μ m; C and D, 50 μ m. M, mucosa; L, lumen; MF, mucosal fold; Cr, crypt; GC, goblet cell; LP, lamina propria. Photomicrographs are a representative of four WT and FMO5 KO male mice.

4.3.6.3 Western Blot Analysis of Faecal Contents

To further explore the difference in RELM β expression, protein isolates from the faeces of WT and FMO5 KO animals were assayed. Western blot analysis of faecal proteins, using an antibody against full-length RELM β , show that the dimer of RELM β is the only species detected, and the amount of dimer is higher in the FMO5 KO (Figure 4.13).

By investigating protein levels in faecal samples, we can deduce what the animal is excreting. Although colonic amounts of the dimer species in WT and FMO5 KO animals are comparable (*see* Figure 4.11), the FMO5 KO animals excrete more of the RELM β dimer in their faeces than do WT mice. We may speculate this is due to the difference in the amount of the monomeric and dimeric state of RELM β in the two animals. In functional studies of resistin, the closely related family member of RELM β , the monomer species was shown to be the active form of the hormone (Patel, 2004). Therefore, in the colon of the FMO5 KO mouse, we propose that RELM β exists as an inactive dimer, which is subsequently excreted and therefore detected in high amounts in the faeces. Whereas in the WT animal the dimer is processed to the monomeric, or active, form of RELM β , which results in less of the dimeric protein being excreted.

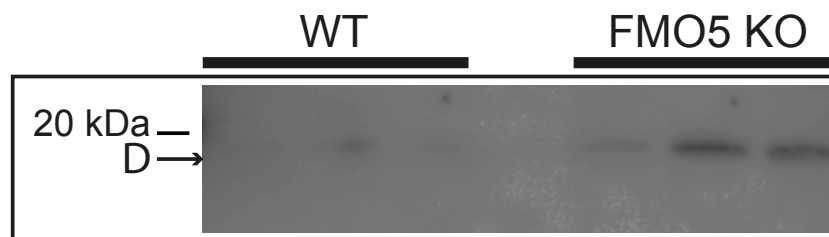


Figure 4.13 – Faecal expression of RELM β in the WT and FMO5 KO mouse. Immunoblot analysis of protein isolated from faecal pellets of WT (n=3) and FMO5 KO (n=3) male mice. The membrane was probed for RELM β and equal loading was confirmed using Colloidal Gold Total Protein Stain (Bio-Rad) (not shown). D, dimer.

4.3.7 *RELM β Expression is Induced in Response to the High-Fat Diet*

It is well known that RELM β is induced in response to a high-fat diet. Both colonic mRNA and serum protein levels were found to be elevated in high-fat diet fed animals (Shojima et al., 2005; Fujio et al., 2008; Hildebrandt et al., 2009). To determine whether the presence of FMO5 influences the ability of an animal to induce RELM β , WT and FMO5 KO animals fed either standard chow or a high-fat diet were monitored for RELM β expression. Protein was isolated from faecal samples and Western blot analysis was conducted with an antibody against a synthetic peptide corresponding the amino acids 2-46 of mouse RELM β (QED Bioscience) (Figure 4.14).

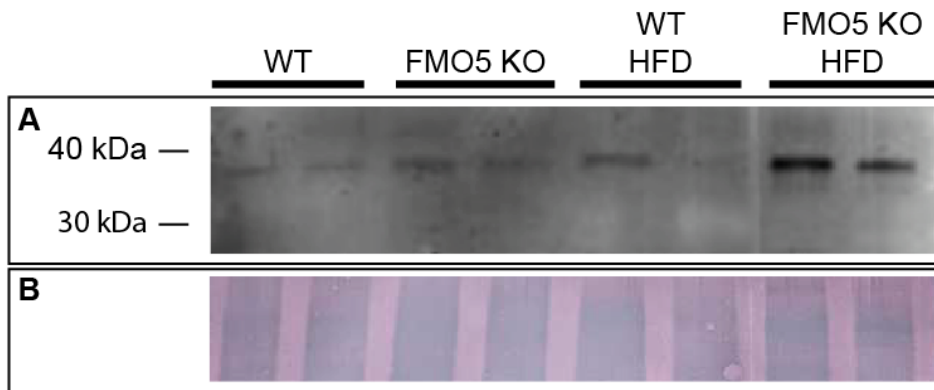


Figure 4.14 – Faecal RELM β expression following high fat feeding. Western blot analysis of protein isolated from faecal samples of WT and FMO5 KO animals fed a standard chow (WT, n=2; FMO5 KO, n=2) or a high fat diet (WT HFD, n=2; FMO5 KO HFD, n=2). The membrane was probed for RELM β (A) and total stain Colloidal Gold Total Protein Stain (Bio-Rad) was used to confirm equal loading (B).

Using this peptide antibody, instead of the monomer and dimer species, a larger band migrating between the 30 and 40 kDa molecular weight marker is detected. This is however the only band detected and it may therefore be that this antibody preferentially recognises a higher oligomeric state of RELM β . In studies of resistin, a closely related family member, Patel et al. describe the detection of a hexamer species. Taking the detected size of the RELM β monomer described by He et al. as 6 kDa, it is possible that with this antibody we are detecting the RELM β hexamer of 36 kDa.

Faecal pellets of WT and FMO5 KO animals fed either a standard chow or high-fat diet were analysed and conditions were run in duplicate. One isolation from WT animals fed a high-fat diet (WT HFD) failed; no RELM β is detected and the total protein stain for the corresponding lane is weaker than other samples. The single successful isolation from the WT HFD condition does however indicate RELM β is induced in high-fat feeding; more RELM β is detected in the faeces of the WT animal fed a high-fat diet (WT HFD) than those from WT animals fed standard chow (WT). Furthermore, this is apparent in the FMO5 KO condition. Higher levels of RELM β are also detected in faeces of FMO5 KO animals fed a high-fat diet (FMO5 KO HFD) than those fed standard chow (FMO5 KO). Therefore, both animals respond in the canonical way to the high-fat diet, in the induction of RELM β .

The higher amount of RELM β detected in the faeces of FMO5 KO animals fed a normal chow diet (*see* figure 4.13) is also observed in high-fat feeding. In both circumstances the absence of FMO5 leads to more of the RELM β protein being excreted. Therefore, in both basal expression and high-fat diet induction, it seems the absence of FMO5 is no hindrance to the production of the RELM β in the colon. The protein is produced, but more is excreted in the FMO5 KO animal.

4.3.8 A difference in Colonic Goblet Cells in the FMO5 KO Animal

As discussed in the introduction to this chapter (*see* 4.1.4), RELM β is proposed to act as a mucosecretagogue (Krimi et al., 2008). When applied apically to human colonic cells, RELM β induced the secretion of mucin protein MUC2. MUC2 is a goblet cell-secreted factor and is a major structural component of the mucus layer (Kim and Ho, 2010). Mucin proteins are packaged into the secretory granules of the goblet cell and basal exocytosis is necessary for the formation of the protective mucus layer.

This study has shown RELM β to exist as both a monomer and dimer in the WT colon. Conversely, the dimer is the only form observed in the FMO5 KO. To investigate the functional consequence of the difference observed in RELM β , mucosecretory function was measured in the WT and FMO5 KO mouse. Sections of WT and FMO5 KO colon were stained with alcian blue (Figure 4.15). Alcian blue stains the mucin polysaccharides of secretory granules and is used to identify and quantify secretory goblet cells. Higher magnifications of WT (Figure 4.15-C) and FMO5 KO (Figure 4.15-D) colonic mucosa shown below indicated a difference in goblet cell number; alcian staining appears less frequent in the FMO5 KO colonic crypts.

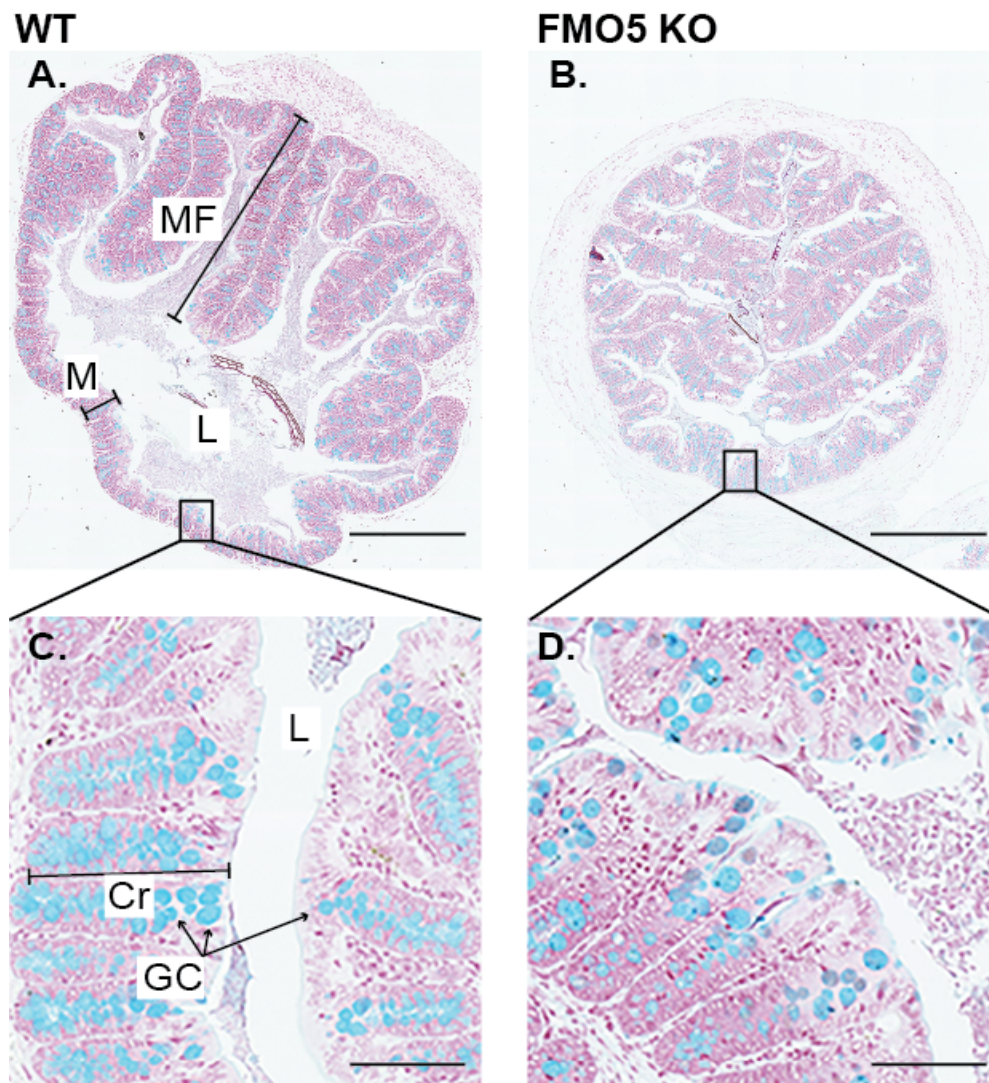


Figure 4.15 – Goblet cell staining of WT and FMO5 KO colonic mucosa. Transverse sections of WT (A) and FMO5 KO (B) colon are stained with alcian blue for goblet cell detection and counter-stained with neutral red. Higher magnifications of WT (C) and FMO5 KO (D) mucosa are shown below. Scale bar: A and B, 500 μm ; C and D, 100 μm . MF, mucosal fold; M, mucosa; L, lumen; Cr, crypt; GC, goblet cell. Photomicrographs are a representative of four WT and FMO5 KO male mice.

Subsequently, a method previously described by Mello et al. was used to quantify goblet cell number in the WT and FMO5 KO colon (de Oliveira Mello et al., 2012). Photomicrographs of alcian blue-stained colon sections of WT and FMO5 KO animals were used for analysis. Six regions of interest, containing at least 3 contiguous crypts, were sampled per photomicrograph and 18 crypts were analysed per biological repeat. Crypt length was measured and the number of goblet cells (alcian blue stained bodies) was recorded for each crypt analysed.

In measurement of crypt length, no difference was observed in the WT and FMO5 KO colon crypts (WT, $151.7 \pm 3.6 \mu\text{m}$, $n=57$; FMO5 KO, $162.1 \pm 5.0 \mu\text{m}$, $n=54$) (Figure 4.16).

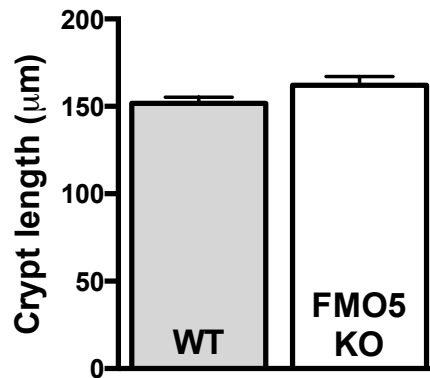


Figure 4.16 – Measurement of colon crypt length in WT and FMO5 KO mice. Colon photomicrographs of WT ($n=3$) and FMO5 KO ($n=3$) male mice were used for quantification. At least 18 crypts per photomicrograph were sampled. Crypt lengths of WT ($n=57$) and FMO5 KO ($n=54$) crypts were measured. Data is expressed as mean \pm SEM.

The number of goblet cells per crypt was however found to be higher in the WT colon (WT, 18.5 ± 0.8 , $n=57$; FMO5 KO, 15.4 ± 0.7 , $n=54$) ($p<0.01$) (Figure 4.17)

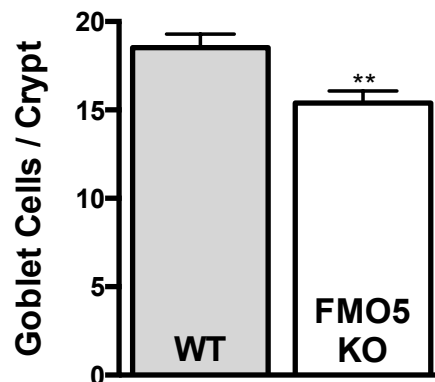


Figure 4.17 – Goblet cell quantification in WT and FMO5 KO colonic crypts. Colon photomicrographs of WT ($n=3$) and FMO5 KO ($n=3$) male mice were used for quantification. At least 18 crypts per photomicrograph were sampled. Counts of goblet cells per crypt for WT ($n=57$) and FMO5 KO ($n=54$) crypts were recorded. Data is expressed as mean \pm SEM (**: $p<0.01$)

Furthermore, when goblet cell number is expressed over crypt length, thus giving a measure of goblet cell number per unit of crypt length (Figure 4.18), the difference in the WT and FMO5 KO becomes more pronounced. Normalised for crypt length, the WT colonic crypt contains more goblet cells (WT, 12.2 ± 0.4 cells. $100\mu\text{m}^{-1}$, n=57; FMO5 KO, 9.5 ± 0.3 cells. $100\mu\text{m}^{-1}$, n=54) ($p < 0.0001$).

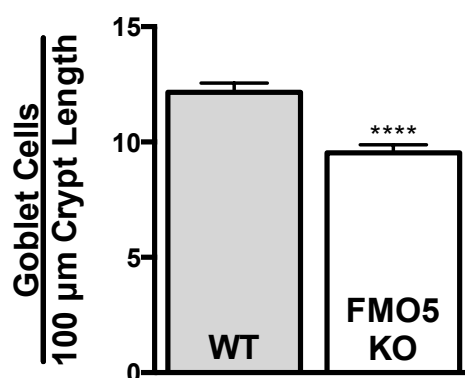


Figure 4.18 – Goblet cell number normalised to colon crypt length in WT and FMO5 KO mice. Colon photomicrographs of WT (n=3) and FMO5 KO (n=3) male mice were used for quantification. At least 18 crypts per photomicrograph were sampled. Goblet cell number is divided by crypt length for WT (n=57) and FMO5 KO (n=54) crypts analysed. Data is expressed as mean ± SEM (*: $p < 0.0001$).

In the absence of FMO5, we observe a difference in the processing of colonic hormone RELM β . The monomer, and proposed active form of RELM β , is absent in the FMO5 KO colon. In line with RELM β acting as a mucosecretagogue, in investigations of the colon mucosa, the absence of the monomer is accompanied by a decrease in goblet cell number in KO crypts.

Goblet cell secretion is necessary for the formation of the mucus layer and secretion is upregulated when the cell is physically or chemically challenged. However, as described in more detail in the introduction to this chapter (*see* 4.1.3), a tight regulation of MUC2 production and mucin secretion is necessary as pathologies are associated with over, as well as under, production. RELM β has been described as a mucosecretagogue (Krimi et al., 2008), and the upregulation of RELM β and overproduction of mucus is a hallmark of several inflammatory disorders of mucosal sites (*see* 4.1.4). A moderate suppression of mucosecretion, mediated by an attenuation of RELM β activation, in the FMO5 KO mouse may therefore be

protective. Of note, the absence of FMO5 does result in detrimental goblet cell ablation (*see* Figure 4.17) and subsequently no gross morphological differences are seen in the luminal integrity of intestinal tissue (*see* 4.3.4), however a small decrease in goblet cell activity when compared to the WT animal may be beneficial to the FMO5 KO.

The RELM β KO mouse is protected from diet induced obesity, also indicating a key role for this protein in the response to a high-fat diet (Hildebrandt et al., 2009). In high-fat feeding the induction of RELM β is observed in both animals, however we deduce that an attenuation in processing, and lack of activity, of RELM β in the FMO5 KO animal leads to the proteins excretion in faeces (*see* Figure 4.14). Therefore, in addition to maintaining a beneficial intestinal environment in the standard chow condition, the absence of FMO5, and proposed inactivity of RELM β , also serves to protect the FMO5 KO animal from diet induced obesity.

4.3.9 *RELMβ* and *FMO5* Expression Following Antibiotic Treatment

To investigate the role of the intestinal microbiota, WT and *FMO5* KO animals were treated with low-dose, broad-spectrum antibiotics to reduce the bacterial load of the intestine (*see* 3.3.3). Metabolic profiling following treatment revealed, although the *FMO5* KO remained unaffected, antibiotic treatment improved glucose tolerance and lowered plasma insulin and glucose in the WT mouse. Consequently, the phenotype of the antibiotic treated WT animals resembled that of the *FMO5* KO. To further understand the convergence in phenotype, intestinal expression of proteins of interest *FMO5* and *RELMβ* were measured following treatment.

4.3.9.1 *Ablation of RELMβ* Expression in Antibiotic Treatment

RELMβ has been well characterised as a goblet cell secreted factor and expression is heavily dependent on the presence of the microbiota. Colonic *RELMβ* protein and mRNA measurements are markedly reduced in germ-free animals and both can be recovered upon conventionalisation (He et al., 2003; Wang et al., 2005). Protein was isolated from faeces of WT animals and WT animals treated with antibiotics. Previously *RELMβ* was detected in WT faeces at very low levels (*see* Figure 4.13), therefore protein samples were first concentrated by acetone-precipitation before being electrophoresed and transferred onto nitrocellulose membrane. Western blot analysis was performed with the peptide *RELMβ* antibody and subsequently the proposed *RELMβ* hexamer was detected (Figure 4.19).

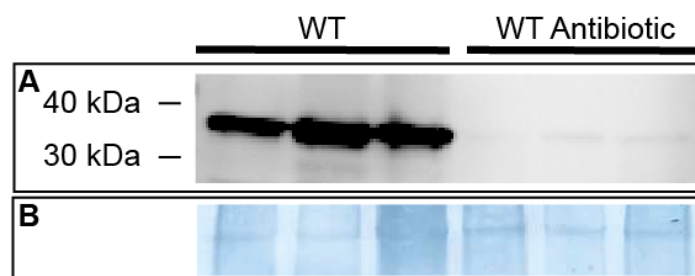


Figure 4.19 – Faecal *RELMβ* expression following antibiotic treatment. Western blot analysis of protein isolated from faecal samples of WT animals (WT) (n=3) and WT animals treated with antibiotics (WT antibiotic) (n=3). The membrane was probed for *RELMβ* (A) and total protein stain amido black was used to confirm equal loading (B).

In agreement with previous studies of RELM β , antibiotic treatment experiments were found to attenuate RELM β expression. The response of RELM β , a protein known to be potently induced by the presence of the microbiota, validates the antibiotic treatment used and the proposed reduction in microbial load of treated animals.

4.3.9.2 *FMO5 Expression is Unchanged in Antibiotic Treatment*

Concentrated protein samples of faecal pellets from WT and antibiotic-treated WT animals were also used to investigate the response of FMO5 to the antibiotic treatment (figure 4.20).

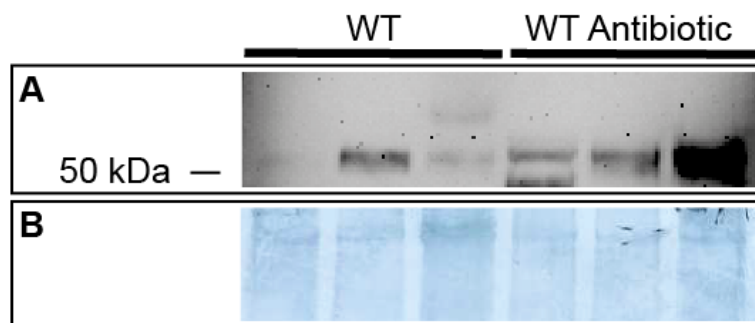


Figure 4.20 – Faecal FMO5 expression following antibiotic treatment. Western blot analysis of protein isolated from faecal samples of WT animals (WT) (n=3) and WT animals treated with antibiotics (WT antibiotic) (n=3). The membrane was probed for FMO5 (A) and total protein stain amido black was used to confirm equal loading (B).

Though there is high variation in the samples, it seems FMO5 expression is unchanged in treatment, indicating expression is not so heavily dependent on the microbiota.

4.4 CONCLUSIONS

FMO5 was found to be expressed in epithelial cells in all sections of the digestive tract analysed. Although no difference was observed in the gross morphology of WT and FMO5 KO intestinal tissue, in microbiota analysis we demonstrate FMO5 expression modifies the commensal bacterial of the intestine. However, further characterisation of the intestinal microbiota in high-fat feeding experiments dispute this to be the cause of the altered energy phenotype of the WT and FMO5 KO. Similar to the RELM β KO mouse, the FMO5 KO is protected from diet-induced obesity independent to the intestinal dysbiosis.

As discussed in chapter 3 (*see* 3.3.3), the antibiotic treatment of the WT animal elicits the expected response in the elimination of the intestinal microbiota; an overall improvement in insulin sensitivity and glucose homeostasis. However, the metabolic phenotype of the FMO5 KO remained unchanged in treatment. In addition, similar to a germ-free model, the KO animal presents with a heightened insulin sensitivity from a young age. We therefore propose the FMO5 KO as a ‘pseudo germ-free’ model; impervious to the presence of the commensal microbes of the intestine.

From investigations into the intestine of WT and FMO5 KO mice, we further propose the absence of FMO5 mimics a germ-free environment by attenuating the necessary processing of RELM β , the microbial sensor of the intestine. In the absence of FMO5, RELM β remains as an inactive dimer resulting in a modest, beneficial reduction in mucosecretion. In high-fat feeding RELM β is induced, however remains as an inactive dimer in the KO. Analogous to the RELM β KO, the FMO5 KO animal is therefore protected from diet induced obesity. In antibiotic treatment, and subsequent attenuation in RELM β expression, the WT animal adopts the pseudo germ-free profile of the FMO5 KO.

***Chapter 5 - Low-grade Inflammation in
Metabolic Disorders***

Chapter 3 describes a heightened insulin sensitivity of the FMO5 KO and its subsequent influence on the gross metabolic phenotype of the animal. Following investigations into the intestine of the WT and FMO5 KO mice, in Chapter 4 we report a disparity in the luminal environment of the two mouse lines. There is a difference in the dimerization state of the colonic hormone RELM β . Only the WT expresses the active monomer and mucosecretion, known to be induced by RELM β , was found to be higher in the WT. In addition to a mucosecretagogue, RELM β is also regarded as an inflammatory mediator. RELM β -activation of macrophages results in inflammatory TNF α release (Hogan et al., 2006; McVay et al., 2006; Krimi et al., 2008). In this chapter a potential link between intestinal inflammation and systemic insulin resistance will be explored.

5.1 INTRODUCTION

5.1.1 Inflammation and Metabolism

Both the metabolic and immune systems are fundamental to the survival of a multicellular organism. The signaling networks have evolved to be closely linked; many bioactive molecules including cytokines, hormones and lipids function in both immune and metabolic roles, and the interplay of the two pathways is now a well-established mediator of an individual's homeostasis. The regulation of metabolism in immunity is clear; in the extremes of obesity the immune system is activated and malnutrition results in immunosuppression, however the reverse is also the case. Immunity relies on metabolic support; the mobilisation of stored lipid helps fight infection, and hence basic inflammation promotes a catabolic state, suppressing anabolic processes including the function of insulin. Therefore, a delicate balance must exist between inflammatory and metabolic signaling in the maintenance of good health, as disorder in one will lead to the imbalance of the other (Hotamisligil, 2006; Shoelson et al., 2007).

Inflammation is the response of an organism to a harmful stimulus, normally resulting in the delivery of plasma components to the site of injury, facilitating the return to a homeostatic state. More recently a distinct, mild inflammatory state has been linked to metabolic disorders. This inflammation occurs in the absence of gross tissue injury

or infection, and the subclinical state has subsequently been referred to as ‘metabolic’ or ‘low-grade’ inflammation. Although mild, the chronic, low-grade inflammatory state has become heavily implicated in the disturbance of energy distribution seen in several metabolic pathologies including diabetes and obesity (Wellen and Hotamisligil, 2005; Monteiro and Azevedo, 2010).

5.1.2 Adipose Tissue

In addition to adipocytes, adipose tissue contains a connective tissue matrix and several immune cells. Whereas brown adipose tissue functions mainly to produce heat through the uncoupling of oxidative phosphorylation in hibernating mammals, white adipose tissue (WAT) is responsible for triglyceride storage when energy is available and the mobilisation of lipids in times of energy deficit. In addition, WAT also secretes bioactive molecules, such as adiponectin and cytokines IL-1 β , IL-6 and TNF α , enabling the organ to communicate with the other metabolically active tissues of the body. Subsequently WAT is now considered to be much more than a passive site of energy storage, with the capacity to regulate food intake, energy homeostasis and insulin signaling (Shoelson et al., 2007; Park et al., 2014).

WAT can be further subdivided into visceral and subcutaneous depots, specifically the former being implicated in the instigation and propagation of metabolic low-grade inflammation. Visceral adipose tissue (VAT) secretion of chemokines, in particular monocyte chemoattractant protein 1, induces macrophage infiltration of adipose tissue. Due to the secretion of their own inflammatory molecules, infiltration of macrophages further propagates the inflammatory response. The resulting interaction between endothelial cells, adipocytes and macrophages potentially leads to the originally local inflammation resulting in a systemic state of low-grade inflammation (Shoelson et al., 2006; Monteiro and Azevedo, 2010; Lam et al., 2011; Kwon and Pessin, 2013; Park et al., 2014).

Insulin signaling is suppressed in the inflammatory state. An increase in adiposity, and resultant increase in inflammatory tone is subsequently now regarded as a prime contributor to the pathogenesis of type 2 diabetes (T2D). The size of specifically VAT depots correlates with inflammatory markers and in cross studies of healthy and

diabetic individuals, markers of inflammation are heavily associated with and actually predict the development of insulin resistance and occurrence of T2D (Duncan et al., 2003; Herder et al., 2007; Sam et al., 2009).

Although elevated fatty acids in circulation alone is known to have an inhibitory effect on insulin signaling, when Miyazaki et al. further investigated the role of visceral fat in peripheral insulin resistance (i.e. muscle and liver), it was not correlated with plasma free fatty acid (FFA) levels. This suggests the relationship is not simply due to an increase in circulating FFA and further corroborates another role of adipose tissue and its association with the development of insulin resistance (Miyazaki et al., 2002). In using conditioned media from human VAT, Lam et al. again demonstrated the inhibitory action of VAT on the insulin pathway of a cultured rat muscle cell line. The inhibition was partly restored when IL-6 was neutralised, implicating a role of adipose tissue derived cytokines in adipose tissue induced diminished insulin signaling (Lam et al., 2011). In addition, several other studies have described the detrimental effect of adipose tissue derived TNF α on insulin sensitivity and the efficacy of TNF α blocking as a therapeutic in humans with inflammatory linked metabolic disorders (Kwon and Pessin, 2013).

Furthermore, even in the absence of full disease development, the associated increase in cytokines with greater adiposity in ageing is proposed to explain the age-related decline in insulin sensitivity. Indeed, anti-inflammatory agents, which decrease inflammatory tone, reduce the risk of development and improve control in already established diabetes (Pickup, 2004; Park et al., 2014). The mechanism of cytokine induced insulin resistance will be discussed further in the following section.

5.1.3 *Inflammation and Insulin Signaling*

5.1.2.1 *Insulin Signaling*

Production of insulin from pancreatic islets is enhanced in response to elevated blood glucose. Circulating insulin then binds to the α subunit of the insulin receptor, which is arranged as a $\alpha_2\beta_2$ heterodimer on the cell surface. Binding of an insulin molecule permits the tyrosine kinase activity of the intracellular β subunit, resulting in autophosphorylation of the dimer. The conformational change further amplifies the intrinsic tyrosine kinase activity of the receptor, which is now able to phosphorylate proximal adaptor molecules, such as insulin receptor substrates 1 and 2 (IRS-1 and IRS-2). IRS1/2 tyrosine phosphorylation activates the phosphatidylinositol-3-kinase (PI3K) and mitogen activated protein kinase (MAPK) pathways. Amongst other cellular effects, the PI3K pathway functions to stimulate glucose uptake in muscle and adipose tissue by the translocation of glucose transporter 4 (GLUT4) into the membrane, the induction of glycogen synthesis in muscle and liver by the activation of glycogen synthase, and inhibition of liver gluconeogenesis by suppressing the expression of the required enzymes (Wellen and Hotamisligil, 2005; Hotamisligil et al., 2006; Kwon and Pessin, 2013; Park et al., 2014).

5.1.2.2 *Insulin Resistance*

A decrease in insulin sensitivity, or increase in insulin resistance, can be defined as a smaller than expected biological response of insulin-sensitive organs to a defined dose of insulin. In the first instance, the pancreatic beta cells respond by producing more insulin. Hyperinsulinaemia, as well as causing metabolic stress, eventually becomes insufficient and a state of hyperglycaemia ensues. The constant activation of the beta cells, due to unresolved hyperglycaemia, causes cellular stress and apoptosis. Additive to the original insulin resistance, the subsequent reduced function of pancreatic beta cells further worsens the physiological state, resulting in T2D. (Kwon and Pessin, 2013)

Insulin resistance is characterised at the cellular level by the interruption of the IRS-PI3K pathway. IRS-1 tyrosine phosphorylation, mediated by the insulin receptor, permits the activation of PI3K and MAPK pathways, however there are also several serine residues of the IRS-1 that can be phosphorylated. Serine phosphorylation

conversely disrupts binding between the insulin receptor and IRS-1 and subsequently decreases the activity of the downstream PI3K and MAPK cascades. As well as its tyrosine kinase activity, the insulin receptor also activates certain serine/threonine kinases capable of catalysing the inhibitory phosphorylation of the receptor itself or IRS-1. Serine phosphorylation may therefore have developed as a negative feedback loop if insulin signaling is overactive or insulin is in excess (Aguirre et al., 2002; Werner et al., 2004; Kwon and Pessin, 2013).

Cytokines

Inhibitory serine phosphorylation of IRS-1 is induced by inflammatory cytokines. Cytokines such as TNF α and IL-6 activate kinases c-Jun N-terminal kinase 1 (JNK) and I κ B kinase (IKK). JNK and IKK are well characterised in diminishing the activity of the insulin pathway, either by direct serine phosphorylation of substrates or by activating genes of the inflammatory response. Since its detection in adipose tissue, a cytokine that has received particular attention in the progression of insulin resistance is TNF α . TNF α is elevated in adipose tissue in obesity, hyperinsulinaemia and in response to high-fat feeding. The cytokine is experimentally shown to induce serine phosphorylation, hence reducing tyrosine phosphorylation and downstream activity of the insulin receptor and IRS-1. As well as lowering whole body insulin and glucose levels, TNF α neutralization specifically restores diminished tyrosine phosphorylation of adipose tissue and muscle tissue in obesity induced insulin resistance. Muscle tissue does not directly produce the cytokine, therefore further highlighting an endocrine/paracrine function of the cytokine. TNF α infusions alone have been shown to reduce insulin sensitivity and gain of function mutations in the TNF α , as well as IL-6, genes are associated with a higher risk of diabetes (Hotamisligil et al., 1993; 1994; Moller, 2000; Gao et al., 2002; Dandona et al., 2004; Pickup, 2004; Hotamisligil et al., 2006).

Higher circulating lipids, ER and mitochondrial stress also activate JNK and IKK and genetic loss-of-function mutations in the two pathways are associated with higher insulin sensitivity and the protection from diet induced insulin resistance (Wellen and Hotamisligil, 2005; Hotamisligil et al., 2006; Shoelson et al., 2007; Monteiro and Azevedo, 2010).

Obesity and Insulin Resistance

A sustained positive energy balance, resulting from over nutrition and a sedentary lifestyle, results in the accumulation of lipid and pathogenesis of obesity. The increase in adipose tissue, and its associated secreted factors, in obesity, makes the obese state itself a prime cause of T2D. Indeed, obesity is characterised by a higher inflammatory tone and inflammatory genes represent one of the most abundantly affected sets in the obesogenic state. Subsequently, obesity is well regarded as an activator of the immune response and consistent with this, weight loss and calorific restriction improves the inflammatory tone of obese individuals. Likewise, the use of anti-inflammatory therapeutics improve the outcome of obesity induced insulin resistance (Wellen and Hotamisligil, 2005; Shoelson et al., 2007; Hotamisligil et al., 1993)

Obesity-induced low-grade inflammation is now well regarded to be the transmitting signal between obesity and the development of insulin resistance. In fact, it is the discriminating factor of the not always uniform relationship between obesity and diabetes. Although a strong link exists between the two pathologies, the former does not always result in the latter. In both animals and humans, inflammatory markers are elevated in specifically obese subjects with accompanying insulin resistance. Those who are obese, yet protected from the development of insulin resistance, do not have an accompanying increase in inflammatory tone. Furthermore, a genetic mutation impairing TNF α synthesis uncouples obesity and diabetes and the TNF α null mouse is protected from obesity induced glucose intolerance and hyperinsulinaemia (Hotamisligil et al., 1993; Moller, 2000; Barbarroja et al., 2010; Kwon and Pessin, 2013).

The activation of inflammatory cellular kinases, mediated by excess lipids and cytokines, therefore dictates a pathogenic feed forward loop in obesity. Larger adipose deposits, and an increase in associated cytokines, initiates insulin resistance which further propagates excessive lipid storage. However, it is clear inflammation induced insulin resistance can also happen independently of obesity. The infusion of inflammatory mediators, in the absence of obesity, is alone effectual in the instigation of insulin resistance. Along with the increased incidence of T2D in other inflammatory diseases, it is clear insulin resistance is also a consequence of the

inflammatory response alone (Wellen and Hotamisligil, 2005). Therefore, in addition to the very well characterised, canonical pathway of obesity-induced inflammation mediating insulin resistance, another loop may exist whereby inflammation, in the absence of obesity, first provides a stimulus for reduced insulin sensitivity.

5.1.4 *The Intestine and Metabolic Endotoxaemia*

There are pronounced differences in the phenotype of the germ-free and conventionalized mouse. Specifically, conventionalisation of the murine digestive tract results in reduced insulin sensitivity and a coincident increase in plasma glucose (*see* 1.2.2). Because of this, research has focused on the intestine and its resident microbes as a potential source of low-grade inflammation, capable of influencing insulin signaling.

Using mouse models, Ding et al. showed ileal TNF α to correlate with obesity and insulin resistance during high-fat feeding and intestinal markers of inflammation predated the development of metabolic syndrome (Ding et al., 2010). Subsequent investigations of high-fat fed mice agreed that the colon tissue itself is more inflamed and intestinal inflammation was identified as an early response to the diet, which could participate in systemic inflammation and whole body insulin resistance (Lam et al., 2012; Kim et al., 2012).

In parallel, Lipopolysaccharide (LPS), a component of gram-negative bacterial cell walls, was also proposed to be a gut-derived trigger for a low-grade inflammatory state. Bacterial-derived LPS can be transported from the lumen into intestinal epithelial cells. Here, chylomicron formation facilitates entry into circulation, and transport of LPS to peripheral tissues. Contact of the antigen with innate immune cells of the host has the potential to evoke the production of inflammatory cytokines. Subsequent activation of kinases JNK and IKK leads to the serine phosphorylation and downregulation of the insulin pathway. Cani et al. demonstrated high-fat feeding increased circulating LPS (or endotoxaemia) in the mouse. This moderate increase in LPS is much lower than that observed in the severe instance of septic shock, and was therefore referred to as “metabolic endotoxaemia”. An LPS infusion alone was able to mimic the increase in inflammatory tone observed in high-fat feeding, along with associated hyperinsulinaemia, hyperglycaemia and increased body weight. Furthermore, the LPS receptor (CD14) knockout was protected from the development of associated inflammation and insulin resistance in response to a high-fat diet. LPS was therefore postulated to be involved in the gut-insulin signaling axis, transmitting the signal of a high-fat diet to the systemic phenotype. Even when fed normal chow,

the CD14 knockout is more insulin responsive, indicating LPS may also be a mediator of insulin sensitivity in physiological conditions. (Cani et al., 2007a)

High-fat feeding is thought to increase the uptake of LPS by upregulating the incorporation into chylomicrons and also by simply increasing gut permeability. Specifically a high-fat diet has been shown to reduce the intestinal epithelial expression of tight junction proteins ZO-1 and Occludin. Thus a 'leaky gut' would be more permissive to LPS entering circulation and further worsening the inflammatory tone (Erridge et al., 2007; Cani et al., 2008a; Delzenne and Cani, 2011; Raybould, 2012; Boroni Moreira and de Cássia Gonçalves Alfenas, 2012).

Human studies have further corroborated a role of LPS, as a high-fat diet increased plasma LPS and elevated LPS is associated with insulin resistance and insulin levels in healthy individuals and is higher in T2D patients. Low doses of LPS induced adipocyte-derived cytokines such as TNF α and IL-6 at both the whole body and cellular level. LPS is now therefore regarded as a bacterial mediator, capable of infiltrating host circulation and instigating the subclinical inflammation seen in the development of insulin resistance (Creely et al., 2006; Cani et al., 2007a; Anderson et al., 2007; Amar et al., 2008; Serino et al., 2011; Hawkesworth et al., 2013).

Intestinal inflammation and/or the infiltration of LPS in the instigation of systemic inflammation is thought to be a potential determinant in whether an individual is prone or resistant to diet-induced insulin sensitivity. As described previously, both humans and mice display different responses to obesity, with only some developing impaired insulin signaling. Although an increased inflammatory tone is known to be key in the development of obesity induced insulin resistance, Serino et al. further implicated gut permeability and circulating LPS in determining the polarised response to a high fat diet. In addition, in patients that underwent gastric bypass surgery to alleviate the obese and diabetic state, T2D resolved itself far before the obesogenic state was improved. This further supports the intestine as a significant site of inflammation, in addition to adipose tissue, in the pathogenesis of acquired diabetes (Serino et al., 2011; Kemp, 2013).

Consequently, the source of LPS generation, the intestinal bacteria, has been the focus of efforts to relieve the stress of metabolic endotoxaemia. Indeed, antibiotic treatment or prebiotic feeding of high-fat diet fed animals reduced intestinal permeability, plasma LPS and improved peripheral inflammation and associated metabolic parameters (Cani et al., 2007b; 2008a; 2009). Caution must however be taken when postulating a causative role in specifically the changes in the microbiota upon high-fat feeding in the instigation of inflammation. The diet associated microbial shift does not always correlate with the susceptibility to diet-induced insulin resistance. In addition, there are several evidences of a high-fat diet induced dysbiosis occurring independently of obesity. Therefore, although the significance of the presence of the microbiota cannot be argued, it is clear the transmission of the signal from the gut to host immunity also involves a host-genetic component (Hildebrandt et al., 2009; La Serre et al., 2010; Boroni Moreira and de Cássia Gonçalves Alfenas, 2012).

5.1.5 Complement Component 3

The complement pathway is a component of the innate immune system. Briefly, activation of the three complement pathways; alternative, classical and lectin, leads to the activation and cleavage of complement component 3 (C3), subsequent production of C3a and C3b and activation of the terminal pathway. Membrane attack complexes formed in the terminal pathway insert themselves into cell membranes, disturb cellular integrity and eventually promote cell lysis. The complement system is ubiquitous and therefore a tight balance of activation and inhibition is necessary in preventing immune dysregulation (Hertle et al., 2014).

C3 is an acute phase reactant (a factor induced in acute inflammation) and production was originally solely attributed to the liver. Since however, C3 synthesis has also been demonstrated in macrophages and adipocytes, where all other components of specifically the alternative pathway are produced, and it is considered an important immune mediator. C3-derived anaphylatoxins C3a and C5a serve to promote initial immune cell infiltration, macrophage proliferation and cytokine release. A further product of C3 cleavage, acylation stimulating protein (ASP), also contributes to the activation of adipocyte inflammatory mechanisms, such as the increased gene expression of inflammatory kinases JNK1 and IKK. Along with being one of the major plasma proteins of the immune complement system, C3 production in adipose tissue in response to local inflammation is postulated to link tissue inflammation with systemic pathologies, such as low-grade chronic inflammation and accompanying insulin resistance (Muscari et al., 2000; Cianflone et al., 2003; Engström et al., 2005; Onat et al., 2011; Wlazlo et al., 2012; Munkonda et al., 2012; Hertle et al., 2014).

Indeed changes in levels of C3, and its cleavage products, are a now well-established marker of inflammatory disorders such as T2D and obesity. Circulating C3 correlates with high-fat feeding, obesity and insulin resistance where it is also associated with systemic low-grade inflammation. C3 levels are actually found to be predictive of impaired glucose tolerance, diabetes and weight gain and subsequently are considered to be not just a marker, but also a mediator of immune disorder development. In support of this, the C3 knockout has lower plasma glucose and C3a and C5a receptor knockout models have ameliorated inflammation and maintained insulin sensitivity

during high-fat feeding (Muscari et al., 2000; Engström et al., 2005; Samaras et al., 2010; Onat et al., 2011; Hertle et al., 2014).

Being a product of adipose tissue, it is unsurprising C3 is found to be elevated in times of increased adiposity such as high-fat feeding and obesity. However, a magnitude of epidemiological studies has specifically shown C3 to be predictive of insulin resistance and T2D independently of obesity and metabolic syndrome. In fact, ASP was found to be elevated in lean T2D subjects, suggesting C3 activation participates in inflammatory insulin resistance even in the absence of increased adiposity (Engström et al., 2005; Onat et al., 2011; Phillips et al., 2012; Wlazlo et al., 2012; Hertle et al., 2014).

5.2 RESEARCH QUESTIONS AND AIMS

- I.** Complement component 3 (C3) is used as an inflammatory marker in the pathogenesis of insulin resistance. In C3 measurement, inflammation of WT and FMO5 KO adipose tissue will be determined.

- II.** Following the observed increase in whole-body insulin sensitivity of the FMO5 KO, insulin sensitivity will be measured in specifically the adipose tissue of the WT and FMO5 KO animal.

- III.** LPS is a bacterial product of the intestine thought to be involved in the progression of low-grade inflammation in the host (*see* 5.1.4). To investigate the ‘leaky gut’ hypothesis and subsequent infiltration of luminal LPS, plasma LPS (endotoxin) will be measured in the WT and FMO5 KO animal.

- IV.** Differences in colonic expression of RELM β indicate an altered processing of the hormone in the WT and FMO5 KO animal (*see* 4.3.6). To clarify whether this results in a difference in how much hormone enters circulation, plasma RELM β will be measured.

- V.** Finally, to characterise any differences in systemic inflammation of the WT and FMO5 KO animal, inflammatory cytokine TNF α will be measured in plasma of the two mouse lines.

5.3 RESULTS

5.3.1 Adipose tissue C3 expression is reduced in the FMO5 KO Mouse

Adipose tissue produces C3 in response to acute infection. Levels are associated with the development of inflammatory-linked metabolic disorders and specifically visceral adipose tissue (VAT) C3 expression is shown to influence insulin function (Engström et al., 2005; Samaras et al., 2010; Hertle et al., 2014). VAT from 10-week old WT and FMO5 KO animals was harvested and probed for C3 (Figure 5.1).

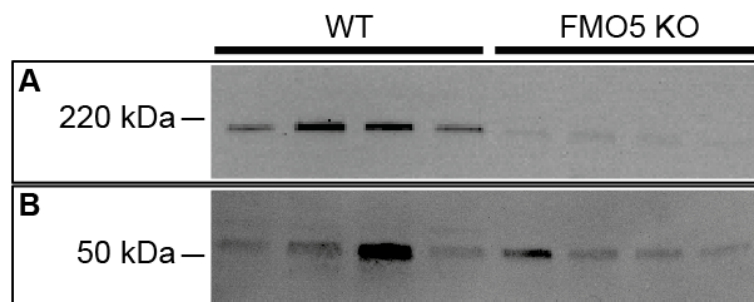


Figure 5.1 – Adipose tissue levels of complement component 3 (C3) in the WT and FMO5 KO animal. Western blot analysis of visceral epididymal adipose tissue of 10-week old WT (n=4) and FMO5 KO (n=4) male mice. The membrane was probed for C3 (A) and enolase was used as a loading control (B)

Consistent with a size of ~185 kDa, a single band for C3 was detected in Western blot analysis. FMO5 KO mice have reduced amounts of adipose tissue C3 when compared to the WT, indicating the FMO5 KO adipose tissue has a lower inflammatory tone. Enolase was used as a loading control and variation in sample loading is evident. Protein determination of adipose tissue lysates is challenging, due to the high lipid content of samples interfering with the protein assay. Regardless, the genotype-related difference in C3 is clearly not an artifact of the imperfect protein loading.

Moreover, there was no difference in liver C3 expression in the WT and FMO5 KO mice (data not shown). The difference in C3 expression is therefore paradoxically detected in adipose tissue, where FMO5 is not expressed, and not evident in the liver; the primary site of FMO5 expression. This suggests the difference observed in C3 is not a direct result of FMO5 mediated catalysis, the action we are seeing is a consequence of its expression in a discrete location.

5.3.2 FMO5 KO Adipose Tissue is more Insulin Sensitive

As early as 10 weeks of age, whole-body measurements revealed the FMO5 KO to be insulin hypersensitive (*see* 3.3.1). A decline in insulin sensitivity of specifically VAT, in response to low-grade inflammation, has been postulated as the mediator of whole-body insulin resistance (Shoelson et al., 2006). Insulin sensitivity was subsequently measured in VAT of WT and FMO5 KO mice. Insulin resistance is characterised by the interruption of the IRS-PI3K pathway, hence phosphorylation of the PI3K substrate; Akt, generating phospho-Akt (pAkt), is a measurable indicator of pathway activation. 10 minutes post insulin stimulation, WT and FMO5 KO mice were culled and VAT was harvested and probed for pAkt (Figure 5.2).

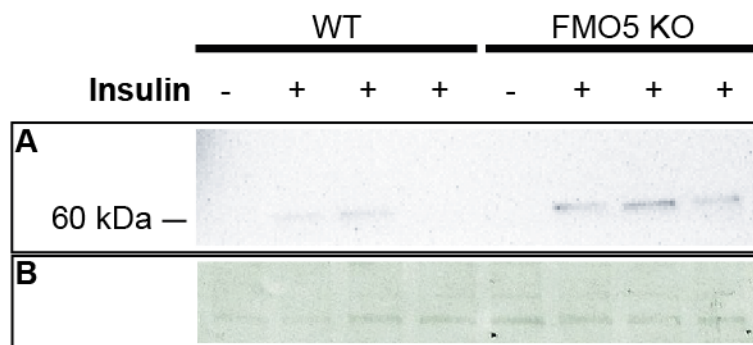


Figure 5.2 – Adipose tissue insulin sensitivity measurement in WT and FMO5 KO animals. Western blot analysis of visceral epididymal adipose tissue from control (-) and insulin stimulated (+) WT and FMO5 KO male mice at 10-weeks of age. The membrane was probed for pAkt (**A**) and total protein stain amido black was used to confirm equal loading (**B**).

At a low dose of insulin (0.5U/Kg), FMO5 KO adipose tissue was more responsive. FMO5 KO insulin treated animals (+) show a consistent increase in pAkt compared to the untreated animal (-). However, in measurements of the WT animal, insulin stimulation did not result in any great deviation from the basal pAkt level.

A low dose of insulin was used, 4 times lower than what is generally used in the study of control versus obese or diabetic groups. We are not measuring obese nor diabetic mice and the dose was selected to be just great enough to instigate a response, however not too great to mask the very slight difference between a control and hyperinsulinsensitive animal. This explains why, in our analyses, the WT mice do not show any response to the stimulation, whereas the hypersensitive FMO5 KO does.

Out of the insulin sensitive organs, VAT has gained the most attention in the investigation of inflammation-induced insulin resistance. In fact, there is disagreement as to whether insulin signaling of muscle and liver is affected in response to low-grade inflammation (Hotamisligil et al., 1993; Moller, 2000; Shoelson et al., 2006; Serino et al., 2011). Nevertheless, future insulin sensitivity measurements of liver and muscle would further characterise the insulin sensitive phenotype of the FMO5 KO animal. Regardless, in the FMO5 KO, we propose a reduced inflammatory tone of visceral adipose tissue results in heightened insulin sensitivity of the tissue.

5.3.3 Plasma Endotoxin Measurement

A wealth of studies has proposed an increase in intestinal permeability, or ‘leaky gut’, and the subsequent infiltration of LPS (endotoxin), as a gut-derived trigger for peripheral and systemic inflammation (Cani et al., 2007a; Boroni Moreira and de Cássia Gonçalves Alfenas, 2012; Delzenne et al., 2011; Delzenne and Cani, 2011). Plasma endotoxin measurements of the WT and FMO5 KO animal however revealed no observable difference in circulating levels (Figure 5.3).

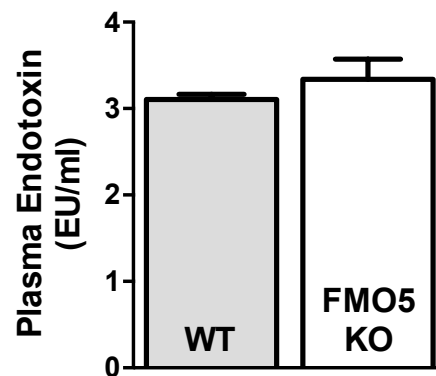


Figure 5.3 – Plasma endotoxin levels in the WT and FMO5 KO animal. Plasma endotoxin was measured in 10-week old WT (n=3) and FMO5 (n=3) male mice. Data is expressed as mean \pm SEM.

Therefore, the protection from the low-grade adipose tissue inflammation, and subsequent increased insulin sensitivity of the FMO5 KO, cannot be specifically attributed to a difference in endotoxaemia. This is in agreement in the gross morphological analysis of WT and FMO5 KO intestinal tissue (*see* 4.3.4); no difference in barrier integrity was observed.

5.3.4 Difference in Plasma RELM β in the WT and FMO5 KO Animal

Along with changes in the intestinal microbiota, differences were observed in the expression of the colonic hormone RELM β . In the WT and FMO5 KO colon no gross difference was observed in RELM β expression levels and the dimeric form of the protein was detected in both genotypes. The active monomer was however specifically found in the colon of the WT animal (*see* Figure 4.11). In addition, faecal detection revealed the FMO5 KO excretes more RELM β (*see* Figure 4.13). Taken together, this suggests a lack of RELM β processing in the KO colon results in less of the luminal hormone infiltrating host tissue/ circulation. The pro-inflammatory nature of RELM β would therefore make it a potential source of variation in inflammation of the WT and FMO5 KO animal. Using a sandwich-based ELISA, RELM β was measured in plasma of WT and FMO5 KO animals fed a standard chow (Figure 5.4).

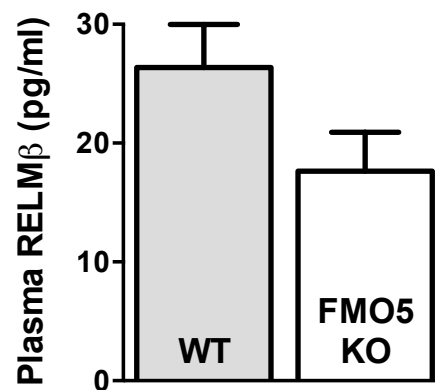


Figure 5.4 – Plasma levels of RELM β in WT and FMO5 KO male mice Plasma RELM β was measured between 9-11 am in 30-week old WT (n=10) and FMO5 KO (n=10) male mice. Data is expressed as mean \pm SEM.

High variation exists between individuals in both colonic and plasma measurements of RELM β (Hildebrandt et al., 2009; Neilson et al., 2011). In plasma measurements, RELM β tended to be higher in the WT animal. However, due to the high variability in measurements, the difference between WT and FMO5 KO levels was not statistically significant when analysed with Student's t-test ($p=0.09$). To investigate the influence of high-fat feeding, measurements were also conducted in high-fat diet (HFD) fed WT and FMO5 KO animals (Figure 5.5).

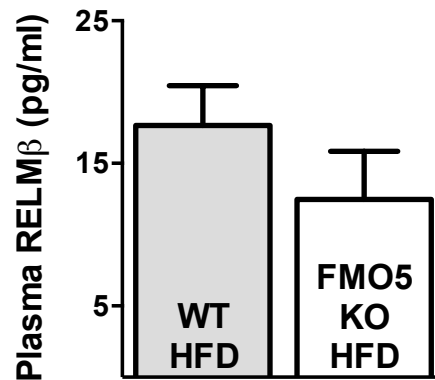


Figure 5.5 – Plasma levels of RELMβ in WT and FMO5 KO male mice fed a high fat diet (HFD). Plasma RELMβ was measured between 9-11 am in high fat diet fed WT (n=6) and FMO5 KO (n=6) male mice. Data is expressed as mean ± SEM.

In high-fat diet fed animals, plasma RELMβ was again higher in WT plasma when compared to FMO5 KO levels. However, due to high variation in samples, results were again not statistically significant. Plasma RELMβ is reported to be elevated in response to high-fat feeding (Shojima et al., 2005). We did not observe this trend in our analysis. In fact, although not significant, the HFD values were lower in both genotypes (Table 5.1). This is likely to be due to the lipaemia in HFD plasma interfering with the ELISA method of detection. Normally this can be overcome by taking plasma from starved animals, thereby reducing the lipid content of plasma, however RELMβ expression is attenuated during fasting.

	RELMβ (pg/ml)	
	WT	FMO5 KO
Standard Chow	26.36 ± 3.63	17.63 ± 3.28
High-Fat Diet	17.65 ± 2.80	12.47 ± 3.37

Table 5.1 – Plasma levels of RELMβ in WT and FMO5 KO male mice fed standard chow or a high fat diet. RELMβ was measured between 9-11 am in standard chow fed (WT: n=10, FMO5 KO: n=10) and high fat diet fed (WT: n=6, and FMO5 KO: n=6) male mice. Data is expressed as mean ± SEM.

5.3.5 Changes in Circulating TNF α in the WT and FMO5 KO Animal

In both *in vivo* and *in vitro*, RELM β activates macrophages resulting in the release of TNF α . McVay et al. specifically described the colon of the RELM β KO mouse to have lower levels of TNF α (McVay et al., 2006). This suggests even breaching the intestinal barrier, and not necessarily entering circulation, RELM β can instigate intestinal inflammation. TNF α is an inflammatory cytokine, well characterised in its ability to diminish the activity of the insulin pathway. It is also known to have a paracrine/endocrine function; mediating effects peripheral to its site of production. To assess a potential role of the observed differences in RELM β , and postulate a link to the difference in insulin sensitivity of the WT and FMO5 KO mouse, plasma TNF α was measured before and after antibiotic treatment (Figure 5.6).

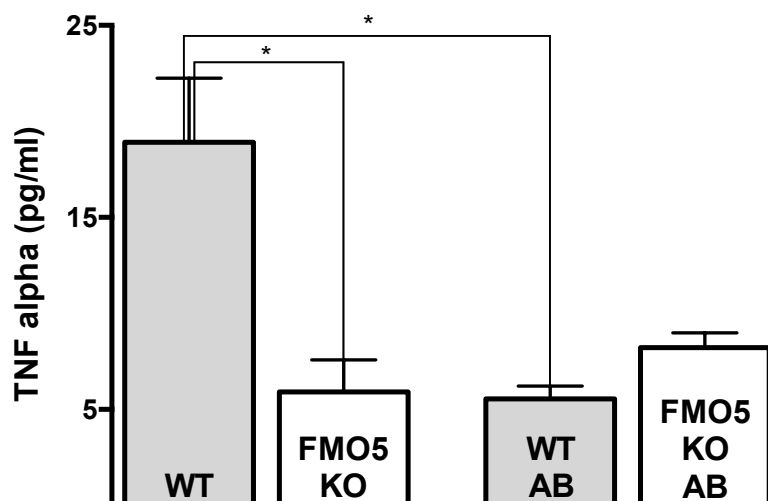


Figure 5.6 – Plasma levels of TNF α in control and antibiotic treated WT and FMO5 KO mice. TNF α was measured between 9-11 am in control treated animals (WT; n=5, FMO5; n=4) and antibiotic treated animals (WT AB; n=3, FMO5 KO AB; n=3) Data is expressed as mean \pm SEM. *: $p < 0.05$.

In the untreated WT and FMO5 KO animals, TNF α was found to be higher in the WT (WT, 18.92 \pm 3.34 pg/ml, n=5; FMO5 KO, 5.91 \pm 1.67 pg/ml, n=4) ($p < 0.05$). Therefore, coincident with higher insulin sensitivity and lower adipose tissue inflammation, the FMO5 KO also has a lower systemic inflammatory tone. Furthermore, circulating TNF α was found to be lower in antibiotic treated WT animals (WT AB, 5.47 \pm 0.67 pg/ml, n=3) when compared to the untreated controls

(WT, 18.92 ± 3.34 pg/ml, n=5;) ($p < 0.05$), whereas the treatment had no effect on TNF α levels in the FMO5 KO.

The effect of the antibiotic treatment on TNF α levels is in parallel with that seen in the gross metabolic measurements. Antibiotic treatment lowers circulating TNF α , plasma glucose and insulin and improves glucose tolerance in specifically the WT animal, whilst eliciting no effect in the FMO5 KO. As a result, The WT animal adopts the apparent ameliorated low-grade inflammation and hyperinsulinsensitivity of the FMO5 KO.

5.4 CONCLUSIONS

The antibiotic treatment was designed to reduce the microbial load of the intestine. In agreement, microbial-induced RELM β expression was attenuated and the caecum became enlarged; an observed characteristic of germ-free mice. We hypothesize the low dose course of antibiotics relieved the burden of the microbiota in the WT animal, ameliorated expression of microbial sensor RELM β , thereby improving inflammatory tone and insulin signaling.

The heightened insulin sensitivity of the FMO5 KO observed from a young age, and the absence of any effect in antibiotic treatment, suggests FMO5 to be a host protein involved in the intestinal microbiota mediated increase in inflammatory tone, and subsequent decline in insulin signaling. A potential mechanism outlined in Chapter 3 is the processing, hence activation, of colonic hormone RELM β .

From what is known about RELM β , and the observed difference in the WT and FMO5 KO animal, alternative processing of the colonic hormone is a good candidate for the altered metabolic phenotype. Although involved in intestinal barrier integrity, microbiota-induced RELM β also has pro-inflammatory properties. Host goblet cells produce the hormone, and it is secreted into the colonic lumen. Here, it is believed to act as a mucosecretagogue; positively regulating the formation of the mucus layer. In agreement, the intestine of the RELM β KO is more permeable. RELM β infiltration of host tissue is however deleterious, as RELM β -activation of macrophages results in inflammatory TNF α release (McVay et al., 2006; Hogan et al., 2006; Krimi et al., 2008). The proposed active, monomeric form of RELM β was specifically found in the WT colon, and there was a trend of higher levels of RELM β in WT plasma. Akin to colonic measurements (*see* Figure 4.11), the absence of FMO5 does not impair RELM β expression; both the WT and FMO5 KO produce the hormone. However it may be FMO5, also expressed in host colonic cells, mediates a change in the dimeric nature of the protein, hence promoting the infiltration and/or proinflammatory actions of the hormone.

Cytokine measurement in plasma is problematic and detection methods often lead to underestimation. Cytokines are active at very low concentrations, often at the lower limit of detection assays, and recognition is further complicated by the short half-life, rapid degradation of cytokines and cytokines existing in multiple forms (e.g. oligomers and glycosylated) (Bienvenu et al., 1998). Furthermore, plasma detection provides no information of origin. Immune cells, ubiquitously found across the body, produce cytokines. Cytokines are pleiotropic; they often elicit various effects in different cell types, and operate in a complicated network involving several other mediators. In this investigation it is possible infiltrating RELM β activates intestinal macrophages and resultant circulating TNF α causes inflammation in peripheral adipose tissue. Alternatively, RELM β itself in circulation has the potential to activate adipose tissue macrophages, provoking an immune response in adipose tissue leading to higher circulating TNF α . Specific tissue measurement of TNF α would resolve this. Using tissue homogenates in ELISA-based detection of cytokines has been described (Matalka et al., 2005; McDuffie et al., 2006; Amsen et al., 2009), however in our analysis it was not successful. Real-time polymerase chain reaction or immunohistochemical investigations of specific tissues would be appropriate for future investigations.

Regardless of the ambiguity in origin of inflammation, it is of note the C3 and TNF α measurements were conducted at 10- and 20- week old mice respectively. The difference observed in these two markers predates the difference in weight and fat pad size recorded in the WT and FMO5 KO. The difference in gross body weight only presents after 21 weeks of age and the visceral fat pad of the FMO5 KO is only reported to be significantly smaller at 30 weeks of age. The elevated levels of C3 and TNF α cannot therefore be directly attributed to an increase adiposity of the WT. Considering the timeline of the phenotype, it seems more likely an increased inflammatory tone, originating from the gut, has a deleterious effect on the insulin signaling of the WT animal, eventually causing an increase in adiposity and body weight in older age.

Chapter 6 - Discussion

6.1 Summary

The flavin-containing monooxygenases (FMOs) catalyse the oxygenation of a broad range of substrates and are fundamental to the Phase I processing of xenobiotic compounds (Cashman, 2003). In the absence of substrate, the enzymes are able to activate molecular oxygen and the activated FMO complex is thought to be the most prominent form in the cell (Ziegler, 2002; Zhang et al., 2007). Due to the resultant broad substrate specificity of the isoforms, and the inefficiency of antibody-mediated catalytic inhibition, the further characterisation of FMOs requires the utilization of mouse knockout models (Shephard and Phillips, 2010). FMO knockout mouse models have clarified the role of particular isoforms in xenobiotic metabolism (Hernandez et al., 2009) and, in further investigations, have also revealed a potential endogenous role of isoforms FMO1 and 5 (Veeravalli et al., 2014; Gonzalez Malagon et al., unpublished).

Several properties of FMO1 and FMO5 indicate an endogenous role of these isoforms and FMO5 in particular has been defined as an atypical FMO. There are very few non-synonymous mutations of *FMO1* and *FMO5* (Furnes et al., 2003; Sevasti B Koukouritaki, 2005; Motika et al., 2007) and, unlike other isoforms, FMO5 is shown to be inducible and large inter-individual variations are reported (Miller et al., 1997; Overby et al., 1997; Rae et al., 2001; Krusekopf and Roots, 2005). In the study of the FMO1,2,4 KO mouse, FMO1 was shown to be a regulator of energy homeostasis as well as a drug metabolising enzyme (Veeravalli et al., 2014). Mutant mice have a higher total energy expenditure, which is not accompanied by an increase in calorific intake. Characterisation of an FMO5 KO mouse further revealed an unexpected role for this isoform in endogenous metabolism (Gonzalez Malagon et al., unpublished). By the age of 30 weeks, KO mice have lower circulating glucose and cholesterol and weigh less when compared to the wild-type (WT). The investigations of this thesis further corroborate an endogenous role of FMO5. Inactivation of *Fmo5* imparts a heightened insulin sensitivity in the animal, coincident with, and perhaps, as a result of a lower inflammatory tone.

In the further characterisation of the FMO5 KO metabolic phenotype, we report the FMO5 KO mouse is protected from the deleterious consequences of high-fat feeding.

Furthermore, although eliciting the canonical response in the WT animal; in improving parameters of insulin sensitivity, antibiotic targeting of the intestinal microbiota produced no measurable affect in the KO mouse.

In novel experiments, we have shown FMO5 to be expressed through the entirety of the WT digestive tract. Faecal microbiota analysis of the WT and FMO5 KO animal revealed FMO5 influences the resident bacteria of the lumen. An increased representation of the Bacteroidetes phyla, and concomitant decrease in the Firmicutes, was reported in the FMO5 KO. This dysbiosis has been extensively linked with a lean phenotype, explained by a difference in energy harvest of the microbiota. This originally proposed the dysbiosis as a cause for the different energy phenotype of the WT and FMO5 KO. However, a disparity in the high-fat feeding experiments indicated this not to be the case. Upon high-fat feeding, the intestinal microbiota of the FMO5 KO became equivalent to the WT, both animals now harboring a profile commonly associated with excessive energy storage. However, the FMO5 KO mouse remained lean, thereby indicating the protection mediated by the absence of FMO5 supersedes the presence of an unfavourable microbiota.

Along with microbiota modulation, the absence of FMO5 changed the processing of colonic hormone RELM β . Both the WT and FMO5 KO animal produce the hormone, however the proposed active monomer of RELM β was only identified in the WT mouse. RELM β has been described as a mucosecretagogue (Krimi et al., 2008) as well as a modulator of host inflammation (McVay et al., 2006; Hogan et al., 2006; Krimi et al., 2008). In the absence of the active monomer, the FMO5 KO mouse exhibits lower levels of mucosecretion in the colon and a lower systemic inflammatory tone. Inflammation is now regarded as a potent contributor to the pathogenesis of insulin resistance (Shoelson et al., 2006). We therefore propose the lower inflammatory tone of the FMO5 KO imparts a higher sensitivity to insulin, thereby preventing age-related increases in cholesterol, glucose and weight gain observed in the WT animal.

The further induction of RELM β in high-fat feeding, and apparent lack of activation in the FMO5 KO, explains the further disparity in high-fat diet fed WT and FMO5

KO animals. Furthermore, we know RELM β to be the microbial sensor of the intestine; induction is dependent on the presence of the microbiota. In antibiotic mediated clearance of the intestinal microbiota, hence ablation of colonic RELM β expression, the inflammatory tone and insulin sensitivity of the WT animal was improved, subsequently resembling that of the FMO5 KO. Akin to overexpression of *Fmo5* in a model of intestinal stress (Zhang et al., 2009), we also show intestinal FMO5 expression is induced in high-fat feeding, however expression was not strictly dependent on the presence of the microbiota. Regardless, the strong influence of FMO5 in the response to an increase or amelioration in intestinal stress described implicates it as a factor in the host's recognition to its commensal bacteria and/or the luminal environment of the intestine.

6.2 Mechanism

From the investigations presented, the processing of RELM β is a good candidate for the actions of FMO5. In the absence of FMO5, although protein expression and localization remains unaffected, a difference in the dimerization of RELM β is observed. This could be explained by the FMO mediated oxidation of cysteamine to cystamine, a powerful thiol oxidant critical for the formation of disulphide bonds and correct protein assembly. Poulsen et al. proposed the FMOs to therefore be implicated in the folding of nascent proteins by influencing the local oxidising environment (Poulsen and Ziegler, 1977). RELM β is rich in cysteine residues, which mediate intramolecular disulphide bonds. The inactivation of *Fmo5* may therefore result in the incorrect folding of the hormone, resulting in a loss of activity.

In addition to modifying the oxidising environment of a cell, FMO activity may also result in the production of reactive oxygen species (ROS). Regardless of substrate availability, the FMO catalytic cycle can short-circuit, resulting in the oxidation of NADPH and the generation of H₂O₂ or a superoxide anion (Siddens et al., 2014). Mammalian epithelial cells have been shown to respond to intestinal microbiota by the rapid generation of ROS (Kumar et al., 2007). Consequently, intestinal epithelia generated ROS is proposed to constitute a microbial-instigated protection and signal cascade in the host (Neish, 2009). *Fmo5* mRNA was found to be the most prominent of all the isoforms in the intestine (Janmohamed et al., 2001; Zhang and Cashman, 2005) and our investigations have localized the protein to the intestinal epithelium of the WT mouse. FMO5 generated ROS may therefore participate and its absence could result in a beneficial dampening of the response to the commensal microbes of the intestine in the FMO5 KO.

6.3 The FMO5 KO Mouse

The investigations of this thesis have focused on the intestinal phenotype of the FMO5 KO, in particular the differences observed in the colon of WT and FMO5 KO animals. The proposal of FMO5 in modulating the cellular environment, and the pervasive expression of the isoform, would however suggest an effect much greater than solely the processing of a colonic hormone. This is supported by additional observations of the FMO5 KO mouse outside the scope of this thesis. For instance, FMO5 is expressed throughout the digestive tract and in investigations of the stomach we also observe differences in the resident bacteria of this organ (*see* Appendix). Akin to the faecal analyses, FMO5 KO animals have higher levels of Bacteroidetes and lower levels of Firmicutes when compared to the WT. In fact, the microbial shift between genotypes is even greater in the stomach. Although the relevance of an altered microbiota remains unclear, this warrants further investigation into the role of FMO5 in sites of the digestive tract other than the colon. In addition, FMO5 is also expressed in murine skin, most concentrated in the sebaceous glands (Janmohamed et al., 2001). Observations of ageing WT and FMO5 KO animals also indicate a role of FMO5 at this site; KO animals maintain a fuller coat of hair and greying of the hair is not as severe as that seen in the WT. Once again at an interface of host cells and commensal bacteria, the skin may therefore present a novel site for functional analysis of FMO5.

Furthermore, Fmo5 mRNA levels indicate it is the most prominent isoform in mouse liver (Janmohamed et al., 2004; Zhang and Cashman, 2005) and work conducted by colleagues has focused on the hepatic consequence of the absence of FMO5. Proteomic analysis in liver samples of 30-week old WT and FMO5 KO mice revealed three enzymes of glucose metabolism to be downregulated in the KO; fructose biphosphate aldolase B, glycerol-3-phosphate dehydrogenase and ketohexokinase. This may be a consequence of the absence of hepatic FMO5 catalysis, however we have since described a lower inflammatory tone and heightened insulin sensitivity of the FMO5 KO from young, resulting in lower plasma glucose at 30 weeks of age. It is therefore possible the downregulation of these hepatic enzymes is secondary to the reduced intestinal inflammation and subsequent lower circulating glucose of the FMO5 KO. Proteomic analysis of younger animals, when glucose and insulin levels

are comparable in the WT and FMO5 KO, would help decipher the cause of the change in protein expression.

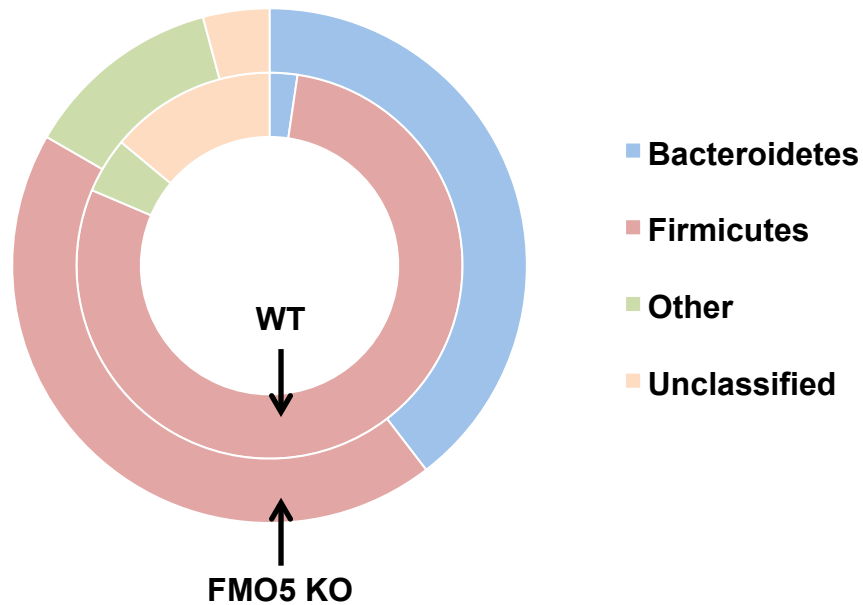
Malic enzyme 1 (ME1) a lipogenic enzyme of the liver was also found to be downregulated in the FMO5 KO mouse. FMO5 mediated ME1 modification was found to be post-transcriptional; ME1 mRNA levels were unchanged in the WT and FMO5 KO mouse. ME1 catalyses the conversion of malate to pyruvate and CO₂, reducing NADP to NADPH. The generated NADPH is required for long chain fatty acid synthesis and also key steps in cholesterol synthesis, therefore the reduction in ME1 may contribute to a decrease in fatty acid biosynthesis and also to the decreased plasma cholesterol of the FMO5 KO mouse. However, what remains unclear is whether the decrease in ME1 is due to the absence of hepatic FMO5 catalysis, or another consequence of a heightened insulin sensitivity of the FMO5 KO. Experiments have revealed adipose tissue of the FMO5 KO to be more insulin sensitive and subsequently lower levels of circulating insulin were detected in comparison to the WT. Additionally, studies have discussed the positive regulation of insulin on ME1 at both the transcriptional and post-transcriptional level (Davis et al., 1988; Katsurada et al., 1988; 1989; Goodridge et al., 1989). If the hepatic insulin sensitivity of the WT and FMO5 KO is comparable, it may therefore be possible higher circulating insulin in the WT results in higher hepatic ME1 expression. Again, ME1 measurement in younger WT and FMO5 KO animals, with equivalent insulin levels, and hepatic insulin sensitivity measurements would prove crucial in determining the cause of the disparity in ME1 expression.

6.4 Conclusions and Future Work

We propose FMO5 to be involved in the host's response to the commensal bacteria of the intestine. The FMO5 KO is impervious to the intestinal stress caused by high-fat feeding and non-responsive to the elimination of the intestinal microbiota. A beneficial dampening in the intestinal epithelial response to the commensal bacteria results in a lower inflammatory tone and resultant modest increase in insulin sensitivity of the FMO5 KO.

The investigations of this thesis propose a potential mechanism in the descriptions of a colonic hormone; FMO5 expression seems necessary for the activation of the microbial sensor RELM β . Moreover, in considering the expression and elusive activity of the isoform, we postulate the endogenous capacity of FMO5 is not mediated by a straight-forward substrate catalysis. Instead, we predict a more global function of FMO5 in regulating the cellular reducing environment and in the production of reactive oxygen species. In doing so, we also predict other site-specific consequences of FMO5 expression, for instance the greying of coat hair in ageing. Cellular measurement of NADP/ NADPH and H₂O₂, in experimental FMO5 overexpression and silencing, would prove fundamental in further mechanistic explanation. Furthermore, the use of stable lines of a specific lineage, for example the goblet cell, would help delineate FMO5's specific, or in fact general, action in the different tissues.

7. Appendix



Appendix I – Phyla-level microbiota analysis of WT and FMO5 KO stomach contents. The stomach contents of three animals was pooled for each condition. Sequence reads were taken from samples of WT (n=44) and FMO5 KO (n=48) 30-week old male mice.

Phylum	Abundance of Phylum (%)	
	WT	FMO5 KO
Bacteroidetes	2	40
Firmicutes	79	44
Other	5	12
Unclassified	14	4

Appendix II – Phyla-level microbiota analysis of WT and FMO5 KO stomach contents. The stomach contents of three animals was pooled for each condition. Sequence reads were taken from samples of WT (n=44) and FMO5 KO (n=48) 30-week old male mice.

		Abundance of Family (%)	
Phylum	Family	WT	FMO5 KO
Bacteroidetes	Rikenellaceae	-	2
	Bacteroidaceae	-	2
	Porphyromonadaceae	2	35
Firmicutes	Clostridiaceae 1	11	2
	Lachnospiraceae	5	6
	Ruminococcaceae	0	2
	Lactobacillaceae	7	21
	Erysipelotrichaceae	55	13

Appendix III – Family-level microbiota analysis of WT and FMO5 KO stomach contents. The stomach content of three animals was pooled for each condition. Sequence reads were taken from samples of WT (n=44) and FMO5 KO (n=48) 30-week old animals.

8. List of Abbreviations

AB	Antibiotic
ASP	Acylation stimulating protein
AUC	Area under the curve
BCA	Bicinchoninic acid
BMI	Body mass index
bp	Base pair
BSA	Bovine Serum Albumin
C3	Complement component 3
CF	Cystic fibrosis
CTFR	Cystic fibrosis transmembrane conductance regulator
CYP	Cytochrome P450
DNA	Deoxyribonucleic acid
dNTP	Deoxynucleotide triphosphate
DPT	10-(<i>N,N</i> -dimethylaminoalkyl)- 2-(trifluoromethyl)phenothiazine
DSS	Dextran sulphate sodium
DTT	Dithiothreitol
ECL	Enhanced chemiluminescence
EDTA	Ethylenediaminetetraacetic acid
ELISA	Enzyme-linked immunosorbent assay
ER	Endoplasmic reticulum
ERK	Extracellular signal-regulated kinase
FAD	Flavin adenine dinucleotide
FFA	Free fatty acids
FIZZ	Found in inflammatory zones
<i>FMO</i>	Flavin-containing monooxygenase gene (human)
<i>Fmo</i>	Flavin-containing monooxygenase gene (mouse)
FMO	Flavin-containing monooxygenase
GI	Gastrointestinal
HDL	High density lipoprotein
HFD	High-fat diet

HRP	Horseradish peroxidase
iAUC	Inverse area under the curve
IBD	Inflammatory bowel disease
IEC	Intestinal epithelial cell
IgA	Immunoglobulin A
IgG	Immunoglobulin G
IHC	Immunohistochemistry
IKK	I κ B kinase
IL	Interleukin
INF γ	Interferon γ
IPTG	Isopropyl β -D-1-thiogalactopyranoside
IRS1/2	Insulin receptor substrate1/2
JNK	c-Jun N-terminal kinase
kDa	Kilo Dalton
KO	Knockout
<i>Lac</i>	Lactose
LAL	Limulus ameocyte lysate
LB	Luria broth
LDL	Low density lipoprotein
LPS	Lipopolysaccharide
MAPK	Mitogen-activated protein kinase
ME1	Malic enzyme 1
mRNA	Messenger ribonucleic acid
MUC2	Mucin 2
NADP ⁺	Nicotine adenine dinucleotide phosphate (oxidised)
NADPH	Nicotine adenine dinucleotide phosphate (reduced)
NFDM	Non-fat dried milk
pAkt	phospho-Akt
PBS	Phosphate buffered saline
PCR	Polymerase chain reaction
PI3K	Phosphatidylinositol-3-kinase
PMSF	Phenylmethylsulfonyl fluoride

<i>Pofut1</i>	Protein O-Fucosyltransferase 1
PPAR γ	Peroxisome proliferator-activated receptor γ
RELM	Resistin like molecule
rRNA	Ribosomal ribonucleic acid
RNA	Ribonucleic acid
ROS	Reactive oxygen species
SDS	Sodium dodecyl sulphate
SDS-PAGE	Sodium dodecyl sulphate polyacrylamide gel electrophoresis
SOC	Super optimal broth with catabolite repression
T2D	Type 2 diabetes
TBS	Tris-buffered saline
TBS-T	Tris-buffered saline – 0.1 % tween
Th1/2	T helper cells1/2
TLR	Toll-like receptor
TMA	Trimethylamine
TMAU	Trimethylaminuria
TNBS	Trinitrobenzene sulphonate
TNF α	Tumour necrosis factor α
VAT	Visceral adipose tissue
WAT	White adipose tissue
WT	Wild-type
X-gal	5-bromo-4-chloro-3-indolyl- β -D-galactopyranoside

9. References

- Aguirre, V., Werner, E. D., Giraud, J., Lee, Y. H., Shoelson, S. E., and White, M. F. (2002). Phosphorylation of Ser307 in insulin receptor substrate-1 blocks interactions with the insulin receptor and inhibits insulin action. *The Journal of biological chemistry* 277, 1531–1537.
- Amar, J., Burcelin, R., Ruidavets, J. B., Cani, P. D., Fauvel, J., Alessi, M. C., Chamontin, B., and Ferrières, J. (2008). Energy intake is associated with endotoxemia in apparently healthy men. *Am J Clin Nutr* 87, 1219–1223.
- Amsen, D., de Visser, K. E., and Town, T. (2009). Approaches to determine expression of inflammatory cytokines. *Methods Mol. Biol.* 511, 107–142.
- Anderson, P. D., Mehta, N. N., Wolfe, M. L., Hinkle, C. C., Pruscino, L., Comiskey, L. L., Tabita-Martinez, J., Sellers, K. F., Rickels, M. R., Ahima, R. S., et al. (2007). Innate Immunity Modulates Adipokines in Humans. *Journal of Clinical Endocrinology & Metabolism* 92, 2272–2279.
- Angelakis, E., Armougom, F., Million, M., and Raoult, D. (2012). The relationship between gut microbiota and weight gain in humans. *Future Microbiology* 7, 91–109.
- Artis, D., Wang, M.-L., Keilbaugh, S. A., He, W., Brenes, M., Swain, G. P., Knight, P. A., Donaldson, D. D., Lazar, M. A., Miller, H. R. P., et al. (2004). RELMbeta/FIZZ2 is a goblet cell-specific immune-effector molecule in the gastrointestinal tract. *Proceedings of the National Academy of Sciences of the United States of America* 101, 13596–13600.
- Arumugam, M., Raes, J., Pelletier, E., Le Paslier, D., Yamada, T., Mende, D. R., Fernandes, G. R., Tap, J., Bruls, T., Batto, J.-M., et al. (2011). Enterotypes of the human gut microbiome. *Nature* 473, 174–180.
- Banerjee, R. R., and Lazar, M. A. (2001). Dimerization of resistin and resistin-like molecules is determined by a single cysteine. *The Journal of biological chemistry* 276, 25970–25973.
- Barbarroja, N., López Pedrera, R., Mayas, M. D., García Fuentes, E., Garrido Sánchez, L., Macías González, M., Bekay, El, R., Vidal Puig, A., and Tinahones, F. J. (2010). The obese healthy paradox: is inflammation the answer? *Biochem J* 430, 141–149.
- Bäckhed, F., Ding, H., Wang, T., Hooper, L. V., Koh, G. Y., Nagy, A., Semenkovich, C. F., and Gordon, J. I. (2004). The gut microbiota as an environmental factor that regulates fat storage. *Proceedings of the National Academy of Sciences of the United States of America* 101, 15718–15723.
- Bäckhed, F., Ley, R. E., Sonnenburg, J. L., Peterson, D. A., and Gordon, J. I. (2005). Host-bacterial mutualism in the human intestine. *Science* 307, 1915–1920.

- Bäckhed, F., Manchester, J. K., Semenkovich, C. F., and Gordon, J. I. (2007). Mechanisms underlying the resistance to diet-induced obesity in germ-free mice. *Proceedings of the National Academy of Sciences of the United States of America* 104, 979–984.
- Bech-Nielsen, G. V., Hansen, C. H. F., Hufeldt, M. R., Nielsen, D. S., Aasted, B., Vogensen, F. K., Midtvedt, T., and Hansen, A. K. (2012). Manipulation of the gut microbiota in C57BL/6 mice changes glucose tolerance without affecting weight development and gut mucosal immunity. *Res. Vet. Sci.* 92, 501–508.
- Benson, A. K., Kelly, S. A., Legge, R., Ma, F., Low, S. J., Kim, J., Zhang, M., Oh, P. L., Nehrenberg, D., Hua, K., et al. (2010). Individuality in gut microbiota composition is a complex polygenic trait shaped by multiple environmental and host genetic factors. *Proceedings of the National Academy of Sciences of the United States of America* 107, 18933–18938.
- Biagi, E., Nylund, L., Candela, M., Ostan, R., Bucci, L., Pini, E., Nikkila, J., Monti, D., Satokari, R., Franceschi, C., et al. (2010). Through Ageing, and Beyond: Gut Microbiota and Inflammatory Status in Seniors and Centenarians. *PLoS ONE* 5, e10667.
- Bienvenu, J. A. D., Monneret, G., Gutowski, M. C., and Fabien, N. (1998). Cytokine assays in human sera and tissues. *Toxicology* 129, 55–61.
- Borbás, T., Benkő, B., Dalmadi, B., Szabó, I., and Tihanyi, K. (2006). Insulin in flavin-containing monooxygenase regulation. *European Journal of Pharmaceutical Sciences* 28, 51–58.
- Boroni Moreira, A. P., and de Cássia Gonçalves Alfenas, R. (2012). The influence of endotoxemia on the molecular mechanisms of insulin resistance. *Nutr Hosp* 27, 382–390.
- Brugman, S., Klatter, F. A., Visser, J., Bos, N. A., Elias, D., and Rozing, J. (2004). Neonatal oral administration of DiaPep277, combined with hydrolysed casein diet, protects against Type 1 diabetes in BB-DP rats. An experimental study. *Diabetologia* 47, 1331–1333.
- Brugman, S., Klatter, F. A., Visser, J. T., Wildeboer-Veloo, A. C., Harmsen, H. J., Rozing, J., and Bos, N. A. (2006). Antibiotic treatment partially protects against type 1 diabetes in the Bio-Breeding diabetes-prone rat. Is the gut flora involved in the development of type 1 diabetes? *Diabetologia* 49, 2105–2108.
- Burcelin, R., Serino, M., Chabo, C., Blasco-Baque, V., and Amar, J. (2011). Gut microbiota and diabetes: from pathogenesis to therapeutic perspective. *Acta Diabetol* 48, 257–273.
- Cani, P. D., Amar, J., Iglesias, M. A., Poggi, M., Knauf, C., Bastelica, D., Neyrinck, A. M., Fava, F., Tuohy, K. M., Chabo, C., et al. (2007a). Metabolic Endotoxemia Initiates Obesity and Insulin Resistance. *Diabetes* 56, 1761–1772.
- Cani, P. D., Neyrinck, A. M., Fava, F., Knauf, C., Burcelin, R. G., Tuohy, K. M.,

- Gibson, G. R., and Delzenne, N. M. (2007b). Selective increases of bifidobacteria in gut microflora improve high-fat-diet-induced diabetes in mice through a mechanism associated with endotoxaemia. *Diabetologia* 50, 2374–2383.
- Cani, P. D., Bibiloni, R., Knauf, C., Waget, A., Neyrinck, A. M., Delzenne, N. M., and Burcelin, R. (2008a). Changes in gut microbiota control metabolic endotoxemia-induced inflammation in high-fat diet-induced obesity and diabetes in mice. *Diabetes* 57, 1470–1481.
- Cani, P. D., Delzenne, N. M., Amar, J., and Burcelin, R. (2008b). Role of gut microflora in the development of obesity and insulin resistance following high-fat diet feeding. *Pathol. Biol.* 56, 305–309.
- Cani, P. D., Possemiers, S., Van de Wiele, T., Guiot, Y., Everard, A., Rottier, O., Geurts, L., Naslain, D., Neyrinck, A., Lambert, D. M., et al. (2009). Changes in gut microbiota control inflammation in obese mice through a mechanism involving GLP-2-driven improvement of gut permeability. *Gut* 58, 1091–1103.
- Carvalho, B. M., Guadagnini, D., Tsukumo, D. M. L., Schenka, A. A., Latuf-Filho, P., Vassallo, J., Dias, J. C., Kubota, L. T., Carvalheira, J. B. C., and Saad, M. J. A. (2012). Modulation of gut microbiota by antibiotics improves insulin signalling in high-fat fed mice. *Diabetologia* 55, 2823–2834.
- Cashman, J. R. (2003). The role of flavin-containing monooxygenases in drug metabolism and development. *Curr Opin Drug Discov Devel* 6, 486–493.
- Chen, G. P., Poulsen, L. L., and Ziegler, D. M. (1995). Oxidation of aldehydes catalyzed by pig liver flavin-containing monooxygenase. *Drug Metab Dispos* 23, 1390–1393.
- Cherrington, N. J., Cao, Y., Rose, R. L., and Hodgson, E. (1998). Physiological Factors Affecting Protein Expression of Flavin-containing Monooxygenases 1, 3 and 5. *Xenobiotica* 28, 673–682.
- Cianflone, K., Xia, Z., and Chen, L. Y. (2003). Critical review of acylation-stimulating protein physiology in humans and rodents. *Biochimica et Biophysica Acta (BBA) - Biomembranes* 1609, 127–143.
- Claus, S. P., Ellero, S. L., Berger, B., Krause, L., Bruttin, A., Molina, J., Paris, A., Want, E. J., de Waziers, I., Cloarec, O., et al. (2011). Colonization-induced host-gut microbial metabolic interaction. *MBio* 2, e00271–10.
- Cliffe, L. J., and Grecis, R. K. (2004). The *Trichuris muris* System: a Paradigm of Resistance and Susceptibility to Intestinal Nematode Infection, in *Advances in Parasitology*, 255–307.
- Cole, J. R., Wang Q, Cardenas E, Fish J, Chai B, Farris, R. J., Kulam-Syed-Mohideen, A. S., McGarrell, D. M., Marsh T, Garrity, G. M., et al. (2009). The Ribosomal Database Project: improved alignments and new tools for rRNA analysis. *Nucleic Acids Res.* 37, D141–5.

- Creely, S. J., McTernan, P. G., Kusminski, C. M., Fisher, F. M., Da Silva, N. F., Khanolkar, M., Evans, M., Harte, A. L., and Kumar, S. (2006). Lipopolysaccharide activates an innate immune system response in human adipose tissue in obesity and type 2 diabetes. *AJP: Endocrinology and Metabolism* 292, E740–E747.
- Dandona, P., Aljada, A., and Bandyopadhyay, A. (2004). Inflammation: the link between insulin resistance, obesity and diabetes. *Trends in Immunology* 25, 4–7.
- Davis, B. B., Magge, S., Mucenski, C. G., and Drake, R. L. (1988). Insulin Mediated Post-transcriptional Regulation of Malic enzymes and Albumin mRNAs. *Biochemical and Biophysical Research Communications* 154, 1081–1087.
- de Oliveira Mello, R., da Silva, C. M. G., Fonte, F. P., Ferraz Silva, D. L., Pereira, J. A., Margarido, N. F., and Martinez, C. A. R. (2012). Evaluation of the number of goblet cells in crypts of the colonic mucosa with and without fecal transit. 39, 139–145.
- Delzenne, N. M., and Cani, P. D. (2011). Gut Microbiota and the Pathogenesis of Insulin Resistance. *Curr Diab Rep* 11, 154–159.
- Delzenne, N. M., Neyrinck, A. M., Bäckhed, F., and Cani, P. D. (2011). Targeting gut microbiota in obesity: effects of prebiotics and probiotics. *Nat Rev Endocrinol* 7, 639–646.
- DeWeerd, S. (2014). Microbiome: A complicated relationship status. *Nature* 508, S61–3.
- Dicksved, J., Halfvarson, J., Rosenquist, M., Järnerot, G., Tysk, C., Apajalahti, J., Engstrand, L., and Jansson, J. K. (2008). Molecular analysis of the gut microbiota of identical twins with Crohn's disease. *ISME Journal* 2, 716–727.
- Ding, S., Chi, M. M., Scull, B. P., Rigby, R., Schwerbrock, N. M. J., Magness, S., Jobin, C., and Lund, P. K. (2010). High-Fat Diet: Bacteria Interactions Promote Intestinal Inflammation Which Precedes and Correlates with Obesity and Insulin Resistance in Mouse. *PLoS ONE* 5, e12191.
- Dolphin, C. T., Janmohamed, A., Smith, R. L., Shephard, E. A., and Phillips, I. R. (1997). Missense mutation in flavin-containing mono-oxygenase 3 gene, FMO3, underlies fish-odour syndrome. *Nat Genet* 17, 491–494.
- Dolphin, C. T., Beckett, D. J., Janmohamed, A., Cullingford, T. E., Smith, R. L., Shephard, E. A., and Phillips, I. R. (1998). The Flavin-containing Monooxygenase 2 Gene (FMO2) of Humans, but Not of Other Primates, Encodes a Truncated, Nonfunctional Protein. *The Journal of biological chemistry* 273, 30599–30607.
- Dolphin, C., Shephard, E. A., Povey, S., Palmer, C. N., Ziegler, D. M., Ayesh, R., Smith, R. L., and Phillips, I. R. (1991). Cloning, primary sequence, and chromosomal mapping of a human flavin-containing monooxygenase (FMO1). *The Journal of biological chemistry* 266, 12379–12385.

- Duescher, R. J., Lawton, M. P., Philpot, R. M., and Elfarra, A. A. (1994). Flavin-containing monooxygenase (FMO)-dependent metabolism of methionine and evidence for FMO3 being the major FMO involved in methionine sulfoxidation in rabbit liver and kidney microsomes. *The Journal of biological chemistry* 269, 17525–17530.
- Duncan, B. B., Schmidt, M. I., Pankow, J. S., Ballantyne, C. M., Couper, D., Vigo, A., Hoogeveen, R., Folsom, A. R., and Heiss, G. (2003). Low-Grade Systemic Inflammation and the Development of Type 2 Diabetes The Atherosclerosis Risk in Communities Study. 1–7. *Diabetes* 52, 1799-1805.
- Engström, G., Hedblad, B., Eriksson, K.-F., Janson, L., and Lindgärde, F. (2005). Complement C3 is a risk factor for the development of diabetes. *Diabetes* 54, 570–575.
- Erridge, C., Attina, T., Spickett, C. M., and Webb, D. J. (2007). A high-fat meal induces low-grade endotoxemia: evidence of a novel mechanism of postprandial inflammation. *Am J Clin Nutr* 86, 1286–1292.
- Eswaramoorthy, S., Bonanno, J. B., Burley, S. K., and Swaminathan, S. (2006). Mechanism of action of a flavin-containing monooxygenase. *Proceedings of the National Academy of Sciences of the United States of America* 103, 9832–9837.
- Fleissner, C. K., Huebel, N., Abd El-Bary, M. M., Loh, G., Klaus, S., and Blaut, M. (2010). Absence of intestinal microbiota does not protect mice from diet-induced obesity. *British Journal of Nutrition* 104, 919–929.
- Fraaije, M. W., Kamerbeek, N. M., van Berkel, W. J. H., and Janssen, D. B. (2002). Identification of a Baeyer-Villiger monooxygenase sequence motif. *FEBS Letters* 518, 43–47.
- Francois, A. A., Nishida, C. R., de Montellano, P. R. O., Phillips, I. R., and Shephard, E. A. (2009). Human flavin-containing monooxygenase 2.1 catalyzes oxygenation of the antitubercular drugs thiacetazone and ethionamide. *Drug Metab Dispos* 37, 178–186.
- Fujio, J., Kushiya, A., Sakoda, H., Fujishiro, M., Ogihara, T., Fukushima, Y., Anai, M., Horike, N., Kamata, H., Uchijima, Y., et al. (2008). Regulation of gut-derived resistin-like molecule β expression by nutrients. *Diabetes Research and Clinical Practice* 79, 2–10.
- Furnes, B., Feng, J., Sommer, S. S., and Schlenk, D. (2003). Identification of novel variants of the flavin-containing monooxygenase gene family in African Americans. *Drug Metab Dispos* 31, 187–193.
- Gagliardi, S., Ogliairi, P., Davin, A., Corato, M., Cova, E., Abel, K., Cashman, J. R., Ceroni, M., and Cereda, C. (2010). Flavin-Containing Monooxygenase mRNA Levels are Up-Regulated in ALS Brain Areas in SOD1-Mutant Mice. *Neurotox Res* 20, 150–158.

- Gao, Z., Hwang, D., Bataille, F., Lefevre, M., York, D., Quon, M. J., and Ye, J. (2002). Serine phosphorylation of insulin receptor substrate 1 by inhibitor kappa B kinase complex. *The Journal of biological chemistry* 277, 48115–48121.
- Geurts, L., Lazarevic, V., Derrien, M., Everard, A., Van Roye, M., Knauf, C., Valet, P., Girard, M., Muccioli, G. G., François, P., et al. (2011). Altered gut microbiota and endocannabinoid system tone in obese and diabetic leptin-resistant mice: impact on apelin regulation in adipose tissue. *Front. Microbio.* 2, 149.
- Gewirtz, A. T. (2006). Dominant-negative TLR5 polymorphism reduces adaptive immune response to flagellin and negatively associates with Crohn's disease. *AJP: Gastrointestinal and Liver Physiology* 290, G1157–G1163.
- Gonzalez Malagon, S.G. (2011). Flavin containing monooxygenase 5 and endogenous metabolism. *University College London*, PhD
- Goodridge, A. G., Crish, J. F., Hillgartner, F. B., and Wilson, S. B. (1989). Nutritional and hormonal regulation of the gene for avian malic enzyme. *J. Nutr.* 119, 299–308.
- Grainge, C., Dulay, V., Ward, J., Sammut, D., Davies, E., Green, B., Lau, L., Cottey, L., Haitchi, H.-M., Davies, D. E., et al. (2012). Resistin-like molecule- β is induced following bronchoconstriction of asthmatic airways. *Respirology* 17, 1094–1100.
- Guilmeau, S., Flandez, M., Bancroft, L., Sellers, R. S., Tear, B., Stanley, P., and Augenlicht, L. H. (2008). Intestinal deletion of Pofut1 in the mouse inactivates notch signaling and causes enterocolitis. *Gastroenterology* 135, 849–860.
- Gylling, H., Hallikainen, M., Pihlajamäki, J., Simonen, P., Kuusisto, J., Laakso, M., and Miettinen, T. A. (2010). Insulin sensitivity regulates cholesterol metabolism to a greater extent than obesity: lessons from the METSIM Study. *Journal of Lipid Research* 51, 2422–2427.
- Hamady, M., and Knight, R. (2009). Microbial community profiling for human microbiome projects: Tools, techniques, and challenges. *Genome Res* 19, 1141–1152.
- Harris, K., Kassis, A., Major, G., and Chou, C. J. (2012). Is the gut microbiota a new factor contributing to obesity and its metabolic disorders? *J Obes* 2012, 879151.
- Hawkesworth, S., Moore, S. E., Fulford, A. J. C., Barclay, G. R., Darboe, A. A., Mark, H., Nyan, O. A., and Prentice, A. M. (2013). Evidence for metabolic endotoxemia in obese and diabetic Gambian women. *Nutrition and Diabetes* 3, e83–6.
- He, W., Wang, M.-L., Jiang, H.-Q., Stepan, C. M., Shin, M. E., Thurnheer, M. C., Cebra, J. J., Lazar, M. A., and Wu, G. D. (2003). Bacterial colonization leads to the colonic secretion of RELM/FIZZ2, a novel goblet cell-specific protein. *Gastroenterology* 125, 1388–1397.

- Heazlewood, C. K., Cook, M. C., Eri, R., Price, G. R., Tauro, S. B., Taupin, D., Thornton, D. J., Png, C. W., Crockford, T. L., Cornall, R. J., et al. (2008). Aberrant mucin assembly in mice causes endoplasmic reticulum stress and spontaneous inflammation resembling ulcerative colitis. *PloS Medicine* 5, 440–460.
- Heikkinen, S., Argmann, C. A., Champy, M.-F., and Auwerx, J. (2007). Evaluation of glucose homeostasis. *Curr Protoc Mol Biol* Chapter 29, Unit 29B.3–29B.3.22.
- Herbert, D. R., Yang, J.-Q., Hogan, S. P., Groschwitz, K., Khodoun, M., Munitz, A., Orekov, T., Perkins, C., Wang, Q., Brombacher, F., et al. (2009). Intestinal epithelial cell secretion of RELM-beta protects against gastrointestinal worm infection. *J. Exp. Med.* 206, 2947–2957.
- Herder, C., Schneitler, S., Rathmann, W., Haastert, B., Schneitler, H., Winkler, H., Bredahl, R., Hahnloser, E., and Martin, S. (2007). Low-Grade Inflammation, Obesity, and Insulin Resistance in Adolescents. *Journal of Clinical Endocrinology & Metabolism* 92, 4569–4574.
- Hernandez, D., Janmohamed, A., Chandan, P., Phillips, I. R., and Shephard, E. A. (2004). Organization and evolution of the flavin-containing monooxygenase genes of human and mouse: identification of novel gene and pseudogene clusters. *Pharmacogenetics* 14, 117–130.
- Hernandez, D., Chandan, P., Janmohamed, A., Phillips, L. R., and Shephard, E. A. (2006a). Deletion of genes from the mouse genome using Cre/loxP technology. *Methods Mol. Biol.* 320, 307–319.
- Hernandez, D., Melidoni, N., Phillips IR, Shephard EA (2006b). Microinjection of targeted embryonic stem cells and establishment of knockout mouse lines for Fmo genes. *Methods in Molecular Biology* 320, 329–341.
- Hernandez, D., Phillips, L. R., and Shephard, E. A. (2006c). Characterization of targeted mouse embryonic stem cell chromosomes: karyotyping and fluorescence in situ hybridization of metaphase spreads. *Methods in Molecular Biology* 320, 321–327.
- Hernandez, D., Janmohamed, A., Chandan, P., Omar, B. A., Phillips, I. R., and Shephard, E. A. (2009). Deletion of the mouse Fmo1 gene results in enhanced pharmacological behavioural responses to imipramine. *Pharmacogenet Genomics* 19, 289–299.
- Hertle, E., Stehouwer, C. D. A., and van Greevenbroek, M. M. J. (2014). The complement system in human cardiometabolic disease. *Molecular Immunology* 61, 135–148.
- Hildebrandt, M. A., Hoffmann, C., Sherrill-Mix, S. A., Keilbaugh, S. A., Hamady, M., Chen, Y.-Y., Knight, R., Ahima, R. S., Bushman, F., and Wu, G. D. (2009). High-Fat diet determines the composition of the murine gut microbiome independently of obesity. *Gastroenterology* 137, 1716–1724.

- Hisamuddin, I. M., Wehbi, M. A., Schmotzer, B., Easley, K. A., Hyland, L. M., Giardiello, F. M., and Yang, V. W. (2005). Genetic polymorphisms of flavin monooxygenase 3 in sulindac-induced regression of colorectal adenomas in familial adenomatous polyposis. *Cancer Epidemiol Biomarkers Prev* 14, 2366–2369.
- Hoenig, M. R., and Sellke, F. W. (2010). Insulin resistance is associated with increased cholesterol synthesis, decreased cholesterol absorption and enhanced lipid response to statin therapy. *Atherosclerosis* 211, 260–265.
- Hogan, S. P., Seidu, L., Blanchard, C., Groschwitz, K., Mishra, A., Karow, M. L., Ahrens, R., Artis, D., Murphy, A. J., Valenzuela, D. M., et al. (2006). Resistin-like molecule beta regulates innate colonic function: barrier integrity and inflammation susceptibility. *J. Allergy Clin. Immunol.* 118, 257–268.
- Holcomb, I. N., Kabakoff, R. C., Chan, B., Baker, T. W., Gurney, A., Henzel, W., Nelson, C., Lowman, H. B., Wright, B. D., Skelton, N. J., et al. (2000). FIZZ1, a novel cysteine-rich secreted protein associated with pulmonary inflammation, defines a new gene family. *The EMBO Journal* 19, 4046–4055.
- Hooper, L. V., and Macpherson, A. J. (2010). Immune adaptations that maintain homeostasis with the intestinal microbiota. *Nat. Rev. Immunol.* 10, 159–169.
- Hopkins, M. J., Sharp, R., and Macfarlane, G. T. (2001). Age and disease related changes in intestinal bacterial populations assessed by cell culture, 16S rRNA abundance, and community cellular fatty acid profiles. *Gut* 48, 198–205.
- Hotamisligil, G. S., Shargill, N. S., and Spiegelman, B. M. (1993). Adipose expression of tumor necrosis factor- α : direct role in obesity-linked insulin resistance. *Science* 259, 87–91.
- Hotamisligil, G. S., Budavari, A., Murray, D., and Spiegelman, B. M. (1994). Reduced tyrosine kinase activity of the insulin receptor in obesity-diabetes. Central role of tumor necrosis factor- α . *Journal of Clinical Investigation* 94, 1543–1549.
- Hotamisligil, G. S. (2006). Inflammation and metabolic disorders. *Nature* 444, 860–867.
- Hough, T. A., Nolan, P. M., Tsipouri, V., Toyne, A. A., Gray, I. C., Goldsworthy, M., Moir, L., Cox, R. D., Clements, S., Glenister, P. H., et al. (2002). Novel phenotypes identified by plasma biochemical screening in the mouse. *Mammalian Genome* 13, 595–602.
- Itoh, H., Beck, P. L., Inoue, N., Xavier, R., and Podolsky, D. K. (1999). A paradoxical reduction in susceptibility to colonic injury upon targeted transgenic ablation of goblet cells. *Journal of Clinical Investigation* 104, 1539–1547.
- Janmohamed, A., Dolphin, C. T., Phillips, I. R., and Shephard, E. A. (2001). Quantification and cellular localization of expression in human skin of genes encoding flavin-containing monooxygenases and cytochromes P450. *Biochemical*

Pharmacology 62, 777–786.

- Janmohamed, A., Hernandez, D., Phillips, I. R., and Shephard, E. A. (2004). Cell-, tissue-, sex- and developmental stage-specific expression of mouse flavin-containing monooxygenases (Fmos). *Biochemical Pharmacology* 68, 73–83.
- Kaila, B., Grant, D., Pettigrew, N., Greenberg, H., and Bernstein, C. N. (2004). Crohn's Disease Recurrence in a Small Bowel Transplant. *The American Journal of Gastroenterology* 99, 158–162.
- Kallus, S. J., and Brandt, L. J. (2012). The intestinal microbiota and obesity. *J. Clin. Gastroenterol.* 46, 16–24.
- Katsurada, A., Iritani, N., Fukuda, H., Noguchi, T., and Tanaka, T. (1988). Transcriptional and posttranscriptional regulation of malic enzyme synthesis by insulin and triiodothyronine. *Biochimica et Biophysica Acta* 950, 113–117.
- Katsurada, A., Iritani, N., Fukuda, H., Matsumura, Y., Noguchi, T., and Tanaka, T. (1989). Effects of insulin and fructose on transcriptional and post-transcriptional regulation of malic enzyme synthesis in diabetic rat liver. *Biochimica et Biophysica Acta* 1004, 103–107.
- Kemp, D. M. (2013). Does chronic low-grade endotoxemia define susceptibility of obese humans to insulin resistance via dietary effects on gut microbiota? *Adipocyte* 2, 188–190.
- Kim, Y. H., Lim, D. S., Lee, J. H., Lim, D.-S., Shim, W. J., Ro, Y. M., Park, G. H., Becker, K. G., Cho-Chung, Y. S., and Kim, M.-K. (2003). Gene expression profiling of oxidative stress on atrial fibrillation in humans. *Exp Mol Med* 35, 336–349.
- Kim, Y. S., and Ho, S. B. (2010). Intestinal Goblet Cells and Mucins in Health and Disease: Recent Insights and Progress. *Curr Gastroenterol Rep* 12, 319–330.
- Kim, K.-A., Gu, W., Lee, I.-A., Joh, E.-H., and Kim, D.-H. (2012). High fat diet-induced gut microbiota exacerbates inflammation and obesity in mice via the TLR4 signaling pathway. *PLoS ONE* 7, e47713.
- Koropatkin, N. M., Cameron, E. A., and Martens, E. C. (2012). How glycan metabolism shapes the human gut microbiota. *Nat. Rev. Microbiol.* 10, 323–335.
- Koukouritaki, S. B., Simpson, P., Yeung, C. K., Rettie, A. E., and Hines, R. N. (2002). Human hepatic flavin-containing monooxygenases 1 (FMO1) and 3 (FMO3) developmental expression. *Pediatr Res* 51, 236–243.
- Krajmalnik-Brown, R., Ilhan, Z. E., Kang, D. W., and DiBaise, J. K. (2012). Effects of gut microbes on nutrient absorption and energy regulation. *Nutr Clin Pract* 27, 201–214.
- Krause, R. J., Lash, L. H., and Elfarra, A. A. (2003). Human kidney flavin-containing monooxygenases and their potential roles in cysteine s-conjugate metabolism and

- nephrotoxicity. *J Pharmacol Exp Ther* 304, 185–191.
- Krimi, R. B., Kotelevets, L., Dubuquoy, L., Plaisancié, P., Walker, F., Lehy, T., Desreumaux, P., Van Seuning, I., Chastre, E., Forgue-Lafitte, M.-E., et al. (2008). Resistin-like molecule β regulates intestinal mucous secretion and curtails TNBS-induced colitis in mice. *Inflamm Bowel Dis* 14, 931–941.
- Krimi, R. B., Letteron, P., Chedid, P., Nazaret, C., Ducroc, R., and Marie, J. C. (2009). Resistin-Like Molecule- Inhibits SGLT-1 Activity and Enhances GLUT2-Dependent Jejunal Glucose Transport. *Diabetes* 58, 2032–2038.
- Krueger, S. K., and Williams, D. E. (2005). Mammalian flavin-containing monooxygenases: structure/function, genetic polymorphisms and role in drug metabolism. *Pharmacol Ther* 106, 357–387.
- Krusekopf, S., and Roots, I. (2005). St. John's wort and its constituent hyperforin concordantly regulate expression of genes encoding enzymes involved in basic cellular pathways. *Pharmacogenet Genomics* 15, 817–829.
- Kumar, A., Wu, H., Collier-Hyams, L. S., Hansen, J. M., Li, T., Yamoah, K., Pan, Z.-Q., Jones, D. P., and Neish, A. S. (2007). Commensal bacteria modulate cullin-dependent signaling via generation of reactive oxygen species. *The EMBO Journal* 26, 4457–4466.
- Kushiyama, A., Shojima, N., Ogihara, T., Inukai, K., Sakoda, H., Fujishiro, M., Fukushima, Y., Anai, M., Hiraku, O., Horike, N., et al. (2005). Resistin-like molecule β activates mapks, suppresses insulin signaling in hepatocytes, and induces diabetes, hyperlipidemia, and fatty liver in transgenic mice on a high fat diet. *The Journal of biological chemistry* 280, 42016–42025.
- Kwon, H., and Pessin, J. E. (2013). Adipokines mediate inflammation and insulin resistance. *Front Endocrinol (Lausanne)* 4, 71.
- La Serre, de, C. B., Ellis, C. L., Lee, J., Hartman, A. L., Rutledge, J. C., and Raybould, H. E. (2010). Propensity to high-fat diet-induced obesity in rats is associated with changes in the gut microbiota and gut inflammation. *AJP: Gastrointestinal and Liver Physiology* 299, G440–G448.
- Lai, W. G., Farah, N., Moniz, G. A., and Wong, Y. N. (2011). A Baeyer-Villiger oxidation specifically catalyzed by human flavin-containing monooxygenase 5. *Drug Metab Dispos* 39, 61–70.
- Lam, Y. Y., Janovská, A., McAinch, A. J., Belobrajdic, D. P., Hatzinikolas, G., Game, P., and Wittert, G. A. (2011). The use of adipose tissue-conditioned media to demonstrate the differential effects of fat depots on insulin-stimulated glucose uptake in a skeletal muscle cell line. *Obes Res Clin Pract* 5, e1–e78.
- Lam, Y. Y., Ha, C. W. Y., Campbell, C. R., Mitchell, A. J., Dinudom, A., Oscarsson, J., Cook, D. I., Hunt, N. H., Caterson, I. D., Holmes, A. J., et al. (2012). Increased gut permeability and microbiota change associate with mesenteric fat inflammation and metabolic dysfunction in diet-induced obese mice. *PLoS ONE*

7, e34233.

- Lang, D. H., Yeung, C. K., Peter, R. M., Ibarra, C., Gasser, R., Itagaki, K., Philpot, R. M., and Rettie, A. E. (1998). Isoform specificity of trimethylamine N-oxygenation by human flavin-containing monooxygenase (FMO) and P450 enzymes: selective catalysis by FMO3. *Biochemical Pharmacology* 56, 1005–1012.
- Lang, D. H., and Rettie, A. E. (2000). In vitro evaluation of potential in vivo probes for human flavin-containing monooxygenase (FMO): metabolism of benzydamine and caffeine by FMO and P450 isoforms. *Br J Clin Pharmacol* 50, 311–314.
- Lawton, M. P., and Philpot, R. M. (1993). Molecular genetics of the flavin-dependent monooxygenases. *Pharmacogenetics* 3, 40–44.
- Ley, R. E., Bäckhed, F., Turnbaugh, P., Lozupone, C. A., Knight, R. D., and Gordon, J. I. (2005). Obesity alters gut microbial ecology. *Proceedings of the National Academy of Sciences of the United States of America* 102, 11070–11075.
- Ley, R. E., Peterson, D. A., and Gordon, J. I. (2006a). Ecological and evolutionary forces shaping microbial diversity in the human intestine. *Cell* 124, 837–848.
- Ley, R. E., Turnbaugh, P. J., Klein, S., and Gordon, J. I. (2006b). Microbial ecology: human gut microbes associated with obesity. *Nature* 444, 1022–1023.
- Ley, R. E. (2010). Obesity and the human microbiome. *Current opinion in Gastroenterology* 26, 5–11.
- Ludwig, W., and Schleifer, K. H. (1994). Bacterial phylogeny based on 16S and 23S rRNA sequence analysis. *FEMS Microbiol Rev* 15, 155–173.
- Malaspina, A., Kaushik, N., and de Bellerocche, J. (2001). Differential expression of 14 genes in amyotrophic lateral sclerosis spinal cord detected using gridded cDNA arrays. *J Neurochem* 77, 132–145.
- Marathe, N. P., Shetty, S. A., Lanjekar, V., Shouche, Y. S., and Ranade, D. (2012). Changes in human gut flora with age: an Indian familial study. *BMC Microbiol* 12, 222.
- Mariat, D., Firmesse, O., Levenez, F., Guimaraes, V., Sokol, H., Dore, J., Corthier, G., and Furet, J. P. (2009). The Firmicutes/Bacteroidetes ratio of the human microbiota changes with age. *BMC Microbiol* 9, 123.
- Matalka, K. Z., Tutunji, M. F., Abu-Baker, M., and Abu Baker, Y. (2005). Measurement of protein cytokines in tissue extracts by enzyme-linked immunosorbent assays: Application to lipopolysaccharide-induced differential milieu of cytokines. *Neuroendocrinology Letters* 26, 231–236.
- McDuffie, E., Obert, L., Chupka, J., and Sigler, R. (2006). Detection of cytokine protein expression in mouse lung homogenates using bead suspension bead array.

- McVay, L. D., Keilbaugh, S. A., Wong, T. M. H., Kierstein, S., Shin, M. E., Lehrke, M., Lefterova, M. I., Shifflett, D. E., Barnes, S. L., Cominelli, F., et al. (2006). Absence of bacterially induced RELM β reduces injury in the dextran sodium sulfate model of colitis. *Journal of Clinical Investigation* 116, 2914–2923.
- Membrez, M., Blancher, F., Jaquet, M., Bibiloni, R., Cani, P. D., Burcelin, R. G., Corthesy, I., Mace, K., and Chou, C. J. (2008). Gut microbiota modulation with norfloxacin and ampicillin enhances glucose tolerance in mice. *The FASEB Journal* 22, 2416–2426.
- Miller, M. M., James, R. A., Richer, J. K., Gordon, D. F., Wood, W. M., and Horwitz, K. B. (1997). Progesterone regulated expression of flavin-containing monooxygenase 5 by the B-isoform of progesterone receptors: implications for tamoxifen carcinogenicity. *Journal of Clinical Endocrinology & Metabolism* 82, 2956–2961.
- Mishra, A., Wang, M., Schlotman, J., Nikolaidis, N. M., DeBrosse, C. W., Karow, M. L., and Rothenberg, M. E. (2007). Resistin-like molecule- β is an allergen-induced cytokine with inflammatory and remodeling activity in the murine lung. *AJP: Lung Cellular and Molecular Physiology* 293, L305–L313.
- Mitchell, S. C., and Smith, R. L. (2001). Trimethylaminuria: the fish malodor syndrome. *Drug Metab Dispos* 29, 517–521.
- Miyazaki, Y., Glass, L., Triplitt, C., Wajcberg, E., Mandarino, L. J., and DeFronzo, R. A. (2002). Abdominal fat distribution and peripheral and hepatic insulin resistance in type 2 diabetes mellitus. *AJP: Endocrinology and Metabolism* 283, E1135–43.
- Moller, D. E. (2000). Potential role of tnf- α in the pathogenesis of insulin resistance and type 2 diabetes. *Trends in Endocrinology & Metabolism* 11, 212–217.
- Monteiro, R., and Azevedo, I. (2010). Chronic inflammation in obesity and the metabolic syndrome. *Mediators of Inflammation* 2010, 1–10.
- Moolenbeek, C., and Ruitenber, E. J. (1981). The “Swiss roll”: a simple technique for histological studies of the rodent intestine. *Laboratory Animals* 15, 57–59.
- Moreno-Indias, I., Cardona, F., Tinahones, F. J., and Queipo-Ortuño, M. I. (2014). Impact of the gut microbiota on the development of obesity and type 2 diabetes mellitus. *Front. Microbio.* 5, 190.
- Motika, M. S., Zhang, J., and Cashman, J. R. (2007). Flavin-containing monooxygenase 3 and human disease. *Expert Opin. Drug Metab. Toxicol.* 3, 831–845.
- Munkonda, M. N., Lapointe, M., Miegueu, P., Roy, C., Gauvreau, D., Richard, D., and Cianflone, K. (2012). Recombinant acylation stimulating protein administration to C3 $^{-/-}$ mice increases insulin resistance via adipocyte

- inflammatory mechanisms. *PLoS ONE* 7, e46883.
- Murphy, E. F., Cotter, P. D., Hogan, A., O'Sullivan, O., Joyce, A., Fouhy, F., Clarke, S. F., Marques, T. M., O'Toole, P. W., Stanton, C., et al. (2013). Divergent metabolic outcomes arising from targeted manipulation of the gut microbiota in diet-induced obesity. *Gut* 62, 220–226.
- Muscari, A., Massarelli, G., Bastagli, L., Poggiopollini, G., Tomassetti, V., Drago, G., Martignani, C., Pacilli, P., Boni, P., and Puddu, P. (2000). Relationship of serum C3 to fasting insulin, risk factors and previous ischaemic events in middle-aged men. *European Heart Journal* 21, 1081–1090.
- Nair, M. G., Guild, K. J., and Artis, D. (2006). Novel Effector Molecules in Type 2 Inflammation: Lessons Drawn from Helminth Infection and Allergy. *The Journal of Immunology* 177, 1393–1399.
- Nair, M. G., Guild, K. J., Du, Y., Zaph, C., Yancopoulos, G. D., Valenzuela, D. M., Murphy, A., Stevens, S., Karow, M., and Artis, D. (2008). Goblet cell-derived resistin-like molecule β augments cd4⁺ t cell production of ifn- γ and infection-induced intestinal inflammation. *Journal of Immunology* 181, 4709–4725.
- Neilson, A. P., Djuric, Z., Land, S., and Kato, I. (2011). Plasma levels of resistin-like molecule beta in humans. *Cancer Epidemiology* 35, 485–489.
- Neish, A. S. (2009). Microbes in gastrointestinal health and disease. *Gastroenterology* 136, 65–80.
- Nimmerfall, F., and Rosenthaler, J. (1980). Significance of the goblet-cell mucin layer, the outer most luminal barrier to passage through the gut wall. *Biochemical and Biophysical Research Communications* 94, 960–966.
- Norkina, O., Burnett, T. G., and De Lisle, R. C. (2004a). Bacterial overgrowth in the cystic fibrosis transmembrane conductance regulator null mouse small intestine. *Infection and Immunity* 72, 6040–6049.
- Norkina, O., Kaur, S., Ziemer, D., and De Lisle, R. C. (2004b). Inflammation of the cystic fibrosis mouse small intestine. *AJP: Gastrointestinal and Liver Physiology* 286, G1032–G1041.
- Ohmi, N., Yoshida, H., Endo, H., Hasegawa, M., Akimoto, M., and Higuchi, S. (2003). S-oxidation of S-methyl-esonarimod by flavin-containing monooxygenases in human liver microsomes. *Xenobiotica* 33, 1221–1231.
- Onat, A., Can, G., Rezvani, R., and Cianflone, K. (2011). Complement C3 and cleavage products in cardiometabolic risk. *Clinica Chimica Acta* 412, 1117–1129.
- Overby, L. H., Buckpitt, A. R., Lawton, M. P., Atta-Asafo-Adjei, E., Schulze, J., and Philpot, R. M. (1995). Characterization of flavin-containing monooxygenase 5 (FMO5) cloned from human and guinea pig: evidence that the unique catalytic properties of FMO5 are not confined to the rabbit ortholog. *Archives of Biochemistry and Biophysics* 317, 275–284.

- Overby, L. H., Carver, G. C., and Philpot, R. M. (1997). Quantitation and kinetic properties of hepatic microsomal and recombinant flavin-containing monooxygenases 3 and 5 from humans. *Chem Biol Interact* 106, 29–45.
- Pai, R., and Kang, G. (2008). Microbes in the gut: A digestible account of host-symbiont interactions. *Indian Journal of Medical Research* 128, 587–594.
- Palmer, C., Bik, E. M., DiGiulio, D. B., Relman, D. A., and Brown, P. O. (2007). Development of the Human Infant Intestinal Microbiota. *PLoS BIOLOGY* 5, 1556–1573.
- Paramsothy, P., Knopp, R. H., Kahn, S. E., Retzlaff, B. M., Fish, B., Ma, L., and Ostlund, R. E. (2011). Plasma sterol evidence for decreased absorption and increased synthesis of cholesterol in insulin resistance and obesity. *Am J Clin Nutr* 94, 1182–1188.
- Park, C. M., Reid, P. E., Walker, D. C., and MacPherson, B. R. (1987). A simple, practical “swiss roll” method of preparing tissues for paraffin or methacrylate embedding. *J Microsc* 145, 115–120.
- Park, M. H., Kim, D. H., Lee, E. K., Kim, N. D., Im, D. S., Lee, J., Yu, B. P., and Chung, H. Y. (2014). Age-related inflammation and insulin resistance: a review of their intricate interdependency. *Arch. Pharm. Res* 12, 1507-1514.
- Pastorelli, L., Salvo, C. D., Mercado, J. R., Vecchi, M., and Pizarro, T. T. (2013). Central role of the gut epithelial barrier in the pathogenesis of chronic intestinal inflammation: lessons learned from animal models and human genetics. *Frontiers in immunology* 4, 1–22.
- Patel, S. D. (2004). Disulfide-Dependent Multimeric Assembly of Resistin Family Hormones. *Science* 304, 1154–1158.
- Peltola, P., Pihlajamäki, J., Koutnikova, H., Ruotsalainen, E., Salmenniemi, U., Vauhkonen, I., Kainulainen, S., Gylling, H., Miettinen, T. A., Auwerx, J., et al. (2006). Visceral obesity is associated with high levels of serum squalene. *Obesity (Silver Spring)* 14, 1155–1163.
- Phillips, C. M., Kesse-Guyot, E., Ahluwalia, N., McManus, R., Hercberg, S., Lairon, D., Planells, R., and Roche, H. M. (2012). Dietary fat, abdominal obesity and smoking modulate the relationship between plasma complement component 3 concentrations and metabolic syndrome risk. *Atherosclerosis* 220, 513–519.
- Phillips, I. R., Dolphin, C. T., Clair, P., Hadley, M. R., Hutt, A. J., McCombie, R. R., Smith, R. L., and Shephard, E. A. (1995). The molecular biology of the flavin-containing monooxygenases of man. *Chem Biol Interact* 96, 17–32.
- Phillips, I., Francois, A., and Shephard, E. A. (2007). The flavin-containing monooxygenases (FMOs): genetic variation and its consequences for the metabolism of therapeutic drugs. *Current Pharmacogenomics* 5, 292–313.
- Pickup, J. C. (2004). Inflammation and activated innate immunity in the pathogenesis

- of type 2 diabetes. *Diabetes Care* 27, 813–823.
- Pihlajamäki, J., Gylling, H., Miettinen, T. A., and Laakso, M. (2004). Insulin resistance is associated with increased cholesterol synthesis and decreased cholesterol absorption in normoglycemic men. *Journal of Lipid Research* 45, 507–512.
- Poulsen, L. L., and Ziegler, D. M. (1977). Microsomal mixed-function oxidase-dependent renaturation of reduced ribonuclease. *Archives of Biochemistry and Biophysics* 183, 563–570.
- Rae, J. M., Johnson, M. D., Lippman, M. E., and Flockhart, D. A. (2001). Rifampin is a selective, pleiotropic inducer of drug metabolism genes in human hepatocytes: studies with cDNA and oligonucleotide expression arrays. *J. Pharmacol. Exp. Ther.* 299, 849–857.
- Rajala, M. W., Obici, S., Scherer, P. E., and Rossetti, L. (2003). Adipose-derived resistin and gut-derived resistin-like molecule- β selectively impair insulin action on glucose production. *Journal of Clinical Investigation* 111, 225–230.
- Rajendhran, J., and Gunasekaran, P. (2011). Microbial phylogeny and diversity: small subunit ribosomal RNA sequence analysis and beyond. *Microbiol. Res.* 166, 99–110.
- Raybould, H. E. (2012). Gut microbiota, epithelial function and derangements in obesity. *J Physiol* 590, 441–446.
- Robins, S. J., Rubins, H. B., Faas, F. H., Schaefer, E. J., Elam, M. B., Anderson, J. W., and Collins, D., (2003). Insulin resistance and cardiovascular events with low HDL cholesterol: the Veterans Affairs HDL Intervention Trial (VA-HIT). *Diabetes Care* 26, 1513–1517.
- Rouer, E., Rouet, P., Delpech, M., and Leroux, J. P. (1988). Purification and comparison of liver microsomal flavin-containing monooxygenase from noraml and streptozotocin-diabetic rats. *Biochemical Pharmacology* 37, 3455–3459.
- Rozee, K. R., Cooper, D., Lam, K., and Costerton, J. W. (1982). Microbial flora of the mouse ileum mucous layer and epithelial surface. *Applied and Environmental Microbiology* 43, 1451–1463.
- Russell, S. L., Gold, M. J., Hartmann, M., Willing, B. P., Thorson, L., Wlodarska, M., Gill, N., Blanchet, M.-R., Mohn, W. W., McNagny, K. M., et al. (2012). Early life antibiotic-driven changes in microbiota enhance susceptibility to allergic asthma. *EMBO reports* 13, 440–447.
- Sahasakul, Y., Takemura, N., and Sonoyama, K. (2012). Different impacts of purified and nonpurified diets on microbiota and toll-like receptors in the mouse stomach. *Bioscience, Biotechnology, and Biochemistry* 76, 1728–1732.
- Sam, S., Haffner, S., Davidson, M. H., D'Agostino, R. B., Feinstein, S., Kondos, G., Perez, A., and Mazzone, T. (2009). Relation of abdominal fat depots to systemic

- markers of inflammation in type 2 diabetes. *Diabetes Care* 32, 932–937.
- Samaras, K., Botelho, N. K., Chisholm, D. J., and Lord, R. V. (2010). Subcutaneous and visceral adipose tissue gene expression of serum adipokines that predict type 2 diabetes. *Obesity (Silver Spring)* 18, 884–889.
- Sausen, P. J., and Elfarra, A. A. (1990). Cysteine conjugate S-oxidase. Characterization of a novel enzymatic activity in rat hepatic and renal microsomes. *The Journal of biological chemistry* 265, 6139–6145.
- Serino, M., Luche, E., Gres, S., Baylac, A., Berge, M., Cenac, C., Waget, A., Klopp, P., Iacovoni, J., Klopp, C., et al. (2011). Metabolic adaptation to a high-fat diet is associated with a change in the gut microbiota. *Gut* 61, 543–553.
- Sevasti B Koukouritaki, R. N. H. (2005). Flavin-containing monooxygenase genetic polymorphism: impact on chemical metabolism and drug development. *Pharmacogenomics* 6, 807–822.
- Shephard, E. A., and Phillips, I. R. (2010). The potential of knockout mouse lines in defining the role of flavin-containing monooxygenases in drug metabolism. *Expert Opin. Drug Metab. Toxicol.* 6, 1083–1094.
- Shoelson, S. E., Lee, J., and Goldfine, A. B. (2006). Inflammation and insulin resistance. *Journal of Clinical Investigation* 116, 1793–1801.
- Shoelson, S. E., Herrero, L., and Naaz, A. (2007). Obesity, inflammation, and insulin resistance. *Gastroenterology* 132, 2169–2180.
- Shojima, N., Ogihara, T., Inukai, K., Fujishiro, M., Sakoda, H., Kushiya, A., Katagiri, H., Anai, M., Ono, H., Fukushima, Y., et al. (2005). Serum concentrations of resistin-like molecules β and γ are elevated in high-fat-fed and obese db/db mice, with increased production in the intestinal tract and bone marrow. *Diabetologia* 48, 984–992.
- Siddens, L. K., Krueger, S. K., Henderson, M. C., and Williams, D. E. (2014). Mammalian flavin-containing monooxygenase (FMO) as a source of hydrogen peroxide. *Biochemical Pharmacology* 89, 141–147.
- Simonen, P. P., Gylling, H. K., and Miettinen, T. A. (2002a). Diabetes contributes to cholesterol metabolism regardless of obesity. *Diabetes Care* 25, 1511–1515.
- Simonen, P. P., Gylling, H., and Miettinen, T. A. (2002b). Body weight modulates cholesterol metabolism in non-insulin dependent type 2 diabetics. *Obes. Res.* 10, 328–335.
- Simonen, P., Kotronen, A., Hallikainen, M., Sevastianova, K., Makkonen, J., Hakkarainen, A., Lundbom, N., Miettinen, T. A., Gylling, H., and Yki-Järvinen, H. (2011). Cholesterol synthesis is increased and absorption decreased in non-alcoholic fatty liver disease independent of obesity. *Journal of Hepatology* 54, 153–159.

- Smithson, K. W., Millar, D. B., Jacobs, L. R., and Gray, G. M. (1981). Intestinal Diffusion Barrier: Unstirred Water Layer or Membrane Surface Mucous Coat? *Science* 214, 1241–1244.
- Song, Y., Liu, C., and Finegold, S. M. (2004). Real-time PCR quantitation of clostridia in feces of autistic children. *Applied and Environmental Microbiology* 70, 6459–6465.
- Specian, R. D., and Oliver, M. G. (1991). Functional biology of intestinal goblet cells. *American Journal of Physiology - Cell Physiology* 260, C183–193.
- Steppan, C. M., Bailey, S. T., Bhat, S., Brown, E. J., Banerjee, R. R., Wright, C. M., Patel, H. R., Ahima, R. S., and Lazar, M. A. (2001a). The hormone resistin links obesity to diabetes. *Nature* 409, 307–312.
- Steppan, C. M., Brown, E. J., Wright, C. M., Bhat, S., Banerjee, R. R., Dai, C. Y., Enders, G. H., Silberg, D. G., Wen, X., Wu, G. D., et al. (2001b). A family of tissue-specific resistin-like molecules. *Proceedings of the National Academy of Sciences of the United States of America* 98, 502–506.
- Stranberg, T. E., Salomaa, V., Vanhanen, H., and Miettinen, T. A. (1996). Associations of fasting blood glucose with cholesterol absorption and synthesis in nondiabetic middle-aged men. *Diabetes* 45, 755–761.
- Strober, W., Fuss, I. J., and Blumberg, R. S. (2002). The immunology of mucosal models of inflammation. *Annu. Rev. Immunol.* 20, 495–549.
- Suh, J. K., Poulsen, L. L., Ziegler, D. M., and Robertus, J. D. (1999). Yeast flavin-containing monooxygenase generates oxidizing equivalents that control protein folding in the endoplasmic reticulum. *Proceedings of the National Academy of Sciences of the United States of America* 96, 2687–2691.
- Swann, J. R., Tuohy, K. M., Lindfors, P., Brown, D. T., Gibson, G. R., Wilson, I. D., Sidaway, J., Nicholson, J. K., and Holmes, E. (2011). Variation in antibiotic-induced microbial recolonization impacts on the host metabolic phenotypes of rats. *J. Proteome Res.* 10, 3590–3603.
- Tachon, S., Zhou, J., Keenan, M., Martin, R., and Marco, M. L. (2012). The intestinal microbiota in aged mice is modulated by dietary resistant starch and correlated with improvements in host responses. *FEMS Microbiology Ecology*.
- Takamura, T., Sakurai, M., Ota, T., Ando, H., Honda, M., and Kaneko, S. (2004). Genes for systemic vascular complications are differentially expressed in the livers of type 2 diabetic patients. *Diabetologia* 47, 638–647.
- Taverne, F., Richard, C., Couture, P., and Lamarche, B. (2013). Abdominal obesity, insulin resistance, metabolic syndrome and cholesterol homeostasis. *Biochemical Pharmacology* 1, 130–136.
- Ternak, G. (2005). Antibiotics may act as growth/obesity promoters in humans as an inadvertent result of antibiotic pollution? *Medical Hypotheses* 64, 14–16.

- Testa, B., and Krämer, S. D. (2007). The biochemistry of drug metabolism - an introduction: part 2. Redox reactions and their enzymes. *Chem Biodivers* 4, 257–405.
- Thomas, F., Hehemann, J.-H., Rebuffet, E., Czjzek, M., and Michel, G. (2011). Environmental and gut bacteroidetes: The food connection. *Front. Microbio.* 2, 1–16.
- Turnbaugh, P. J., Ley, R. E., Mahowald, M. A., Magrini, V., Mardis, E. R., and Gordon, J. I. (2006). An obesity-associated gut microbiome with increased capacity for energy harvest. *Nature* 444, 1027–1031.
- Turnbaugh, P. J., Bäckhed, F., Fulton, L., and Gordon, J. I. (2008). Diet-induced obesity is linked to marked but reversible alterations in the mouse distal gut microbiome. *Cell Host & Microbe* 3, 213–223.
- Turnbaugh, P. J., Hamady, M., Yatsunenko, T., Cantarel, B. L., Duncan, A., Ley, R. E., Sogin, M. L., Jones, W. J., Roe, B. A., Affourtit, J. P., et al. (2009a). A core gut microbiome in obese and lean twins. *Nature* 457, 480–484.
- Turnbaugh, P. J., Ridaura, V. K., Faith, J. J., Rey, F. E., Knight, R., and Gordon, J. I. (2009b). The effect of diet on the human gut microbiome: a metagenomic analysis in humanized gnotobiotic mice. *Sci Transl Med* 1, 6ra14–6ra14.
- Tynes, R. E., Sabourin, P. J., and Hodgson, E. (1985). Identification of distinct hepatic and pulmonary forms of microsomal flavin-containing monooxygenase in the mouse and rabbit. *Biochemical and Biophysical Research Communications* 126, 1069–1075.
- Van der Sluis, M., De Koning, B. A. E., De Bruijn, A. C. J. M., Velcich, A., Meijerink, J. P. P., Van Goudoever, J. B., Büller, H. A., Dekker, J., Van Seuning, I., Renes, I. B., et al. (2006). Muc2-Deficient Mice Spontaneously Develop Colitis, Indicating That MUC2 Is Critical for Colonic Protection. *Gastroenterology* 131, 117–129.
- Veeramah, K. R., Thomas, M. G., Weale, M. E., Zeitlyn, D., Tarekegn, A., Bekele, E., Mendell, N. R., Shephard, E. A., Bradman, N., and Phillips, I. R. (2008). The potentially deleterious functional variant flavin-containing monooxygenase 2*1 is at high frequency throughout sub-Saharan Africa. *Pharmacogenet Genomics* 18, 877–886.
- Veeravalli, S., Omar, B. A., Houseman, L., Hancock, M., Malagon, S. G. G., Scott, F., Janmohamed, A., Phillips, I. R., and Shephard, E. A. (2014). The phenotype of a flavin-containing monooxygenase knockout mouse implicates the drug-metabolizing enzyme FMO1 as a novel regulator of energy balance. *Biochemical Pharmacology* 90, 88–95.
- Venema, K. (2010). Role of gut microbiota in the control of energy and carbohydrate metabolism. *Curr Opin Clin Nutr Metab Care* 13, 432–438.
- Vijay-Kumar, M., Sanders, C. J., Taylor, R. T., Kumar, A., Aitken, J. D., Sitaraman,

- S. V., Neish, A. S., Uematsu, S., Akira, S., Williams, I. R., et al. (2007). Deletion of TLR5 results in spontaneous colitis in mice. *Journal of Clinical Investigation*.
- Vijay-Kumar, M., Aitken, J. D., Carvalho, F. A., Cullender, T. C., Mwangi, S., Srinivasan, S., Sitaraman, S. V., Knight, R., Ley, R. E., and Gewirtz, A. T. (2010). Metabolic syndrome and altered gut microbiota in mice lacking Toll-like receptor 5. *Science* 328, 228–231.
- Walker, A. W., Ince, J., Duncan, S. H., Webster, L. M., Holtrop, G., Ze, X., Brown, D., Stares, M. D., Scott, P., Bergerat, A., et al. (2011). Dominant and diet-responsive groups of bacteria within the human colonic microbiota. *International Society for Microbial Ecology* 5, 220–230.
- Wang, M.-L., Shun, M. E., Knight, P. A., Artis, D., Silberg, D. G., Suh, E., and Wu, G. D. (2005). Regulation of RELM/FIZZ isoform expression by Cdx2 in response to innate and adaptive immune stimulation in the intestine. *AJP: Gastrointestinal and Liver Physiology* 288, G1074–G1083.
- Wang, Q., Garrity, G. M., Tiedje, J. M., and Cole, J. R. (2007). Naive Bayesian classifier for rapid assignment of rRNA sequences into the new bacterial taxonomy. *Applied and Environmental Microbiology* 73, 5261–5267.
- Wellen, K. E., and Hotamisligil, G. S. (2005). Inflammation, stress, and diabetes. *Journal of Clinical Investigation* 115, 1111–1119.
- Werner, E. D., Lee, J., Hansen, L., Yuan, M., and Shoelson, S. E. (2004). Insulin resistance due to phosphorylation of insulin receptor substrate-1 at serine 302. *The Journal of biological chemistry* 279, 35298–35305.
- Williams, D. E., Ziegler, D. M., Nordin, D. J., Hale, S. E., and Masters, B. S. (1984). Rabbit lung flavin-containing monooxygenase is immunochemically and catalytically distinct from the liver enzyme. *Biochemical and Biophysical Research Communications* 125, 116–122.
- Wirtz, S., Neufert, C., Weigmann, B., and Neurath, M. F. (2007). Chemically induced mouse models of intestinal inflammation. *Nat Protoc* 2, 541–546.
- Wlazlo, N., van Greevenbroek, M. M. J., Ferreira, I., Jansen, E. J. H. M., Feskens, E. J. M., van der Kallen, C. J. H., Schalkwijk, C. G., Bravenboer, B., and Stehouwer, C. D. A. (2012). Low-grade inflammation and insulin resistance independently explain substantial parts of the association between body fat and serum C3: The CODAM study. *Metabolism* 61, 1787–1796.
- Yang, R.-Z., Huang, Q., Xu, A., McLenithan, J. C., Eison, J. A., Shuldiner, A. R., Alkan, S., and Gong, D.-W. (2003). Comparative studies of resistin expression and phylogenomics in human and mouse. *Biochemical and Biophysical Research Communications* 310, 927–935.
- Youn, B.-S., Yu, K.-Y., Park, H. J., Lee, N. S., Min, S. S., Youn, M. Y., Cho, Y. M., Park, Y. J., Kim, S. Y., Lee, H. K., et al. (2004). Plasma Resistin Concentrations Measured by Enzyme-Linked Immunosorbent Assay Using a Newly Developed

Monoclonal Antibody Are Elevated in Individuals with Type 2 Diabetes Mellitus. *The Journal of Clinical Endocrinology & Metabolism* 89, 150–156.

- Zaph, C., Troy, A. E., Taylor, B. C., Berman-Booty, L. D., Guild, K. J., Du, Y., Yost, E. A., Gruber, A. D., May, M. J., Greten, F. R., et al. (2007). Epithelial-cell-intrinsic IKK- β expression regulates intestinal immune homeostasis. *Nature* 446, 552–556.
- Zhang, J., and Cashman, J. R. (2005). Quantitative analysis of FMO gene mRNA levels in human tissues. *Drug Metab Dispos* 34, 19–26.
- Zhang, J., Cerny, M. A., Lawson, M., Mosadeghi, R., and Cashman, J. R. (2007). Functional activity of the mouse flavin-containing monooxygenase forms 1, 3, and 5. *J. Biochem. Mol. Toxicol.* 21, 206–215.
- Zhang, J., Chaluvadi, M. R., Reddy, R., Motika, M. S., Richardson, T. A., Cashman, J. R., and Morgan, E. T. (2009). Hepatic flavin-containing monooxygenase gene regulation in different mouse inflammation models. *Drug Metab Dispos* 37, 462–468.
- Ziegler, D. M., and Mitchell, C. H. (1972). Microsomal oxidase. IV. Properties of a mixed-function amine oxidase isolated from pig liver microsomes. *Archives of Biochemistry and Biophysics* 150, 116–125.
- Ziegler, D. M. (2002). An overview of the mechanism, substrate specificities, and structure of FMOs. *Drug Metab Rev* 34, 503–511.
- Zoetendal, E. G., Akkermans, A. D. L., Akkermans-van Vliet, W. M., de Visser, J. A. G. M., and de Vos, W. M. (2001). The Host Genotype Affects the Bacterial Community in the Human Gastrointestinal Tract. *Microbial Ecology in Health and Disease* 13, 129–134.
- Zoetendal, E. G., Rajilic-Stojanovic, M., and De Vos, W. M. (2008). High-throughput diversity and functionality analysis of the gastrointestinal tract microbiota. *Gut* 57, 1605–1615.
- Zuo, H. J., Xie, Z. M., Zhang, W. W., Li, Y. R., Wang, W., Ding, X. B., and Pei, X. F. (2011). Gut bacteria alteration in obese people and its relationship with gene polymorphism. *World J Gastroenterol* 17, 1076–1081.